

CLASSIFIED  
FOR PUBLIC RELEASE

PL/PA 16 DEC 96

Sensor and Simulation Notes

Note 141

February 1972

Numerical Determination of the Step Wave Response of a  
Thin-Wire Scattering Element Arbitrarily Located Above  
a Perfectly Conducting Ground Plane

by

F. M. Tesche\*

Northrop Corporate Laboratories  
Pasadena, California

Abstract

This note presents a numerical technique for determining the behavior of induced currents and charges on a perfectly conducting thin-wire scattering element which is arbitrarily located above a perfectly conducting ground plane. From the parallel plate problem as presented in SSN 135, an integro-differential equation for the wire current is deduced from the limiting case of one of the plates receding to infinity. After a brief discussion of the method of solution, the frequency and time domain behavior of the current at three points on the wire and the linear charge density at both ends of the wire are presented for an assumed incident step wave. The variation of these quantities as a function of the angle of inclination and height above the ground plane of the scattering element is studied. Summary curves showing the variation of the fundamental resonant frequency and the corresponding damping constant are plotted, along with curves of the late time (static) charge densities and the field enhancement factor.

---

\*

Now with The Dikewood Corporation, Albuquerque, New Mexico.

PL 96-11951

### Acknowledgement

I would like to express my appreciation to Drs. Kelvin Lee and Carl Baum for their technical assistance and advice. In addition, thanks go to Mrs. G. Peralta for the typing and to Mrs. E. Ravndal for preparing the numerous curves. The assistance of Mrs. Mary Carroll at Dikewood in the final preparation of this note is gratefully acknowledged.

## I. Introduction

In this note, the behavior of a thin, perfectly conducting wire scatterer located arbitrarily above a perfectly conducting plane is studied in both the frequency and time domain. This idealized model can be thought of as representing a missile located in a parallel plate simulator in such a manner that the effect of one of the plates may be neglected. On the other hand, this model might represent the interaction problem of an EMP incident on a missile which is located above a conducting ground plane. In both cases, it is desirable to know the time history of the currents and charges induced on the structure by the EMP, and to evaluate the effect of the conducting ground plane on these quantities.

In a previous note in this series<sup>(11)</sup>, an integral equation for the current on a thin-wire scattering element which is arbitrarily located within two perfectly conducting parallel plates is formulated and solved. Typical results in the frequency domain are presented. The effect of both parallel plates is taken into account by using the Green's function for the region between the plates. It is noted that the problem of studying a thin-wire antenna or scattering element above a single conducting plate is simply a special case of the more general parallel plate problem. By keeping the positions of one plate and the wire fixed and letting the other plate recede to infinity, the resulting geometry of the problem is then equivalent to that under consideration in this note.

After a brief discussion of the integral equation for the wire current and the numerical method for its solution, results of the numerical computation are presented. Of special interest is the behavior of the induced current at the midpoint and at two points located one quarter of the way from the ends of the wire. In addition, the behavior of the charge density at both ends of the wire is investigated. From these results, summary curves are presented which show the behavior of the damping constant for the fundamental mode and the shift of the first resonant frequency as a function of the position of the scatterer. The static (late time) behavior of the charge at the ends of the scattering element is presented as a function of the wire position and inclination, and the field enhancement factor at the wire ends is defined and plotted. .

It should be pointed out that by assuming one of the two parallel plates in the analysis in Note 135 to be infinitely far away from the other plate and scatterer, no singularities or resonances are expected in the Green's function as the frequency is increased. The more general problem which takes into account both plates will be considered in a future note.

## II. Formulation of the Integral Equation

Consider for a moment the case of a thin-wire scattering element located between two parallel plates, as shown in Figure 1. The total length of the wire is denoted by  $L$ , its radius by  $a$ , and the distance from the plate at  $x = 0$  to the center of the wire element is denoted by  $h$ . The second plate is located at  $x = d$ . The angles  $\theta$  and  $\phi$  describe the inclination of the wire in the usual spherical coordinate system. The symbol  $\hat{\xi}$  represents the unit vector in the direction of the wire.

In Note 135, an integral equation for the induced current on the wire is derived for the special case of  $\phi = 0$ . In this manner, the angle  $\theta$  is contained in a plane perpendicular to the two parallel plates. For this case, the integral equation is of the following form

$$-j\omega\epsilon_0 E^{\text{inc}}(\xi) = \int_0^L I(\xi') \left[ -\mathcal{L} \sum_{n=-\infty}^{\infty} \frac{e^{-jkR_n^{(1)}}}{4\pi R_n^{(1)}} + \mathcal{L}' \sum_{n=-\infty}^{\infty} \frac{e^{-jkR_n^{(2)}}}{4\pi R_n^{(2)}} \right] d\xi', \quad (1)$$

where

$$\mathcal{L}' = \frac{\partial^2}{\partial \xi^2} + k^2 \quad (2)$$

$$\mathcal{L} = -\frac{\partial}{\partial \xi_n} \frac{\partial}{\partial \xi} + k^2 \cos^2 \theta \quad (3)$$

denote operators, and the distances  $R_n$  are given by

$$R_n^{(1)} = \left[ \left( (L - \xi - \xi') \sin \theta - 2(h + nd) \right)^2 + \left( (\xi - \xi') \cos \theta \right)^2 \right]^{1/2} \quad (4)$$

$$R_n^{(2)} = \left[ \left( (\xi - \xi') \sin \theta - 2nd \right)^2 + \left( (\xi - \xi') \cos \theta \right)^2 \right]^{1/2} \quad n \neq 0 \quad (5)$$

$$R_0^{(2)} = \left[ (\xi - \xi')^2 + a^2 \right]^{1/2} \quad n = 0 \quad (6)$$

In this equation,  $E^{\text{inc}}(\xi)$  is the tangential component of the incident electric

field falling on the wire, either from an incident wave or from a driving source for the active antenna problem. For a TEM wave propagating in the  $+\hat{z}$  direction and for the special case of  $\phi = 0$ , the incident field is given by

$$E^{inc}(\xi) = E_0 \sin \theta e^{-jk\xi \cos \theta}, \quad (7)$$

where the phase of the incident field has been chosen as zero at the point  $\xi = 0$ . The time variation in this problem is  $e^{j\omega t}$  and is suppressed.

For the more general case of  $\phi \neq 0$ , the integral equation above must be modified slightly. Assuming that  $\theta, \phi \neq 0$ , it is possible to pass a plane through the scatterer which is perpendicular to the two parallel plates. The resulting geometry, as seen in that plane, is shown in Figure 2. Note that the angle  $\gamma$ , which is that between the wire and the  $\hat{x}$  axis, is given by

$$\cos \gamma = \sin \theta \cos \phi \quad (8)$$

and the angle complementary to  $\gamma$  is given by

$$\beta = \frac{\pi}{2} - \cos^{-1}(\sin \theta \cos \phi) \quad (9)$$

From Figure 2 it is seen that the wire scatterer has the same position relative to the parallel plates as in the  $\phi = 0$  case, except that the angle  $\theta$  has been replaced by  $\beta$ . Hence, by substituting  $\beta$  as calculated from equation 9 into the equations (2), (3), (4), (5), and (6), the correct integral equation results for the case of the scatterer having an arbitrary orientation.

The incident electric field for the scattering case must also be slightly changed for  $\phi \neq 0$ . Looking at Figure 1, it is noted that the tangential component of  $E^{inc}$  is given by

$$E^{inc}(\xi) = E_0 \cos \gamma e^{-jk\xi \cos \theta} \quad (10)$$

or equivalently, by

$$E^{inc}(\xi) = E_0 \sin \theta \cos \phi e^{-jk\xi \cos \theta}. \quad (11)$$

To treat the case of the wire scatterer near just one plane, it is now possible to let  $d$  go to infinity so that the infinite summations in Eq. (1) reduce to a single term. By doing this, the resulting structure is shown in Figure 3 and the integral equation takes the form

$$-j\omega\epsilon E_0 \sin \theta \cos \phi e^{-jk\xi \cos \theta} = \int_0^L I_0(\xi') \left[ -\mathcal{L} \frac{e^{-jkR_0^{(1)}}}{4\pi R_0^{(1)}} + \mathcal{L}' \frac{e^{-jkR_0^{(2)}}}{4\pi R_0^{(2)}} \right] d\xi' \quad (12)$$

with

$$R_0^{(1)} = \left[ \left( (L - \xi - \xi') \sin \beta - 2h \right)^2 + \left( (\xi - \xi') \cos \beta \right)^2 \right]^{1/2} \quad (13)$$

$$R_0^{(2)} = \left[ (\xi - \xi')^2 + a^2 \right]^{1/2} \quad (14)$$

and the  $\mathcal{L}$  and  $\mathcal{L}'$  operators are defined in terms of the angle  $\beta$ . The first term in the kernel of Eq. (12) gives the effect of the image of the wire and the second term gives the effect of the wire itself.

It should be pointed out that in deriving the integral equation for the current on the scatterer, the thin-wire approximation has been used. That is to say, the current on the surface of the wire is assumed to be represented by a line current flowing along the axis of the wire. For source and observation points well separated, the difference in effects between the actual current and the filamentary current is negligible. As the source and observation points become closer, the thin-wire approximation becomes less and less correct, and in some cases, it breaks down completely. This effect has been discussed in the literature<sup>(7,9)</sup> and it is found that if  $\Delta$  represents the size of one zone or cell on the antenna over which the current is assumed constant for the numerical solution, the thin-wire approximation is then valid for

$$\Delta \geq 5a. \quad (15)$$

For the case  $\Delta = 5a$ , it can be shown that the error in the kernel in the thin-wire approximation is of the order of 1.8%.

Assuming that the nominal figure of 10 cells per wavelength is used, it can be shown that for a scattering body having a diameter-to-length ratio of  $2a/L = .01$ , the maximum frequency that can be treated by the thin-wire method is given by  $kL \approx 18$ . It might be that for some cases the response of the scatterer above this value of  $kL$  is negligible so that the thin-wire approximation is adequate. In the most general case, however, it is necessary to use the exact Green's function at higher frequencies. This point is discussed further in the Appendix I.

To solve the integral equation (12) at high frequencies, it is necessary to replace the portion of the kernel that has the singularity in it by the exact kernel. For the other part which accounts for the image of the wire, the thin-wire kernel is still valid. The exact Pocklington equation for a single wire in free space is<sup>(6)</sup>

$$-j\omega\epsilon E^{inc}(\xi) = \int_0^L \int_0^{2\pi} J(\xi') \left( \frac{\partial^2}{\partial \xi^2} + k^2 \right) \frac{e^{-jkR}}{4\pi R} a d\phi d\xi' \quad (16)$$

where

$$R = \left[ (\xi - \xi')^2 + 4a^2 \sin^2(\phi/2) \right]^{1/2} \quad (17)$$

The free space kernel, denoted by  $K_{fs}$ , may be defined as the integral over  $\phi$  in the above expression. Thus,

$$K_{fs} = \frac{1}{2\pi} \int_0^{2\pi} \frac{e^{-jkR}}{4\pi R} d\phi \quad (18)$$

Replacing the free space portion of the kernel in Eq. (12) by this last equation results in the integro-differential equation for the present problem.

$$-j\omega\epsilon E_0 \sin \theta \cos \phi e^{-jk\xi \cos \theta} = \int_0^L I(\xi) \left[ -\mathcal{L} \frac{e^{-jkR_0^{(1)}}}{4\pi R_0^{(1)}} + \mathcal{L}' K_{fs}(\xi, \xi') \right] d\xi' \quad (19)$$

The solution to this integral equation, which is valid for frequencies such that  $kL > 18$ , can then be used to determine the time response of the thin-wire scatterer over the ground plane.

### III. Numerical Solution of the Integro-Differential Equation

The technique of solving the integro-differential equation in (19) is described by Harrington<sup>(3)</sup> and is often referred to as the method of moments. Basically this involves expanding the unknown current on the wire in a set of basis functions, and then, with a similar set of testing functions, forming a set of non-singular linear algebraic equations for the unknown constants multiplying each of the basis functions. The effect of the operators  $\mathcal{L}$  and  $\mathcal{L}'$  are accounted for by defining them to be finite difference operators.

This method is briefly illustrated as follows. Let the integral equation be represented as

$$y = \mathcal{O}x \quad (20)$$

where  $y(\xi)$  is a known function defined over the domain  $0 \leq \xi \leq L$  and  $\mathcal{O}$  is the integral operator defined over the same domain.  $x(\xi')$  is an unknown function to be determined.

By defining a set of basis functions  $\phi_i(\xi')$ , the unknown can be expanded in terms of these as

$$x(\xi') = \sum_i \alpha_i \phi_i(\xi') \quad (21)$$

Substituting this relation into Eq. (20) and using the assumed linearity of the operator  $\mathcal{O}$ , Eq. (20) may be written as

$$y(\xi) = \sum_i \alpha_i \mathcal{O}\phi_i(\xi'). \quad (22)$$

By defining a set of testing functions  $w_j(\xi)$ , and a suitable inner product  $\langle w_j(\xi), f(\xi) \rangle$ , where  $f(\xi)$  can be any function defined over the same domain as  $y$  and  $x$ , the operation of this inner product on Eq. (22) yields

$$\langle w_j, y \rangle = \sum_i \alpha_i \langle w_j, \mathcal{O}\phi_i \rangle. \quad (23)$$

Denoting the inner products  $\langle w_j, y \rangle$  by  $V_j$ , and  $\langle w_j, \mathcal{O}\phi_i \rangle$  by  $Z_{ji}$ , Eq. (23) then

represents a matrix equation of the form

$$V_j = Z_{ji} \alpha_i \quad (24)$$

or equivalently

$$[V] = [Z][\alpha]. \quad (25)$$

By inverting the matrix  $Z$  by standard numerical algorithms, the coefficients  $\alpha_i$  can be determined as

$$[\alpha] = [Z]^{-1}[V] \quad (26)$$

and then substituted into Eq. (21) to obtain the function  $x(\xi)$ .

In any practical problem only a finite number of basis functions can be used to approximate the function  $x(\xi)$ . Moreover, the choice of the functional forms of the basis and testing functions is arbitrary. In this study, the basis functions are chosen to be pulses. This implies that if the scatterer were divided into  $N$  zones or cells, the current would be constant within each cell. The testing functions are defined as impulse functions, which is equivalent to the point-matching method of solution. For a more concise description of this technique, with special emphasis on the treatment of the differential operators  $\mathcal{L}$  and  $\mathcal{L}'$ , the reader is referred to Refs. (3, 8, and 9).

After the current distribution on the wire has been determined via the solution of Eq. (19), the linear charge density on the wire may be evaluated through the use of the continuity equation

$$-j\omega\sigma(\xi_0) = \left. \frac{dI(\xi)}{d\xi} \right|_{\xi=\xi_0} \quad (27)$$

Of special interest is the charge density at the ends of the wire at  $\xi = 0$  and  $L$ . Note that in the thin-wire scattering problem, there is some ambiguity in defining the total charge at the ends of the scatterer. This arises from the fact that it is assumed that the effect of charges on the end-

caps of the wire can be neglected, or equivalently, that the wire is really a hollow, open cylinder. King<sup>(4)</sup> briefly considers this problem in defining the charge at the ends of a driven antenna. In this note, the quantity to be presented will be the normalized line charge density evaluated at the wire-ends. The normalization factor will be the late time line charge density occurring on the same wire and with the wire in free space and the incident electric field being parallel to the wire element. This quantity is denoted by  $\sigma_{\infty}$ . Note that this is the charge density occurring on the wire in the static limit.

#### IV. Construction of the Time Response

To obtain the response of the thin-wire structure with a step wave incident, the Fast Fourier Transform technique is employed.<sup>(1,2)</sup> By solving Eq. (19) with  $E_0 = 1$  at a number of different frequencies, the Fourier transform of the delta function time response of the current can be defined. This spectrum, referred to as the transfer function of the system, can then be used to find the response due to an arbitrary incident waveform. This is done by multiplying the Fourier spectrum of the incident waveform by the transfer function and then taking the inverse Fourier transform.

In treating the scattering problem, it was observed that by taking the frequency spectrum between  $kL = 0$  and  $kL = 40$ , adequate representation of the time response is obtained. There are some slight oscillations in the early portion of the time response curve due to truncating the frequency spectrum. These oscillations were found to be less than .5% of the peak value in a typical case, and have been suppressed in the final plots of the time domain results. By increasing the maximum frequency from  $kL = 40$  to  $kL = 80$ , these oscillations virtually disappeared with no other change in the resulting time plots.

## V. Numerical Results and Discussion

Using the previously described numerical techniques, the behavior of a thin cylinder having a diameter to length ratio of .01 (corresponding to  $\Omega = 2 \ln(L/a) = 10.597$ ) was studied. The numerical computation was done on a CDC 6600 computer. With 256 unique sample points in the frequency domain and 10 cells per wavelength along the wire, the total computation time was around four minutes per case.

In presenting the frequency and time history of the currents and charges on the wire, two basic cases have been considered. Case 1, which is presented in Figures 4 through 7, is for  $\theta = 90^\circ$  and variable  $\phi$  and  $h/L$ . In this manner, the wave vector  $\bar{k}$  is always perpendicular to the wire. The incident plane wave pulse hits every point on the wire at the same time.

The other case for which time and frequency plots are given is for  $\phi = 0$  and various  $\theta$  and  $h/L$ . This is presented in Figures 8 through 11. In this case,  $\bar{k}$  has a component parallel to the wire, indicating that there are possible phase variations of the incident field along the wire. In both cases, the reference time  $t = 0$  is taken to be when the incident pulse first hits the wire.

It should be noted that each numbered figure actually contains ten graphs, labeled a through j. The first five (a through e) show the magnitude of the currents and charges in the frequency domain at various points of the structure for three different inclination angles. This is the transfer function or Fourier transform of the delta function time response of the wire. The next five curves (f through j) give the time domain behavior of the currents and charges at the same points on the wire as in the preceding five plots. The time domain analysis assumes a step wave incident.

In presenting the current and charge data, it is convenient to normalize these quantities by suitable factors. To this end, the following quantities are defined.  $I_0$  is the magnitude of the maximum time domain current flowing at the midpoint of the scattering element which is located in free space with the incident step electric field perpendicular to the wire element.  $\sigma_\infty$  is the magnitude of the linear charge density at either end of the wire in free space which is obtained in the limit as  $t \rightarrow \infty$ . As in the definition of  $I_0$ , it is assumed that the incident step E field is perpendicular to the wire. In this

way, the reference case for normalizing all frequency and time plots is given by the problem defined by the parameters  $h = \infty$ ,  $\theta = 90^\circ$ , and  $\phi = 0^\circ$ .

If the incident pulse electric field has a magnitude of  $E_0$  volts/meter, the previously defined normalizing quantities have the following values

$$I_0 = 1.78 \times (E_0 L) \text{ milliamps}$$

$$\sigma_\infty = 0.95 \times (\epsilon_0 E_0 L) \text{ Coulombs/meter}$$

for the scatterer of length  $L$  and  $2a/L = .01$ .

From these time and frequency plots it is easy to get an idea of the effect of the ground plane on the behavior of the induced charges and currents. For the wire located at  $h/L = 1$ , it is noted that there is very little apparent effect of the ground plane on the currents. A much more noticeable effect is due to the scatterer being tilted with respect to the  $\bar{k}$  vector giving rise to phase variations in the incident electric field. Notice that the curves of the time behavior of the charges and currents eventually settle down to the function that is of the form  $c_1 \cos(\omega_0 t + \phi) e^{-t/\tau}$ . For late time, it is then possible to describe most of the charges and currents by the knowledge of the fundamental resonant frequency  $\omega_0$  and corresponding damping constant  $\tau$ . A study of these two parameters as a function of scatterer location and inclination will aid in assessing the interaction of the ground plane with the thin wire.

Figure 12 portrays the percentage change of the resonant frequency of the wire relative to the free-space case as a function of  $h/L$  for three values of the inclination angle  $\beta$ . This is defined as  $(k_0 L - k_{0\infty} L)/k_{0\infty} L \times 100\%$ . It should be noted that the shift of the resonant frequency is a function only of  $\beta$ , not of its constitutive parts,  $\theta$  and  $\phi$ . Figure 13 shows the normalized damping constant  $\tau/\tau_\infty$  for the fundamental mode as a function of  $h/L$  for various values of  $\beta$ . As in Figure 12, the damping constant for the wire in free space,  $\tau_\infty$ , is the normalizing factor. These reference values are calculated to be

$$(\omega_0)_{fs} = 2.939 \times (c/L) \text{ rad/sec}$$

and

$$\tau_\infty = 3.868 \times (c/L) \text{ seconds}$$

Notice that this value of  $\tau_{\infty}$ , when defined in terms of the half-length of the thin-wire scatterer, becomes  $\tau_{\infty} = 7.737 \times (c/(L/2))$  which compares favorably with the free-space damping constant presented in a previous note where the H-field formulation is employed<sup>(5)</sup>.

Figure 14 presents the damping constants as a function of the angle  $\beta$  for various  $h/L$  values, normalized to the damping constant at  $\beta = 90^{\circ}$  for the same  $h/L$  value. In this manner, all of the normalized damping constants go to 1 as  $\beta$  approaches  $90^{\circ}$ . A table of the normalized values of the damping constants is presented along with the curves.

In looking at the behavior of the charge densities at the ends of the scatterer, one quantity of interest is the late time (static) charge,  $\sigma_s$ , and how it varies as a function of  $h/L$ . Figure 15 presents plots of  $\sigma_s/\sigma_{\infty}$  vs.  $h/L$  for various values of the angle  $\beta$ . As in the cases of the resonant frequency and damping constant, the static charge depends only on  $\beta$ , not on  $\theta$  and  $\phi$ . The solid curve represents the behavior of the charge density at  $\xi = 0$  which is the end nearest the ground plane. The dotted curve is for the charge at  $\xi = L$  which is farther away. As expected, the charge at the end near the ground plane is more affected by its presence than is the charge at the far end. Notice that for each value of the angle  $\beta$  considered, there is a minimum value of  $h/L$  which can be considered. At this point, the end of the wire touches the ground plane and the boundary condition that  $I = 0$  at that end is no longer correct.

For the present problem, the condition that  $I = 0$  at the wire ends is assured by the numerical technique used to solve for the current distribution<sup>(3)</sup>. Hence, it is assumed that the thin-wire never comes into contact with the ground plane. In Figures 7 and 11 where  $h/L = .5$  and  $\theta = 90^{\circ}$ , it is to be assumed that the wire does not quite touch the ground plane. In the physical problem, the current at this wire end is not exactly zero due to the finite capacitance between the end-cap of the wire and its image. As the wire end gets very close to the ground plane, this end-cap effect may give rise to substantial errors. A more rigorous account of this effect can be made in a manner similar to that used in reference (6).

Another quantity of interest involving the charge density is the ratio of the maximum charge density in the time domain for the wire near the ground

plane, relative to the same quantity for the wire in free space with the incident E field parallel to the wire. This quantity is often referred to as the field enhancement factor at the ends of the wire. In figure 16, this ratio  $\sigma_m/\sigma_m(90^\circ, \infty)$  is plotted as a function of  $h/L$  for various combinations of  $\theta$  and  $\phi$ . Note that this plot is for the end of the scatterer nearest the ground plane ( $\xi = 0$ ). The variation of the charge at the opposite end with  $h/L$  was so small that the results were not plotted. For reference, it is noted that the normalizing factor in these curves has the value

$$\sigma_m(90^\circ, \infty) = 1.72 \times (\epsilon_0 E_0 L) \text{ Coulombs/meter.}$$

From the data presented in the previously described curves, it is seen that for this thin scatterer, the effect of the perfectly conducting ground plane on the charge densities is almost negligible if the height is such that  $h/L > 1$ . The variation in the resonant frequency and damping constant, however, is more pronounced.

It is interesting to compare the results presented here with those given in another reference<sup>(6)</sup> where the scattering properties of a thicker cylinder are considered. In that note, the thick cylinder was located at  $\theta = 90^\circ$ ,  $\phi = 0^\circ$  above a perfectly conducting ground plane and studies of its behavior as a function of height above the ground were made. In that case, the effects of the end-caps of the cylinder are not neglected as in the present analysis. Indeed, they are quite important in accounting for the coupling between the cylinder and its image. It is seen from that analysis that the general trends in the damping constants, field enhancement factors, etc., are roughly similar to those presented here for the  $\theta = 90^\circ$  case.

## VI. Summary

Using the electric field Pocklington integro-differential equation for the induced currents on a thin wire scatterer between two parallel plates, the special case of one plate being at infinity is considered. In this way, the two doubly infinite summations occurring in the Green's function for the parallel plate case reduce to simply two terms. The resulting equation is then solved numerically and plots of the frequency and time domain behavior of the induced currents at three points on the wire are presented for varying wire orientations. Similarly, plots of the charge densities at both ends of the wire are presented. Summary curves showing the behavior of the fundamental resonant frequency and corresponding damping constant as functions of the wire orientation are given, and a study of the late time behavior of the charge density is carried out. The field enhancement factor at the wire end nearest the ground plane is also studied. For practical purposes, it is seen that for  $h/L > 1$ , the thin-wire structure can be regarded as being located in free space, since the interaction between the wire and the plane is small.

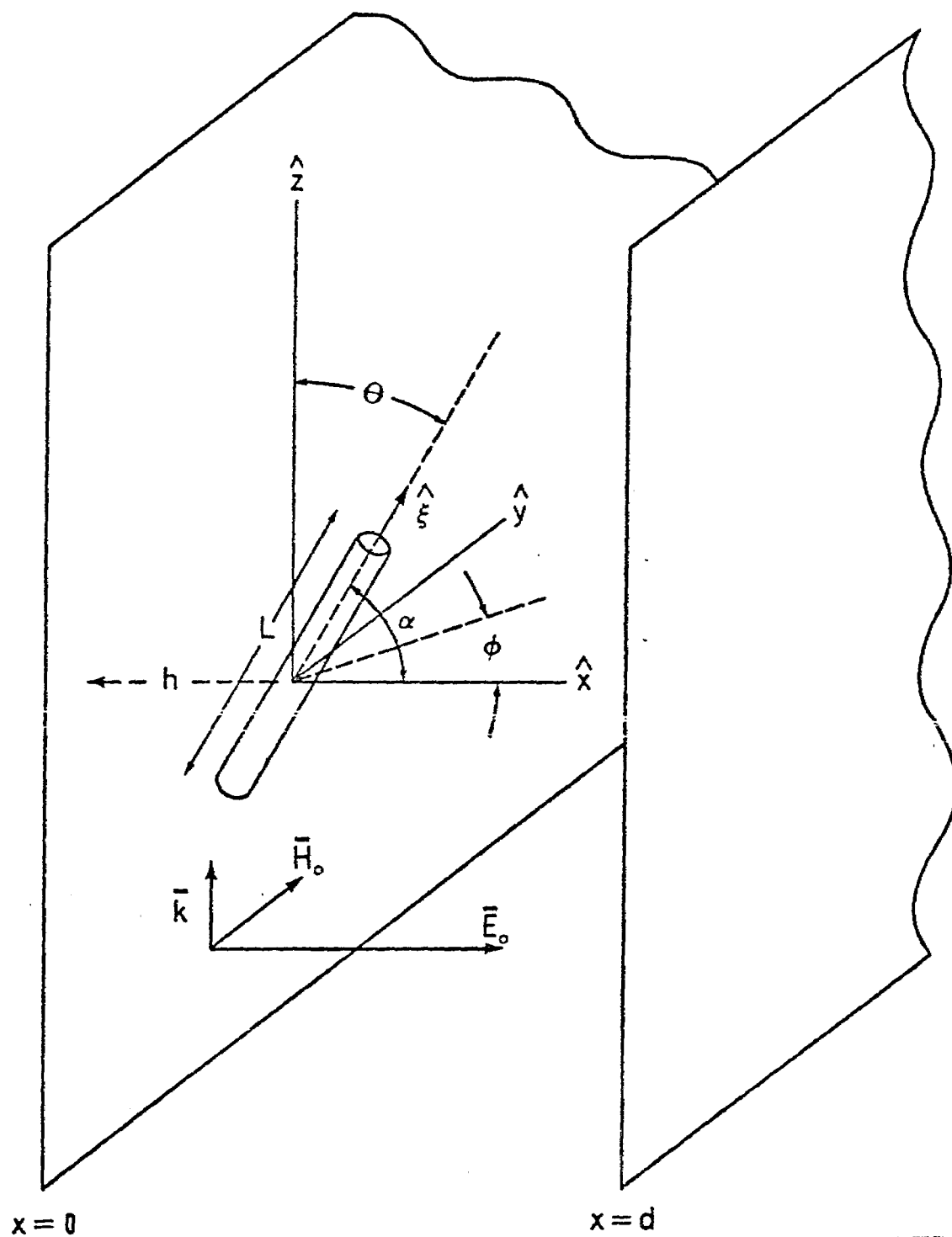


Figure 1. Geometry of the general scattering problem involving a thin-wire element within a parallel plate region. The wire radius is  $a$ .

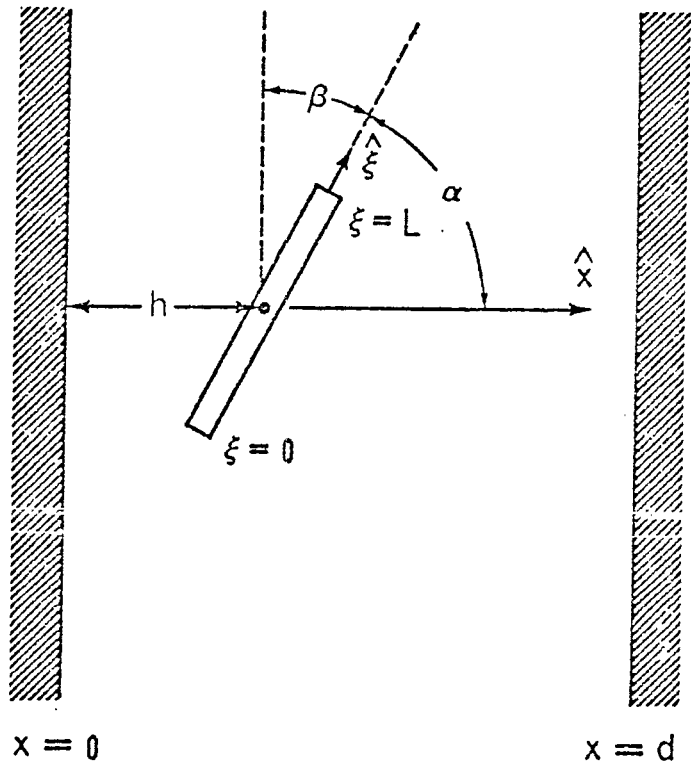


Figure 2. View of the scattering element from a plane perpendicular to the two parallel plates and containing the thin-wire element of radius  $a$ .

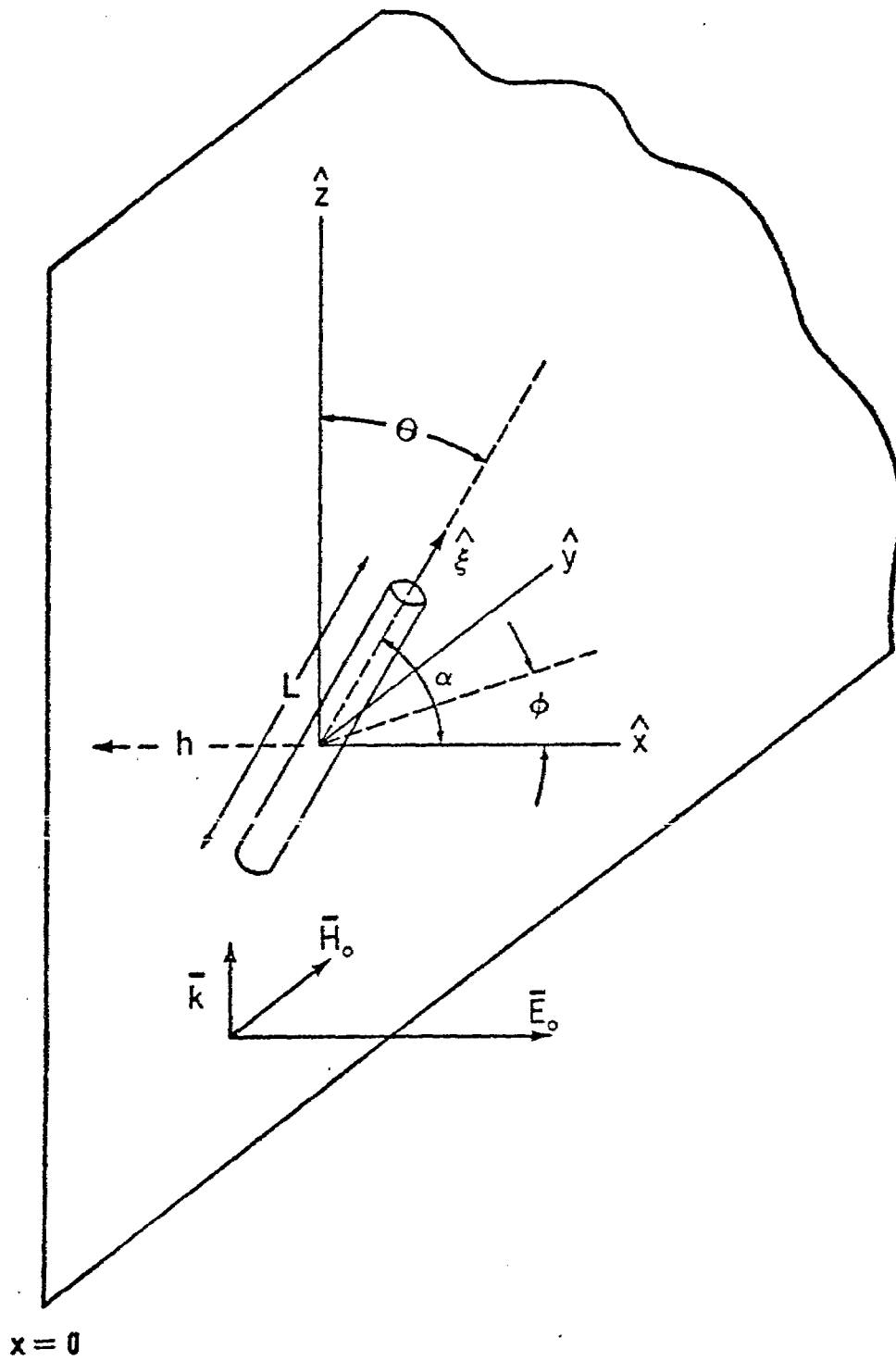


Figure 3. The resulting scattering problem obtained by letting  $d$  approach infinity.

In order to summarize the different combinations of parameters for which numerical data are presented in Figures 4 - 11, the following table is provided.

FIGURE	h/L	$\theta$	$\phi$
4	100.0	$90^\circ$	$0^\circ, 30^\circ, 60^\circ$
5	1.0	$90^\circ$	$0^\circ, 30^\circ, 60^\circ$
6	.75	$90^\circ$	$0^\circ, 30^\circ, 60^\circ$
7	.50	$90^\circ$	$0^\circ, 30^\circ, 60^\circ$
8	100.0	$90^\circ, 60^\circ, 30^\circ$	$0^\circ$
9	1.0	$90^\circ, 60^\circ, 30^\circ$	$0^\circ$
10	.75	$90^\circ, 60^\circ, 30^\circ$	$0^\circ$
11	.50	$90^\circ, 60^\circ, 30^\circ$	$0^\circ$

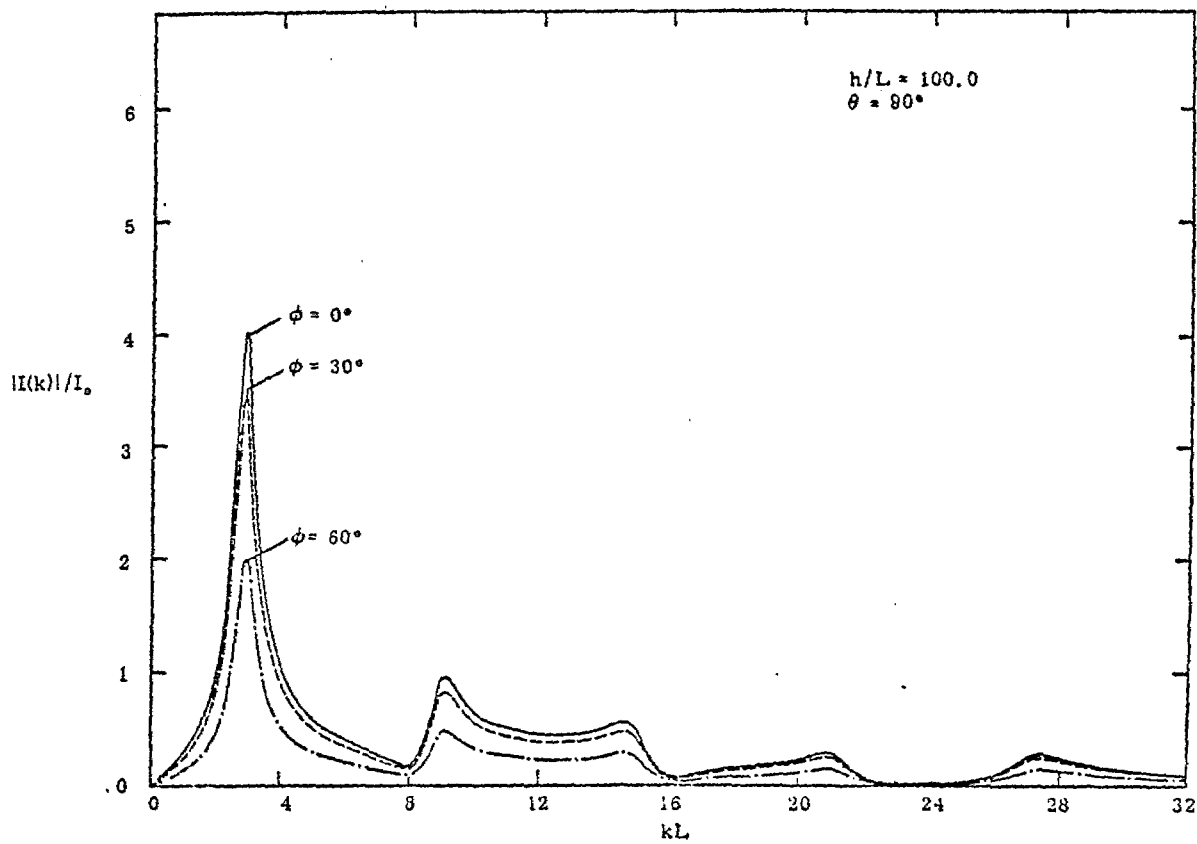


Figure 4a. Magnitude of the impulse spectrum of the current observed at the point  $\xi = .25L$ .

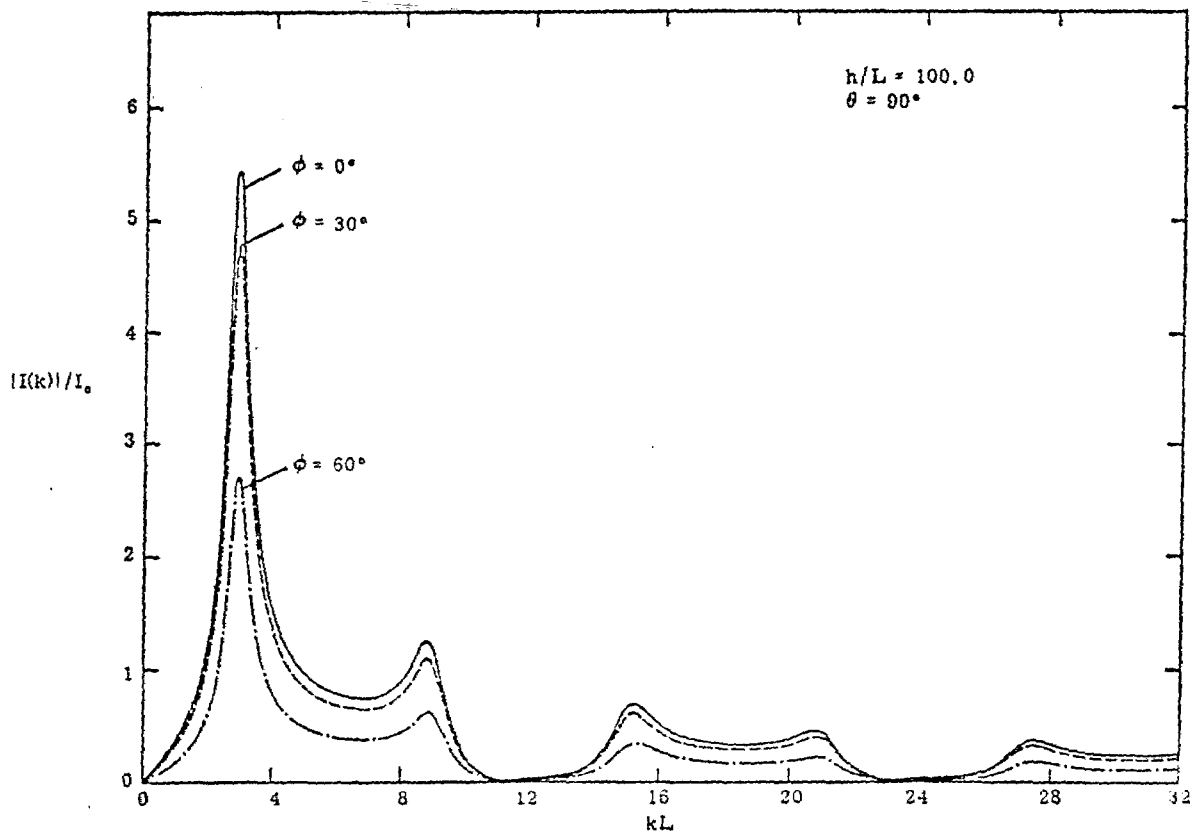


Figure 4b. Magnitude of the impulse spectrum of the current observed at the point  $\xi = .5L$ .

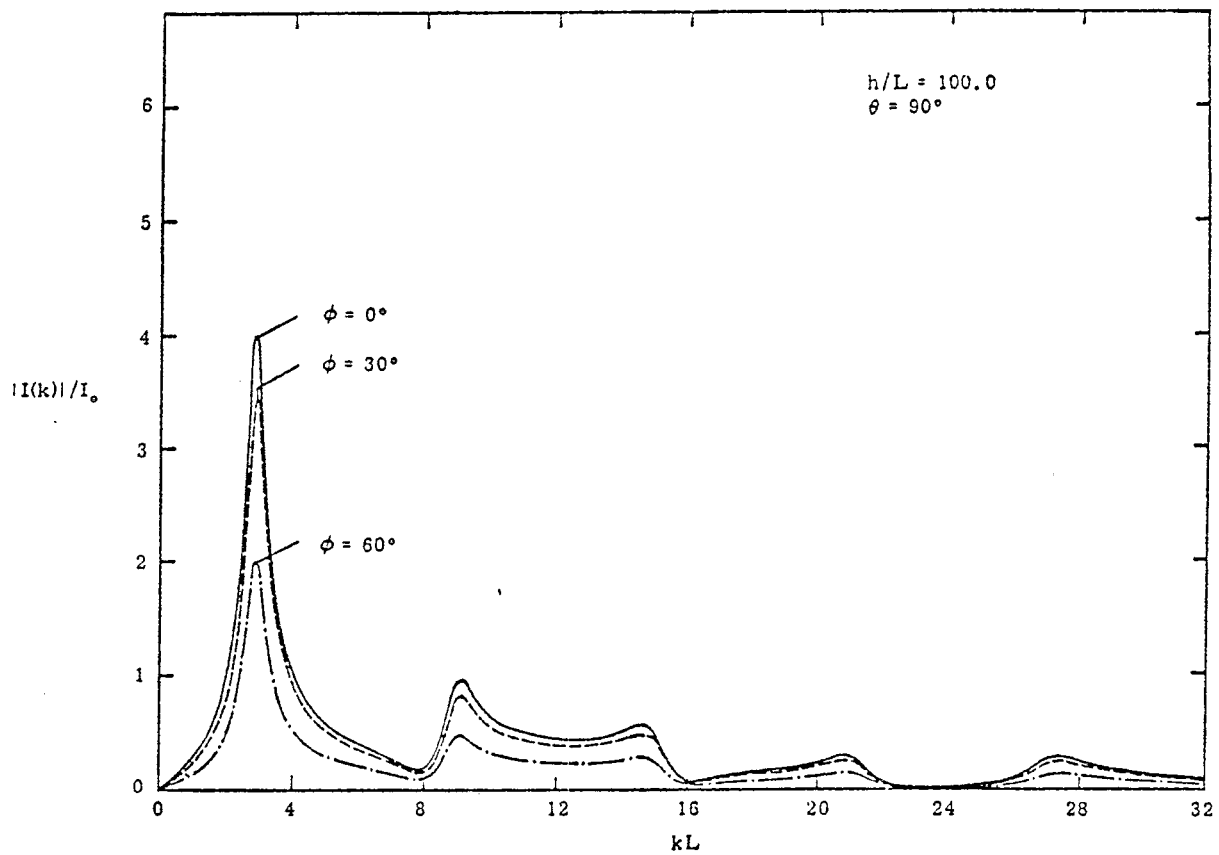


Figure 4c. Magnitude of the impulse spectrum of the current observed at the point  $\xi = .75L$ .

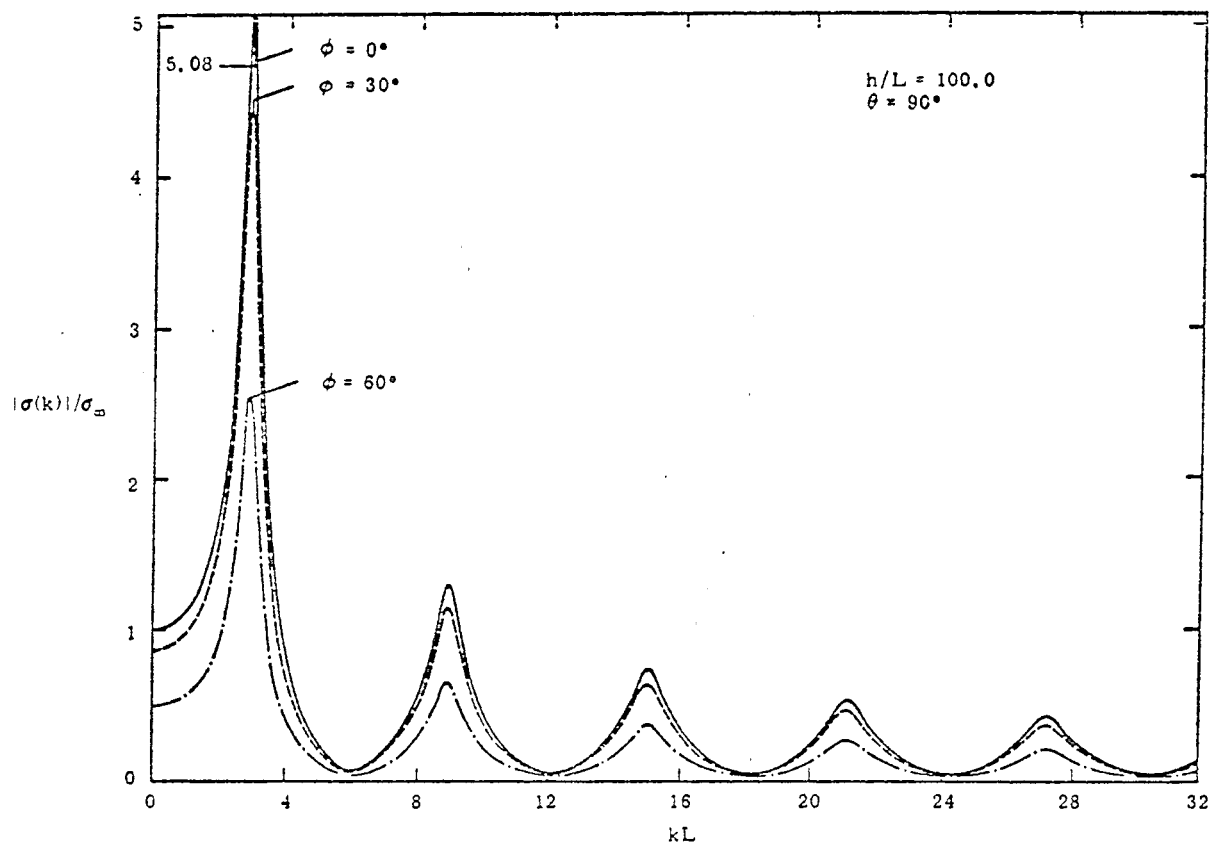


Figure 4d. Magnitude of the impulse spectrum of the linear charge density observed at the point  $\xi = 0$ .

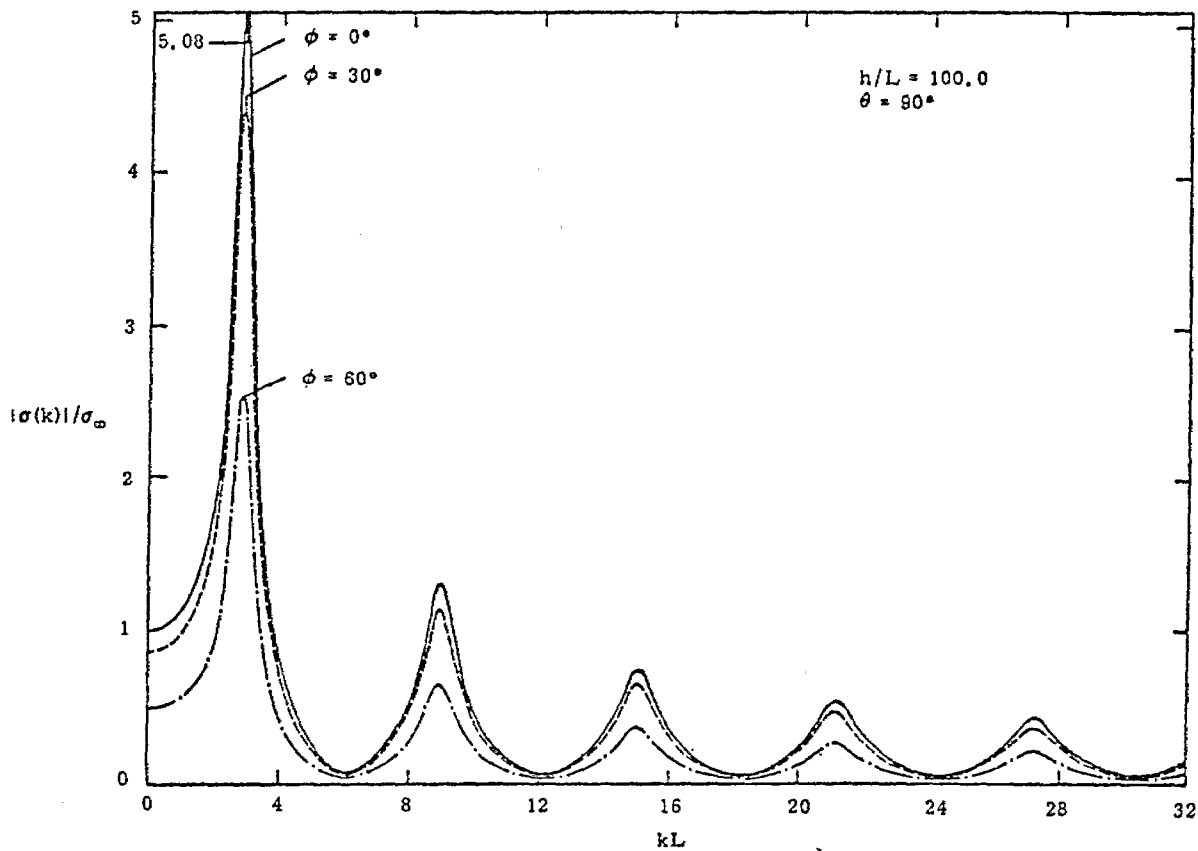


Figure 4e. Magnitude of the impulse spectrum of the linear charge density observed at the point  $\xi = L$ .

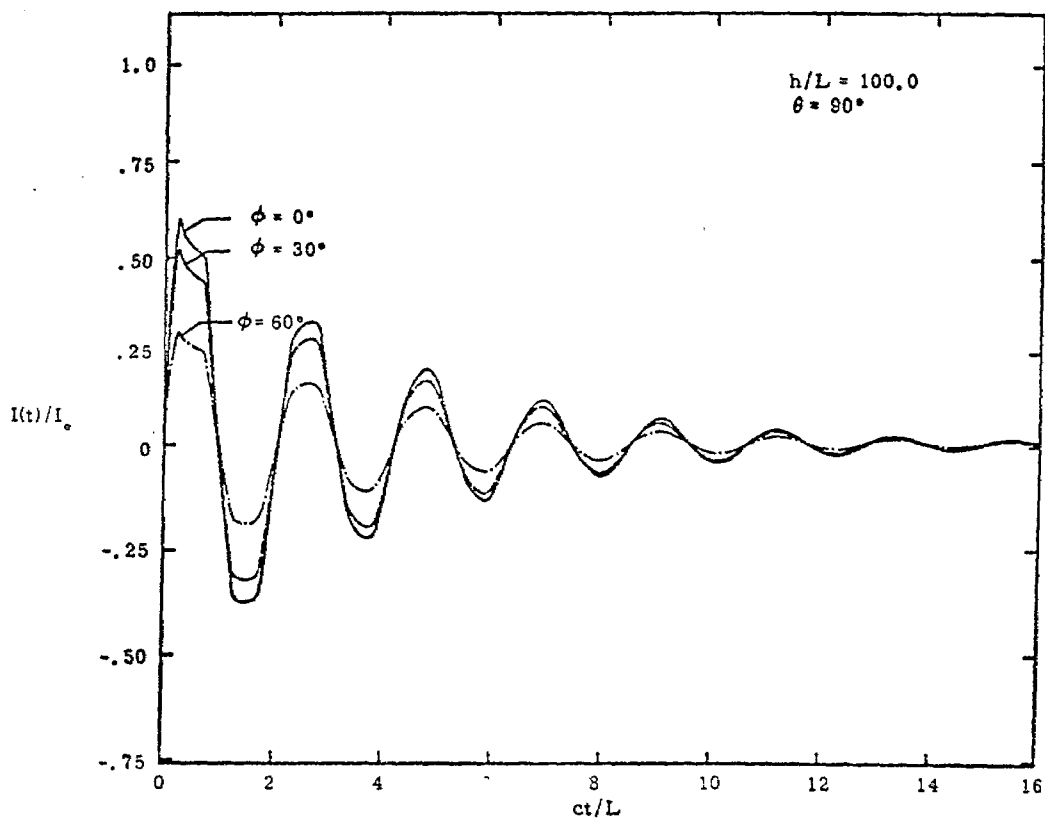


Figure 4f. Time response of the current at  $\xi = .25L$  for an incident step wave.

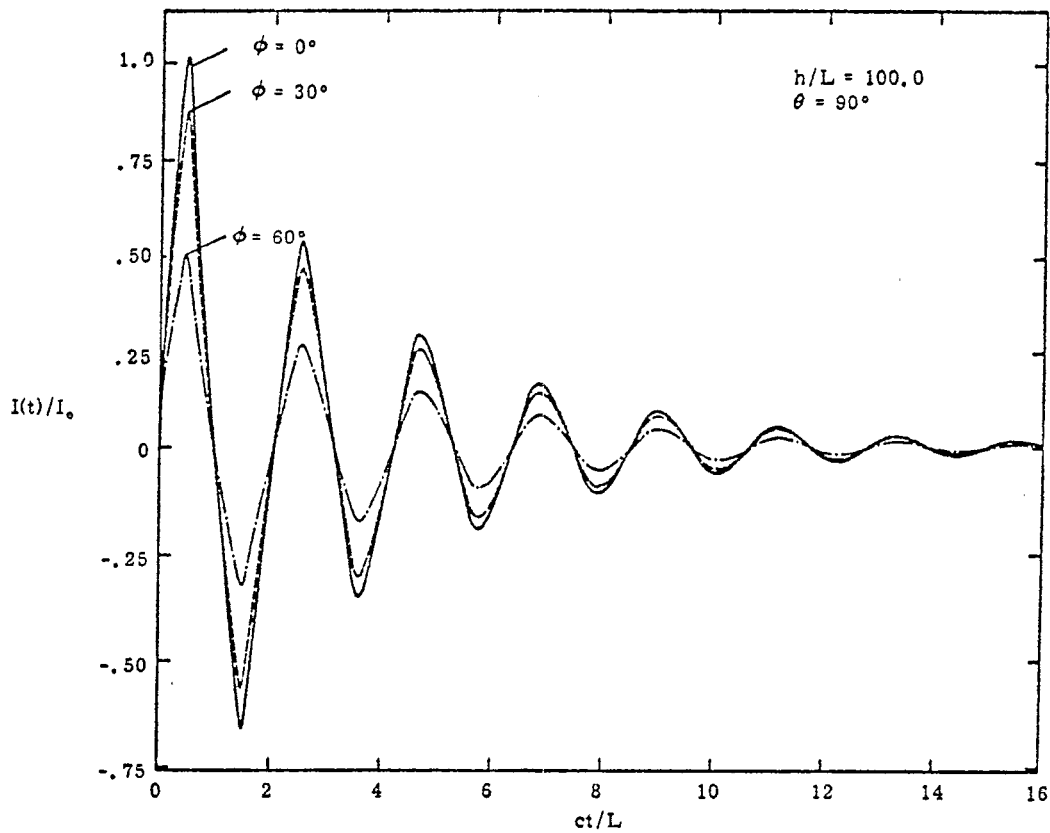


Figure 4g. Time response of the current at  $\xi = .5L$  for an incident step wave.

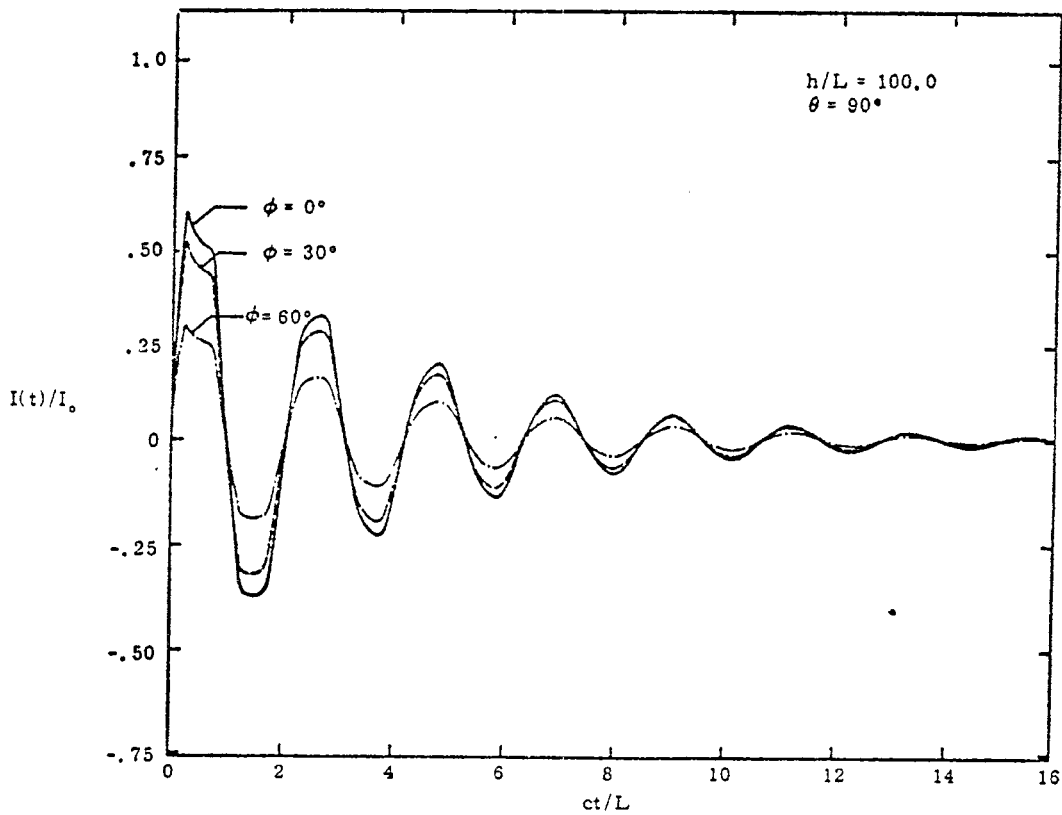


Figure 4h. Time response of the current at  $\xi = .75L$  for an incident step wave.

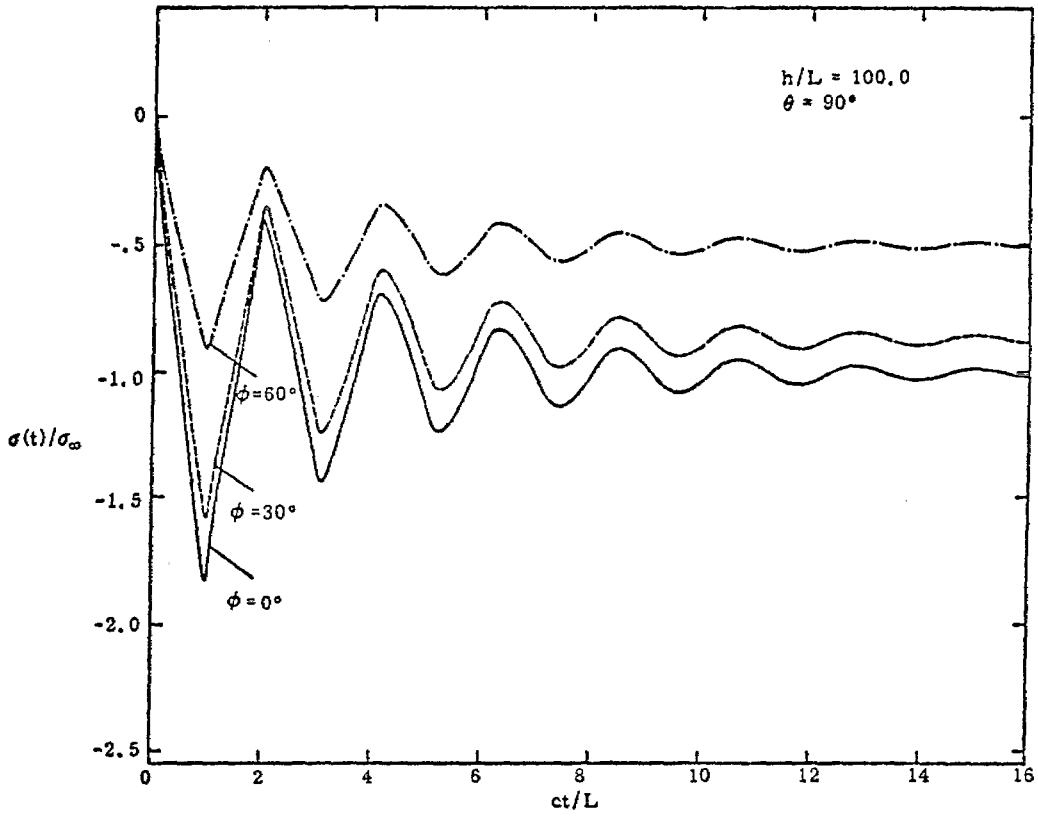


Figure 4i. Time response of the charge density at  $\xi = 0$  for an incident step wave.

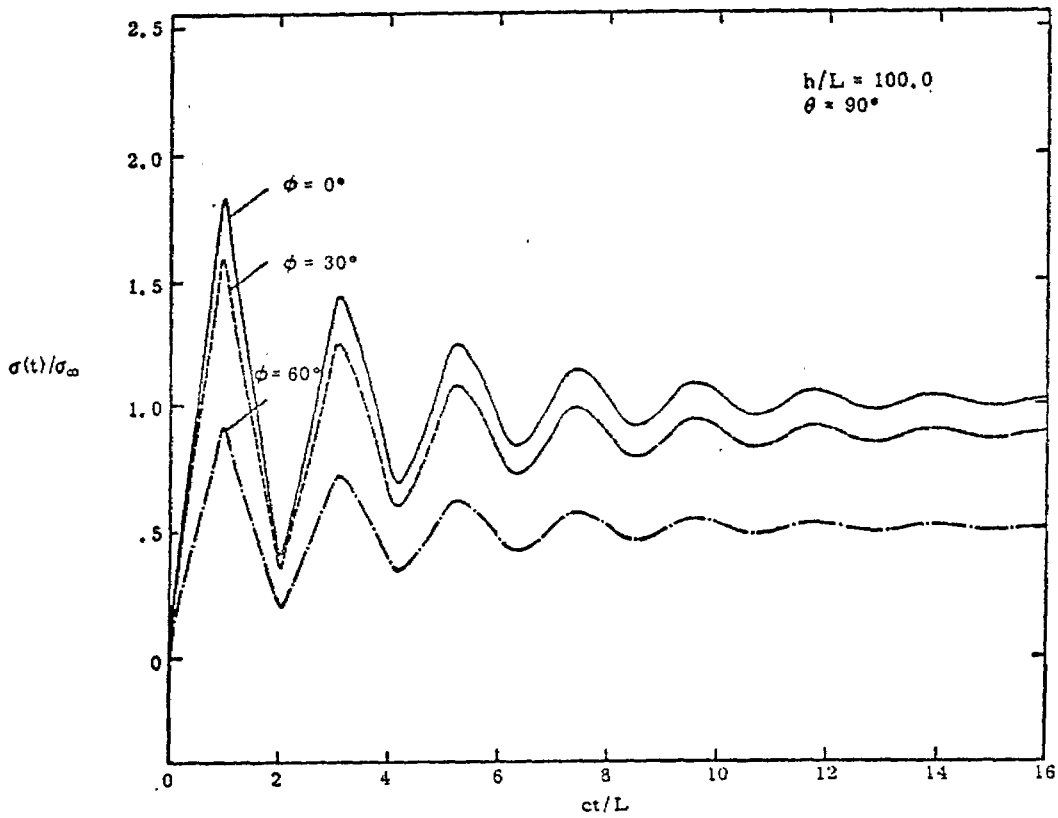


Figure 4j. Time response of the charge density at  $\xi = L$  for an incident step wave.

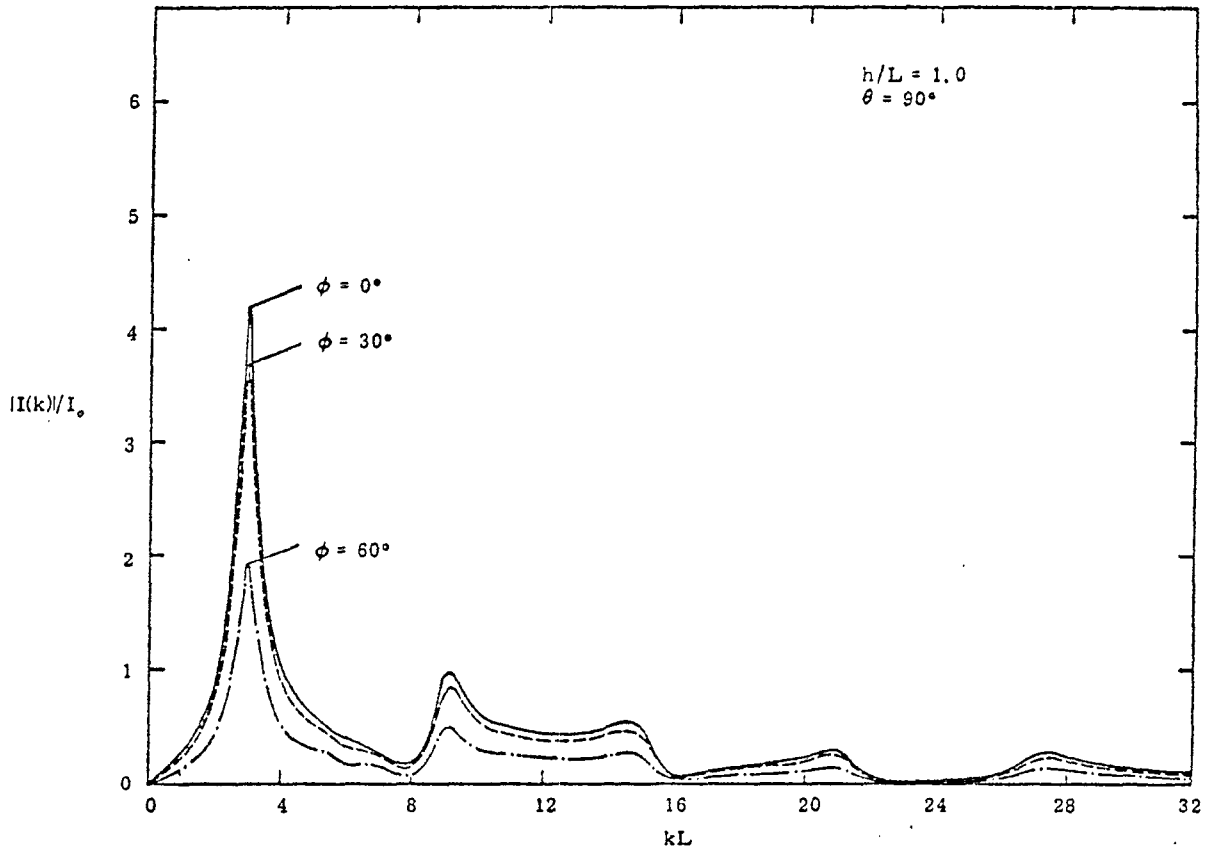


Figure 5a. Magnitude of the impulse spectrum of the current observed at the point  $\xi = .25L$ .

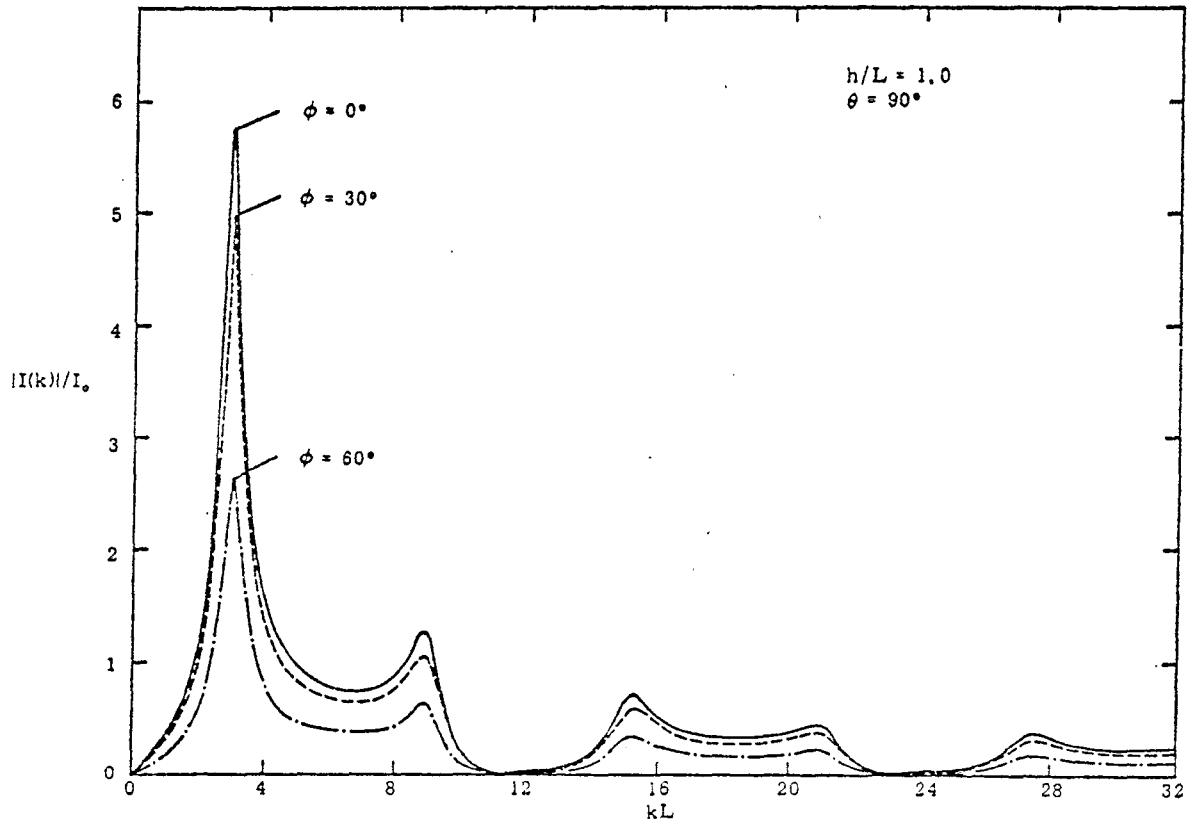


Figure 5b. Magnitude of the impulse spectrum of the current observed at the point  $\xi = .5L$ .

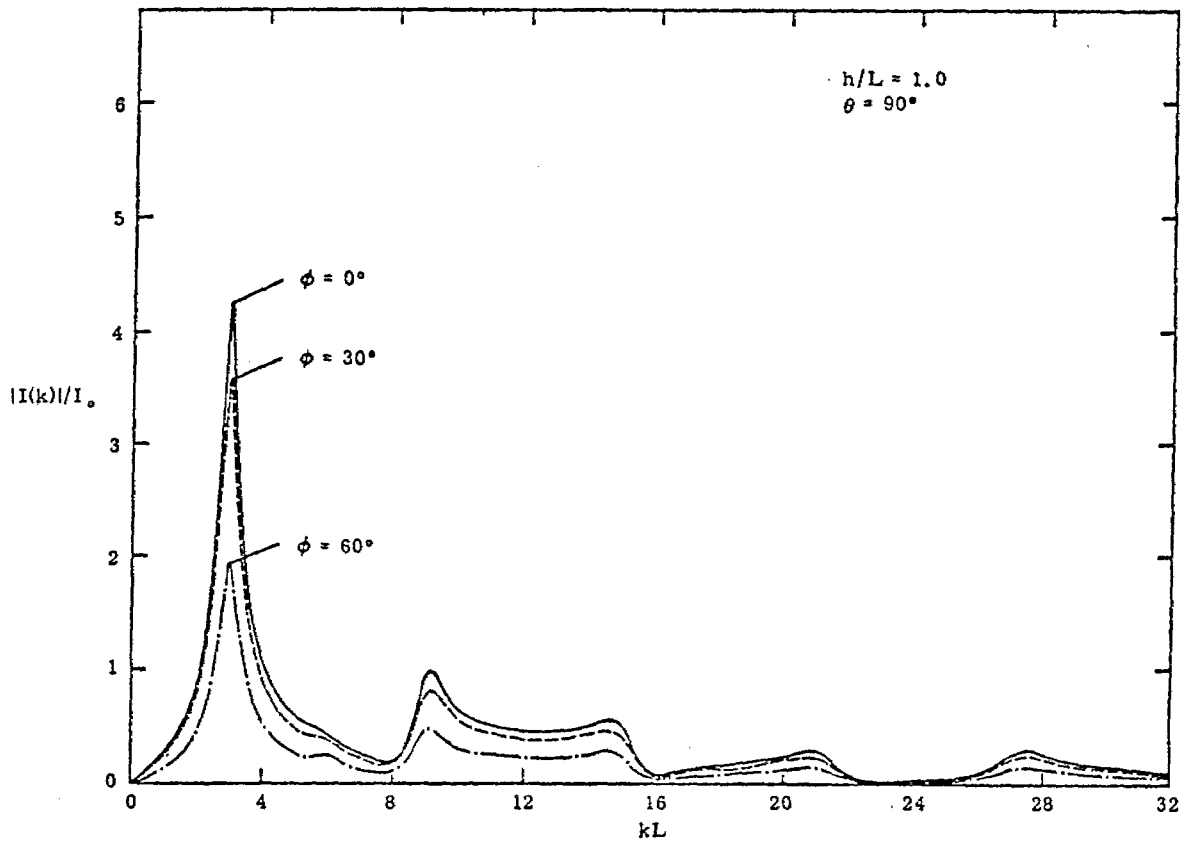


Figure 5c. Magnitude of the impulse spectrum of the current observed at the point  $\xi = .75L$ .

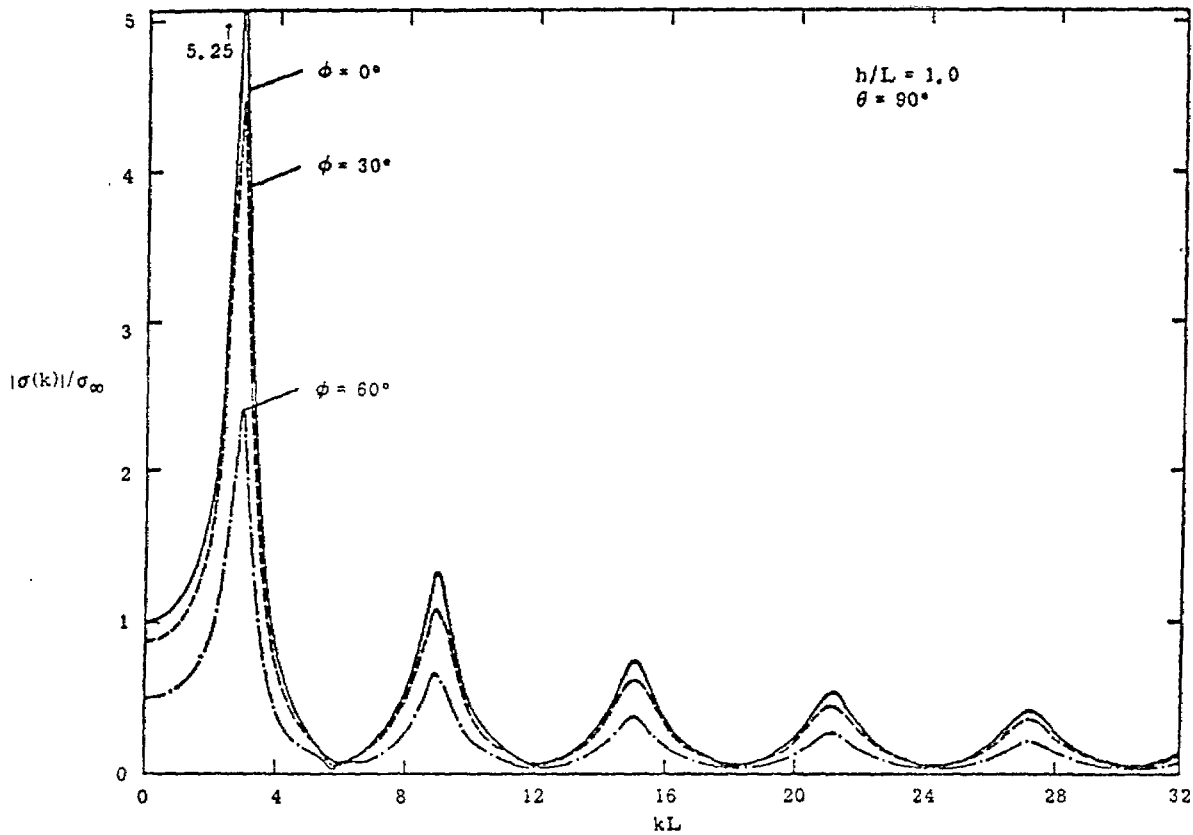


Figure 5d. Magnitude of the impulse spectrum of the linear charge density observed at the point  $\xi = 0$ .

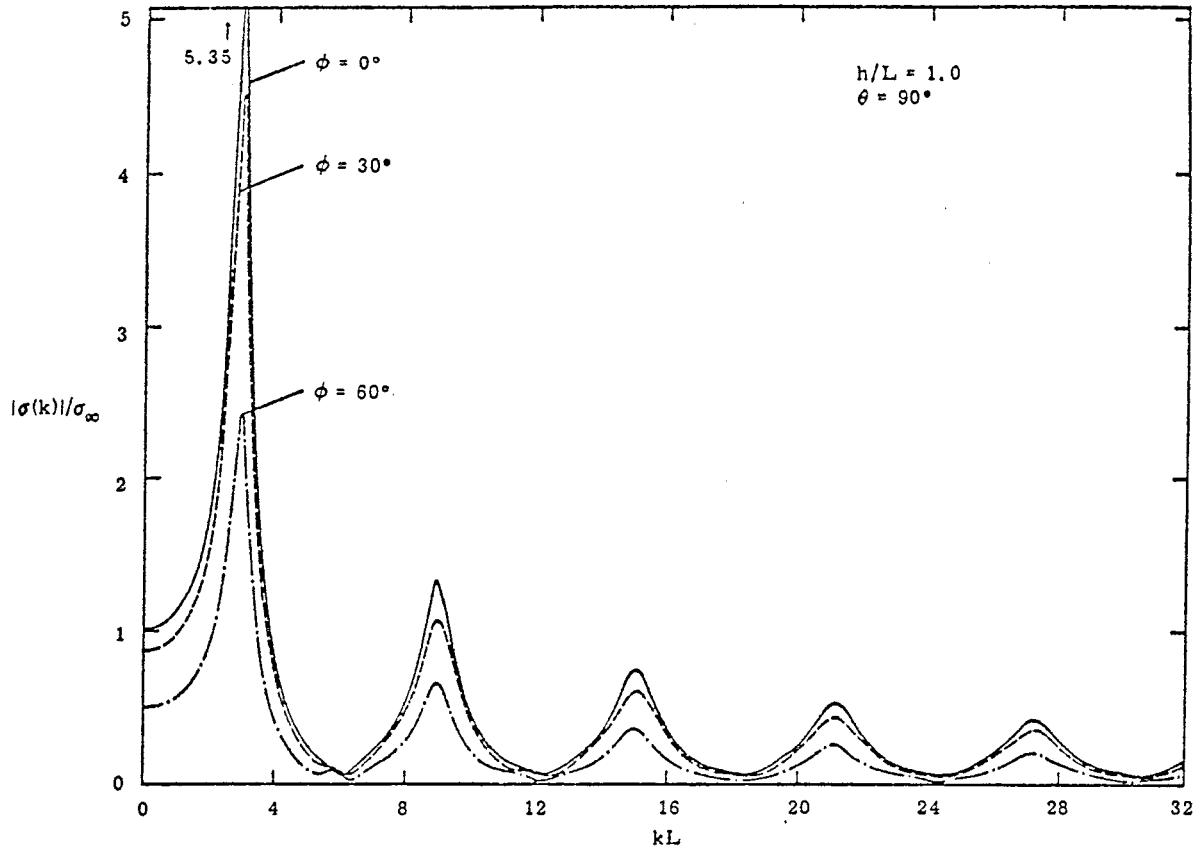


Figure 5e. Magnitude of the impulse spectrum of the linear charge density observed at the point  $\xi = L$ .

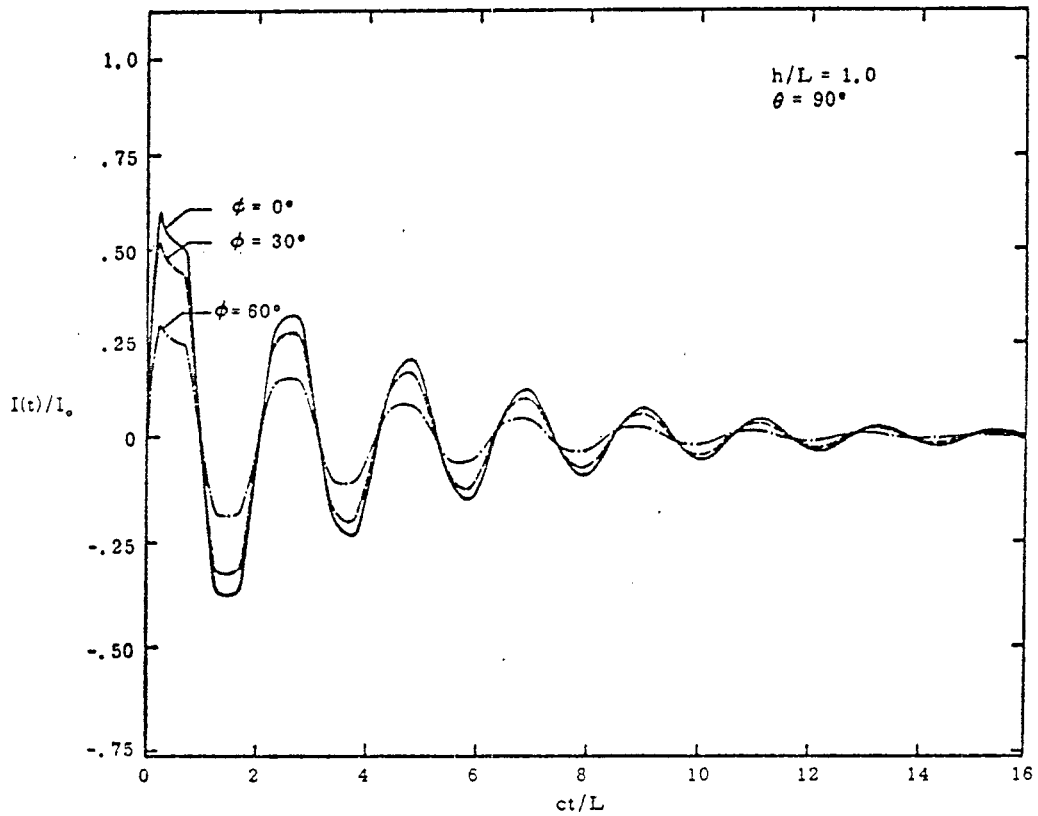


Figure 5f. Time response of the current at  $\xi = .25L$  for an incident step wave.

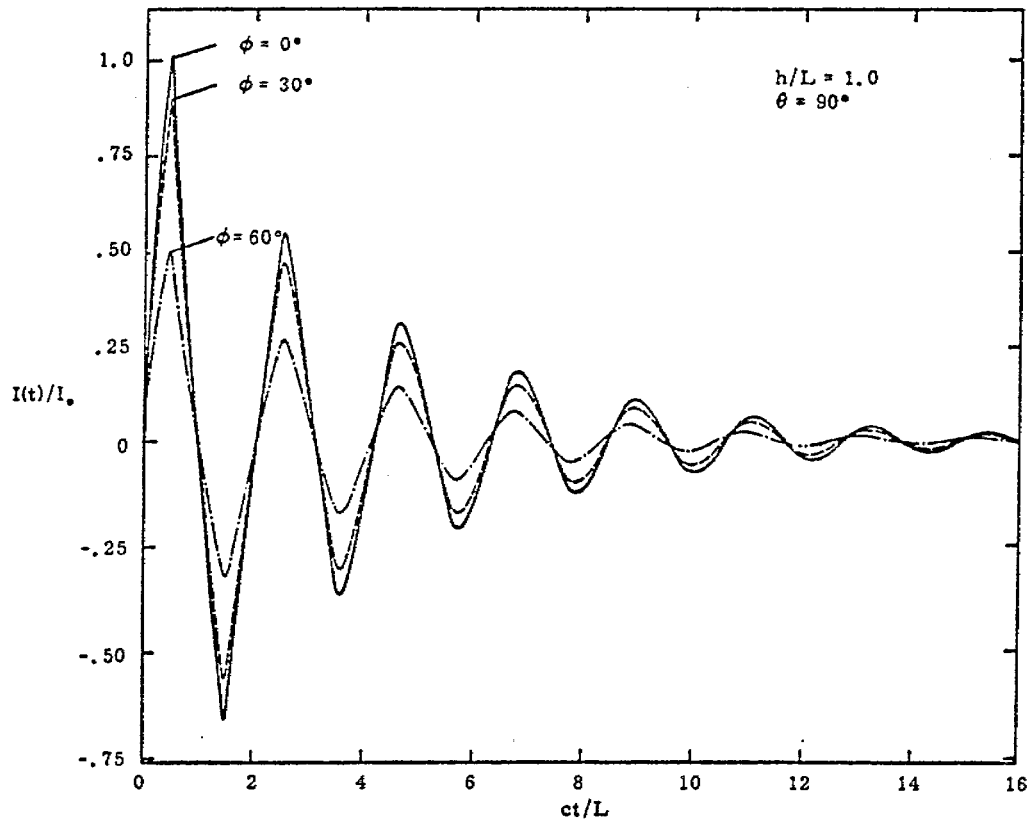


Figure 5g. Time response of the current at  $\xi = .5L$  for an incident step wave.

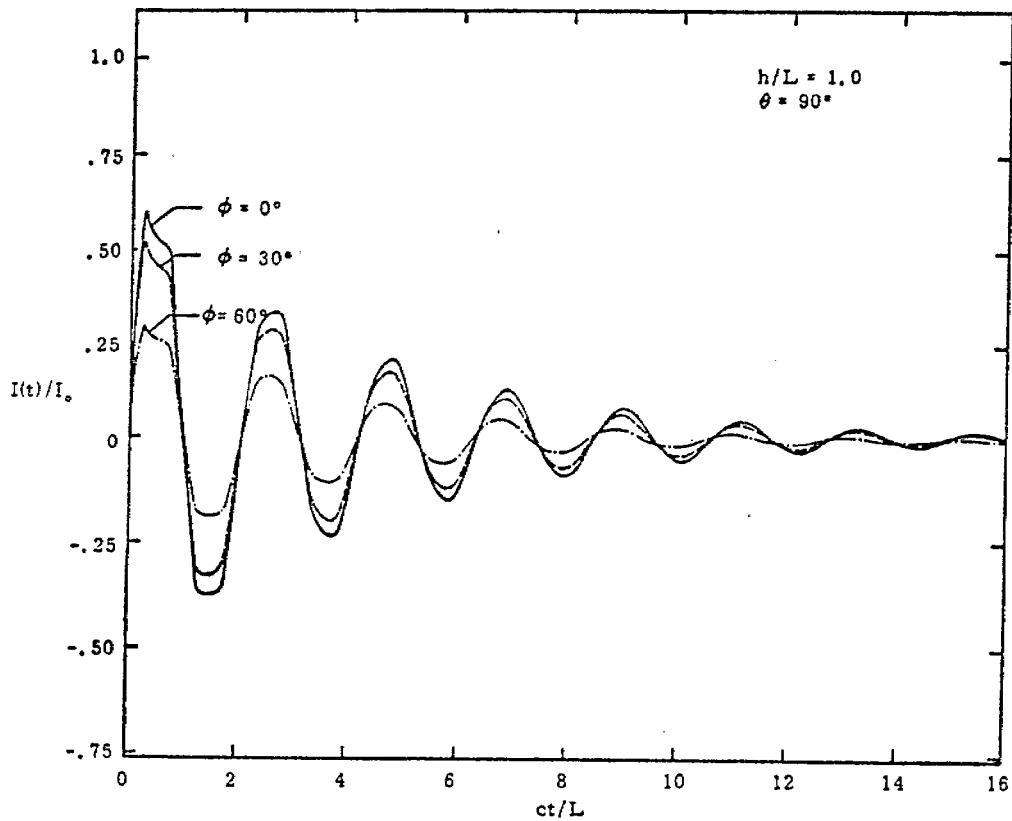


Figure 5h. Time response of the current at  $\xi = .75L$  for an incident step wave.

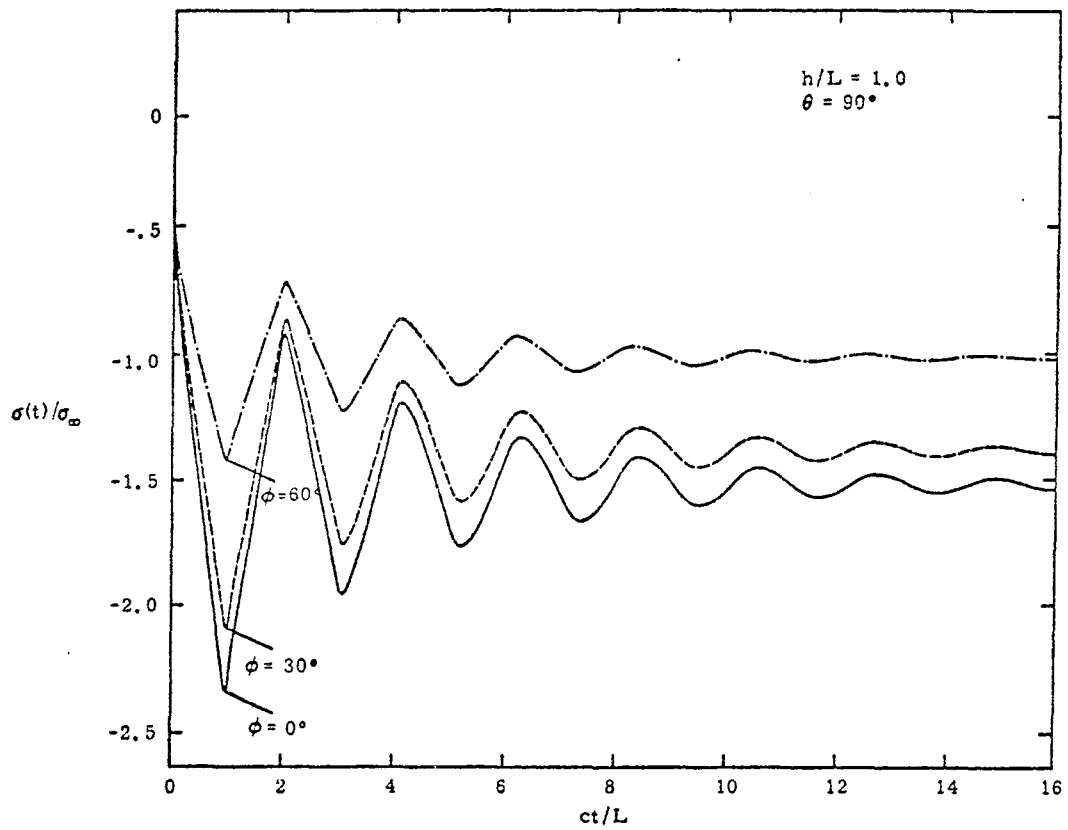


Figure 5i. Time response of the charge density at  $\xi = 0$  for an incident step wave.

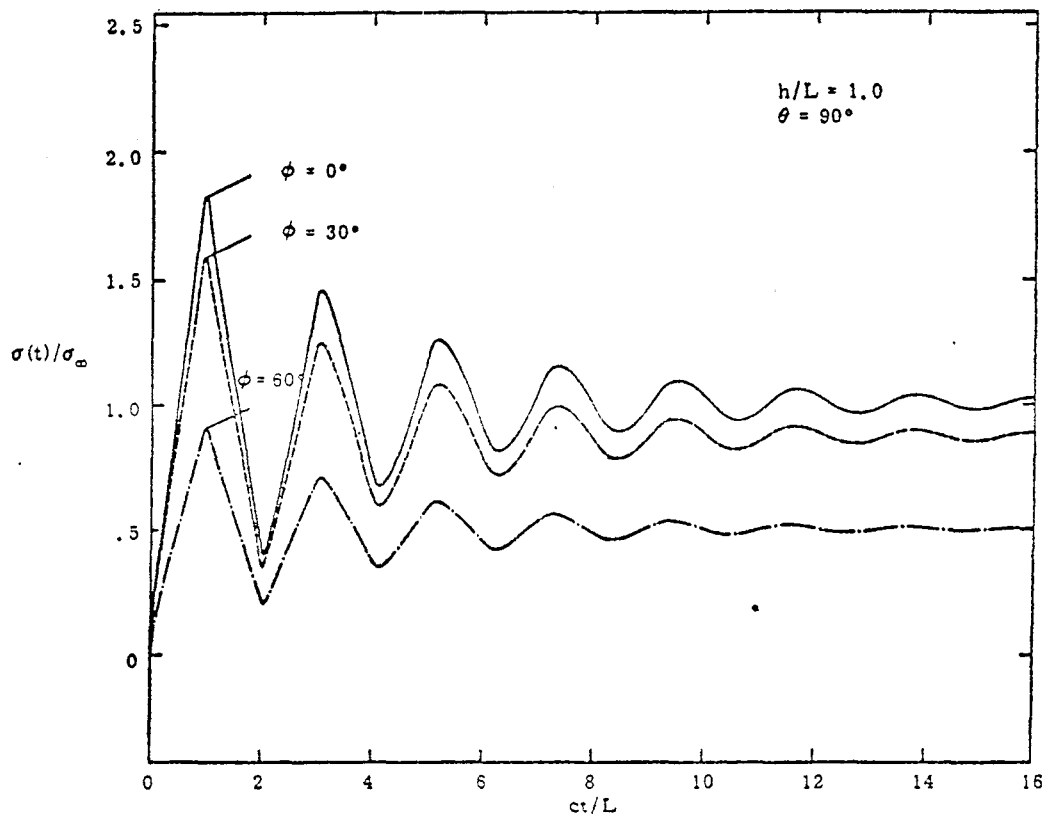


Figure 5j. Time response of the charge density at  $\xi = L$  for an incident step wave.

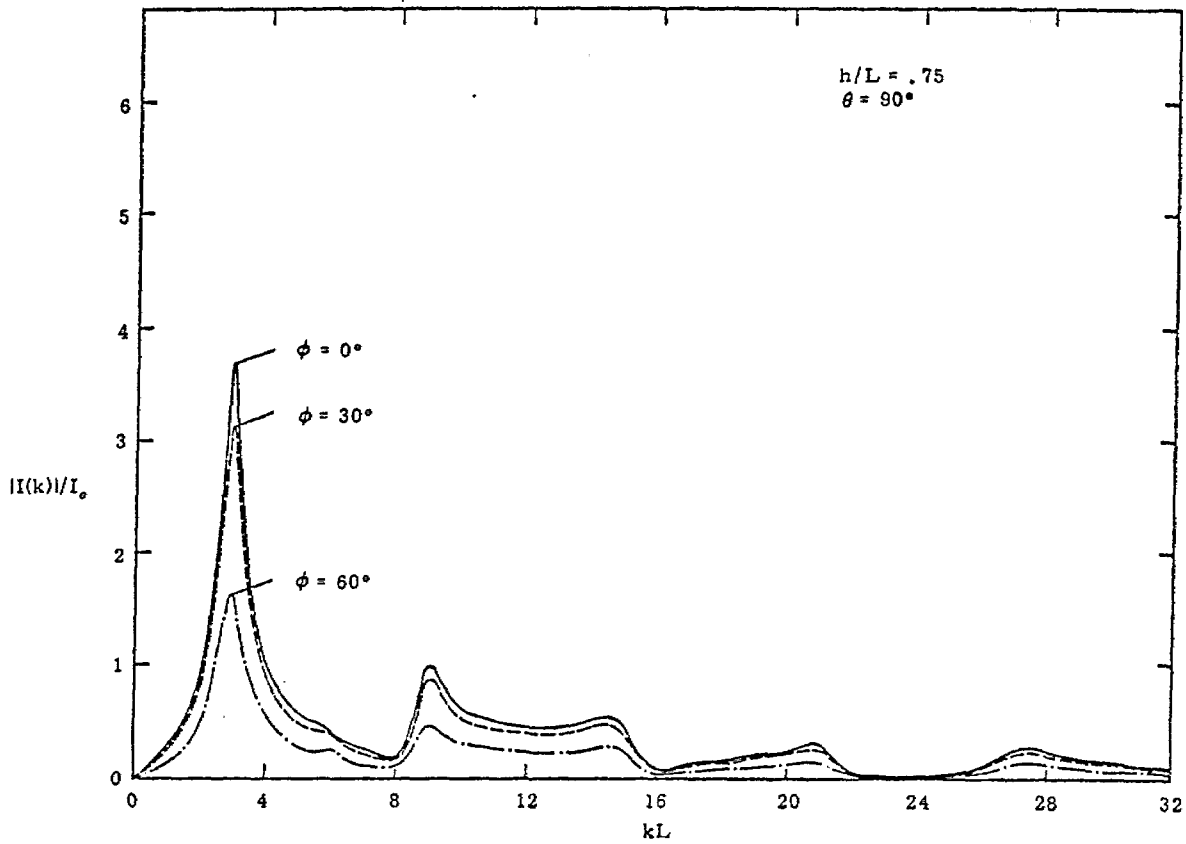


Figure 6a. Magnitude of the impulse spectrum of the current observed at the point  $\xi = .25L$ .

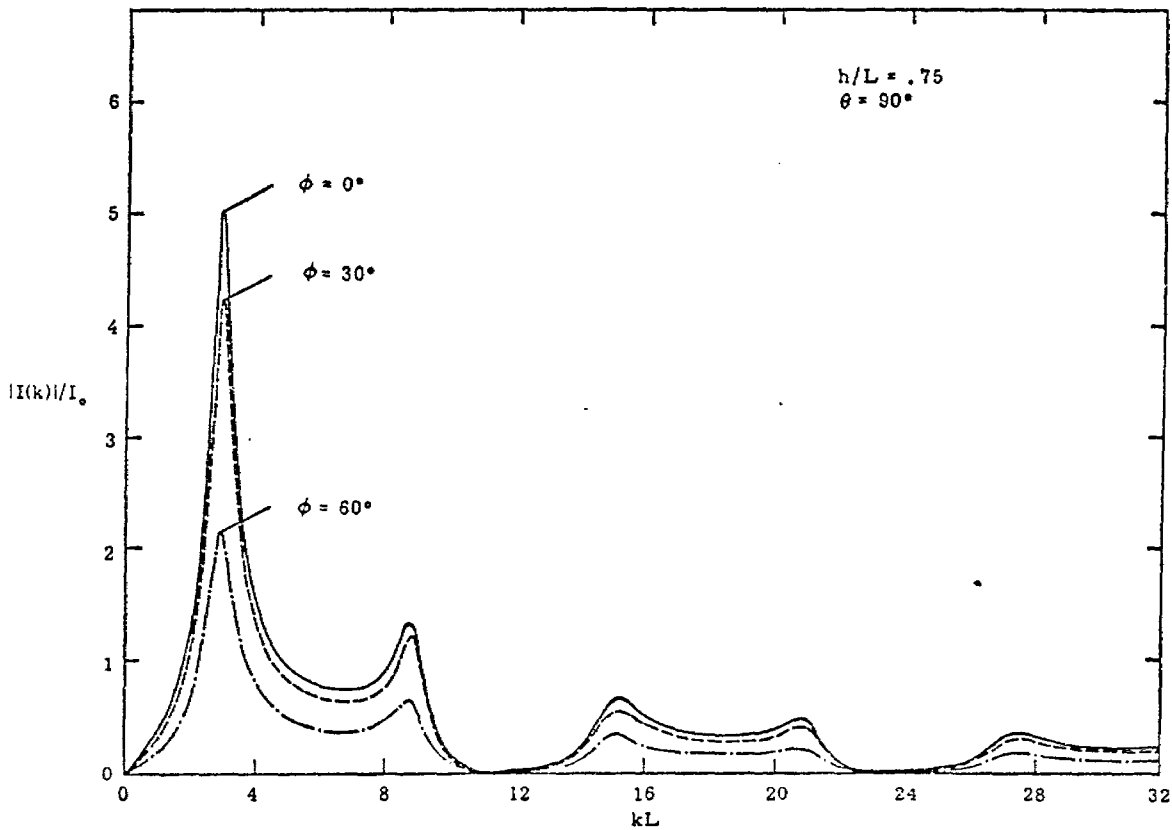


Figure 6b. Magnitude of the impulse spectrum of the current observed at the point  $\xi = .5L$ .

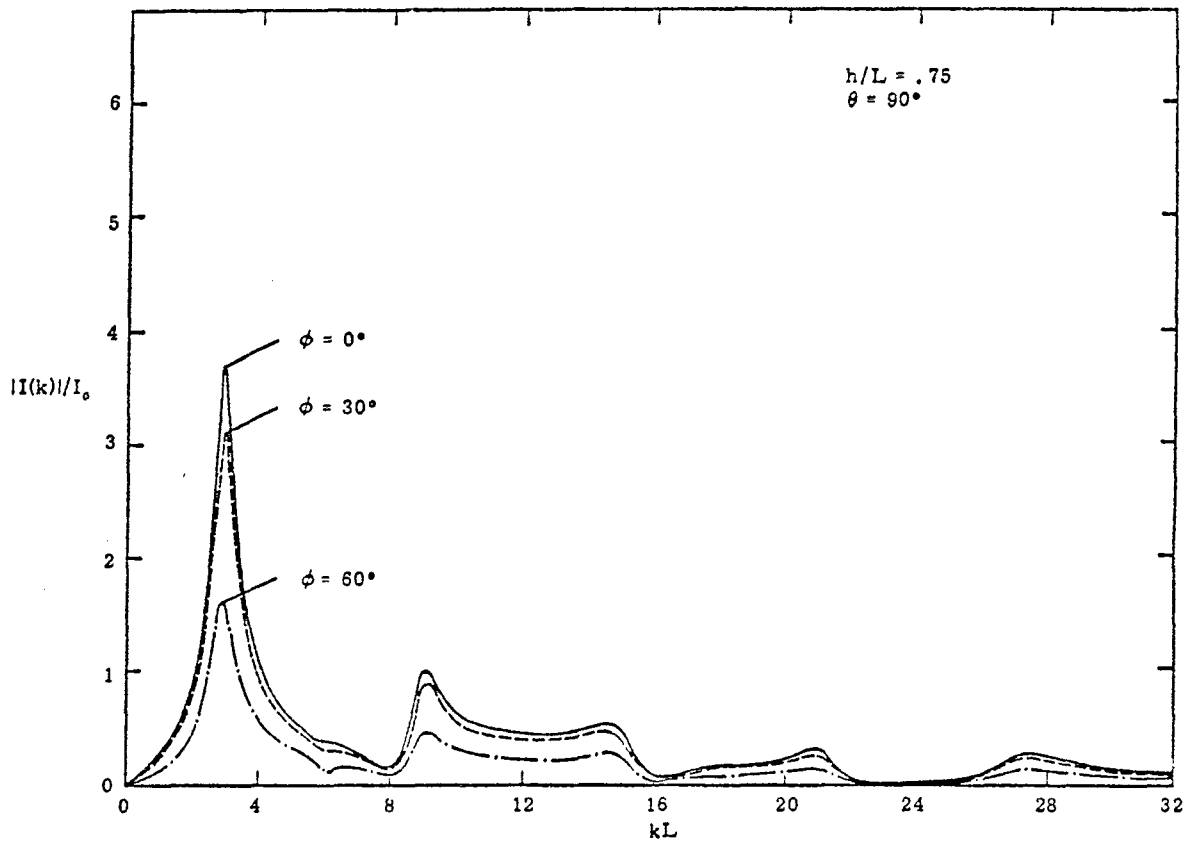


Figure 6c. Magnitude of the impulse spectrum of the current observed at the point  $\xi = .75L$ .

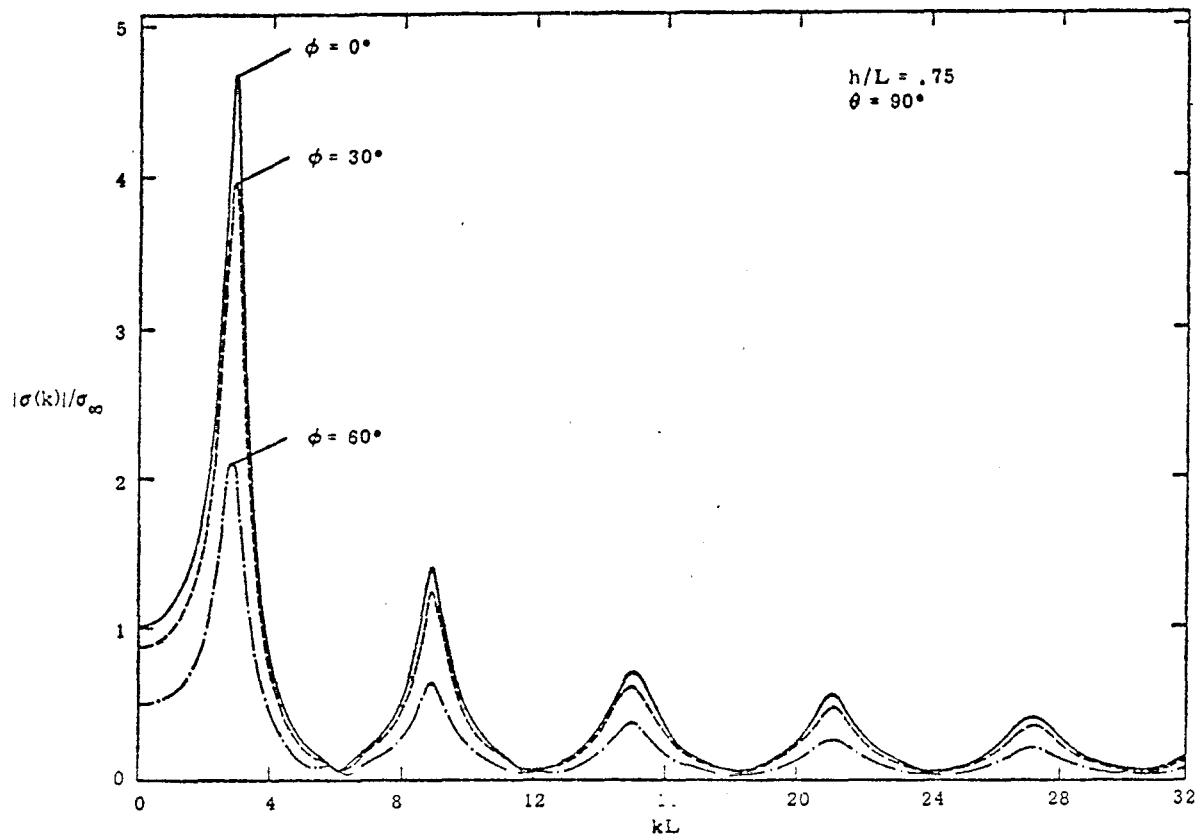


Figure 6d. Magnitude of the impulse spectrum of the linear charge density observed at the point  $\xi = 0$ .

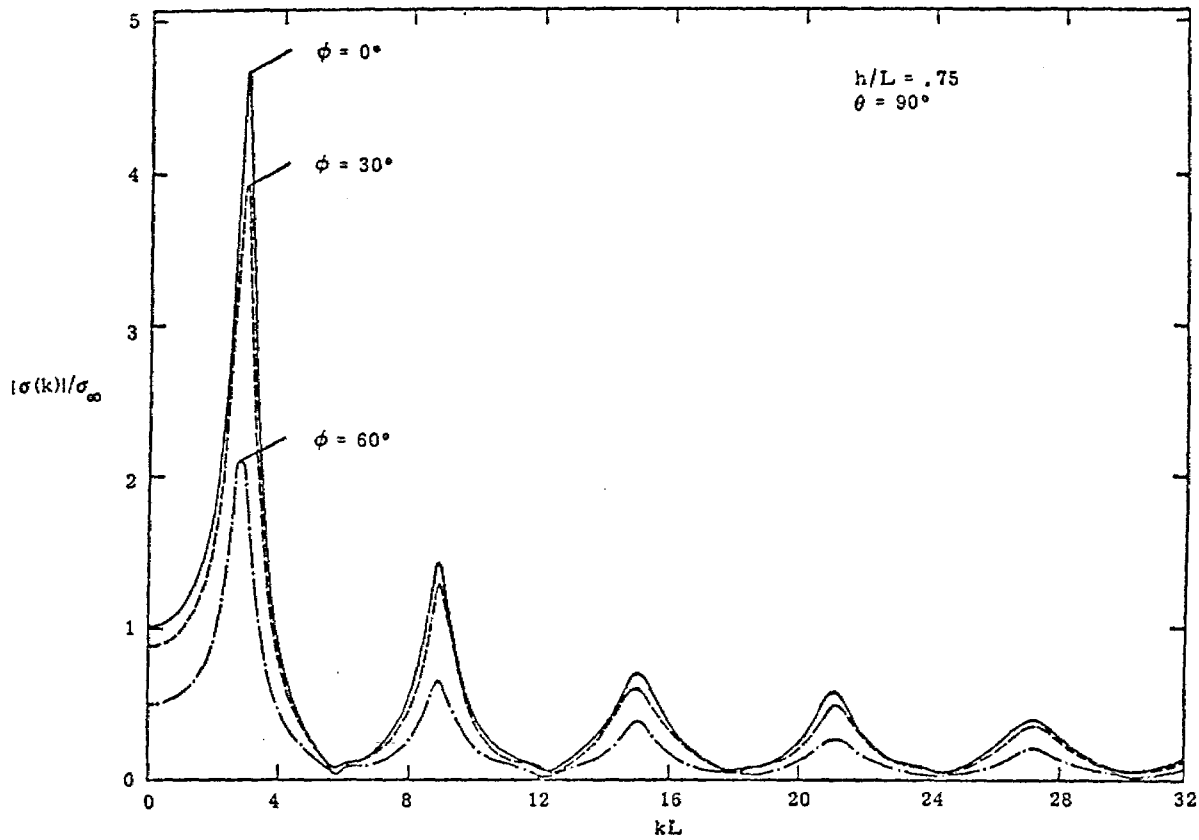


Figure 6e. Magnitude of the impulse spectrum of the linear charge density observed at the point  $\xi = L$ .

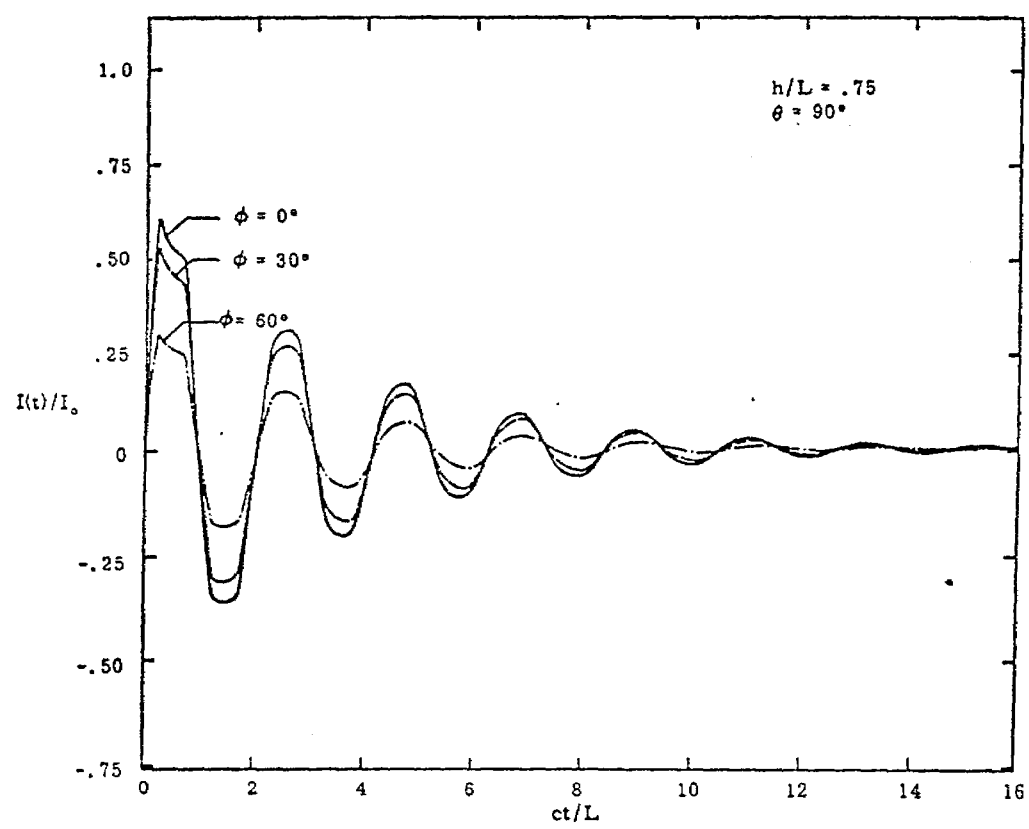


Figure 6f. Time response of the current at  $\xi = .25L$  for an incident step wave.

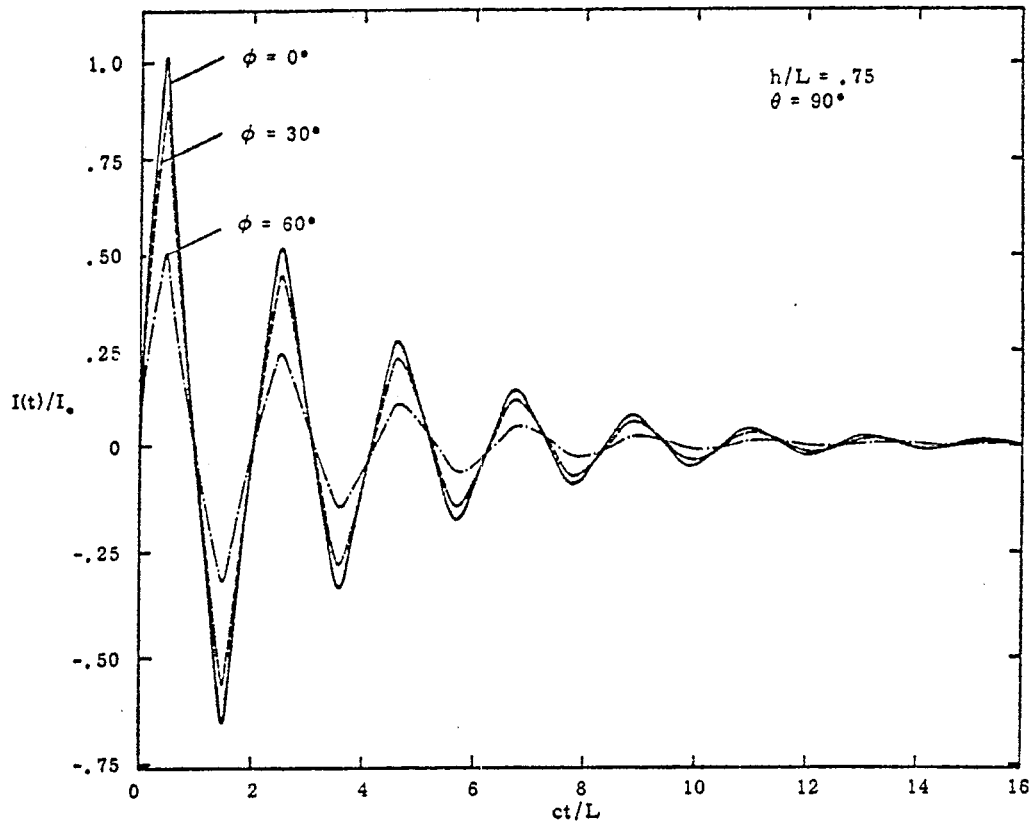


Figure 6g. Time response of the current at  $\xi = .5L$  for an incident step wave.

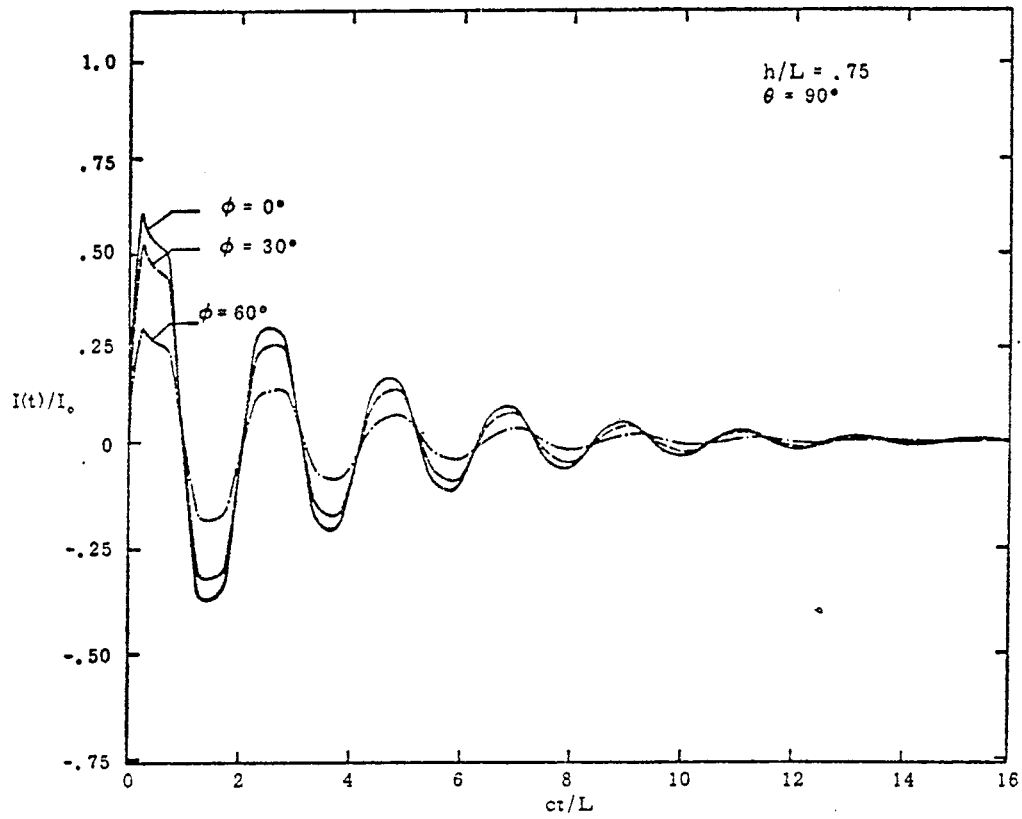


Figure 6h. Time response of the current at  $\xi = .75L$  for an incident step wave.

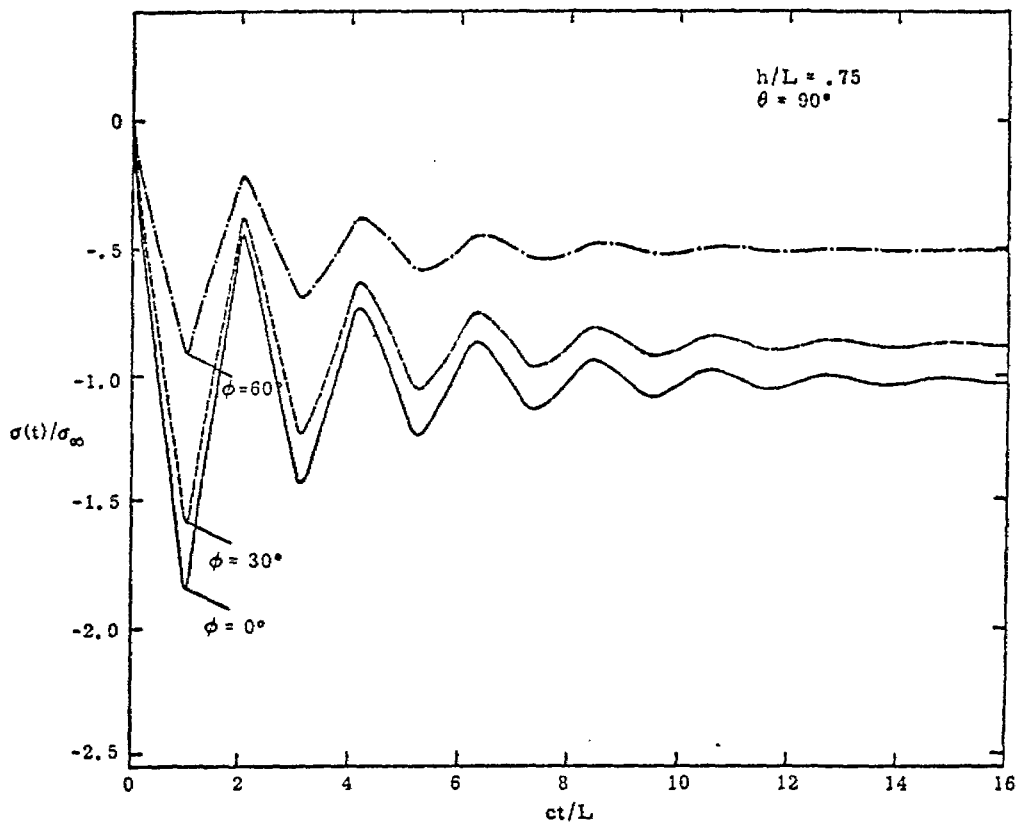


Figure 6i. Time response of the charge density at  $\xi = 0$  for an incident step wave.

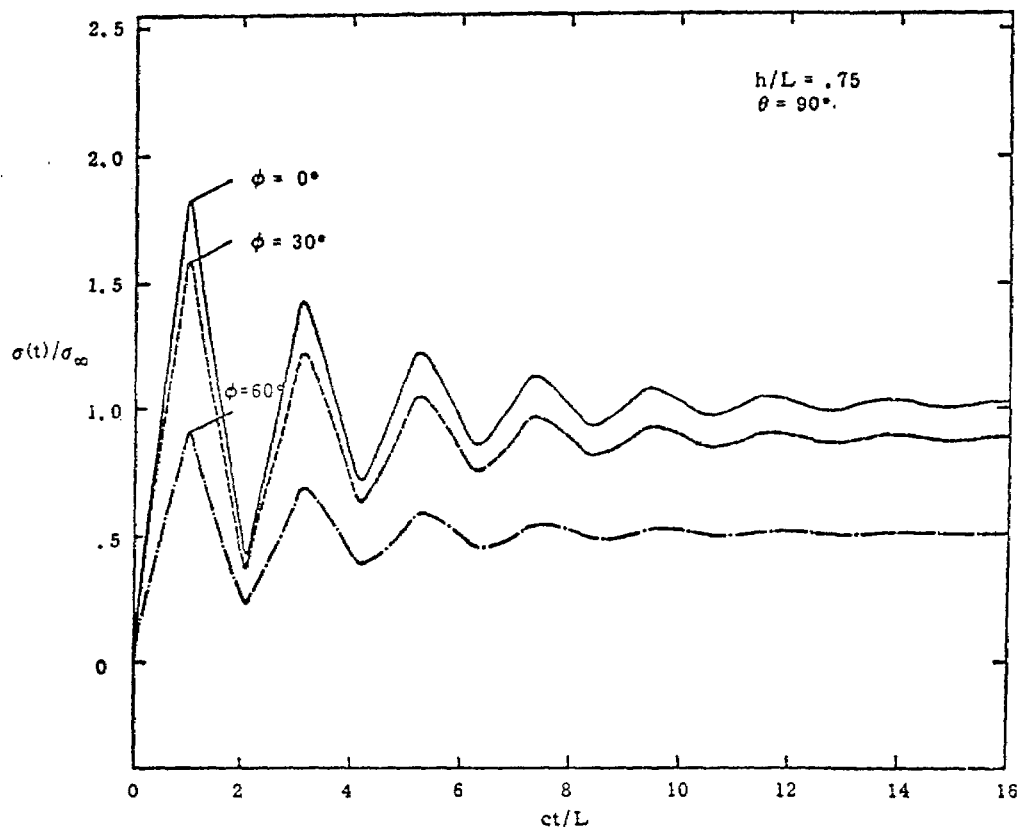


Figure 6j. Time response of the charge density at  $\xi = L$  for an incident step wave.

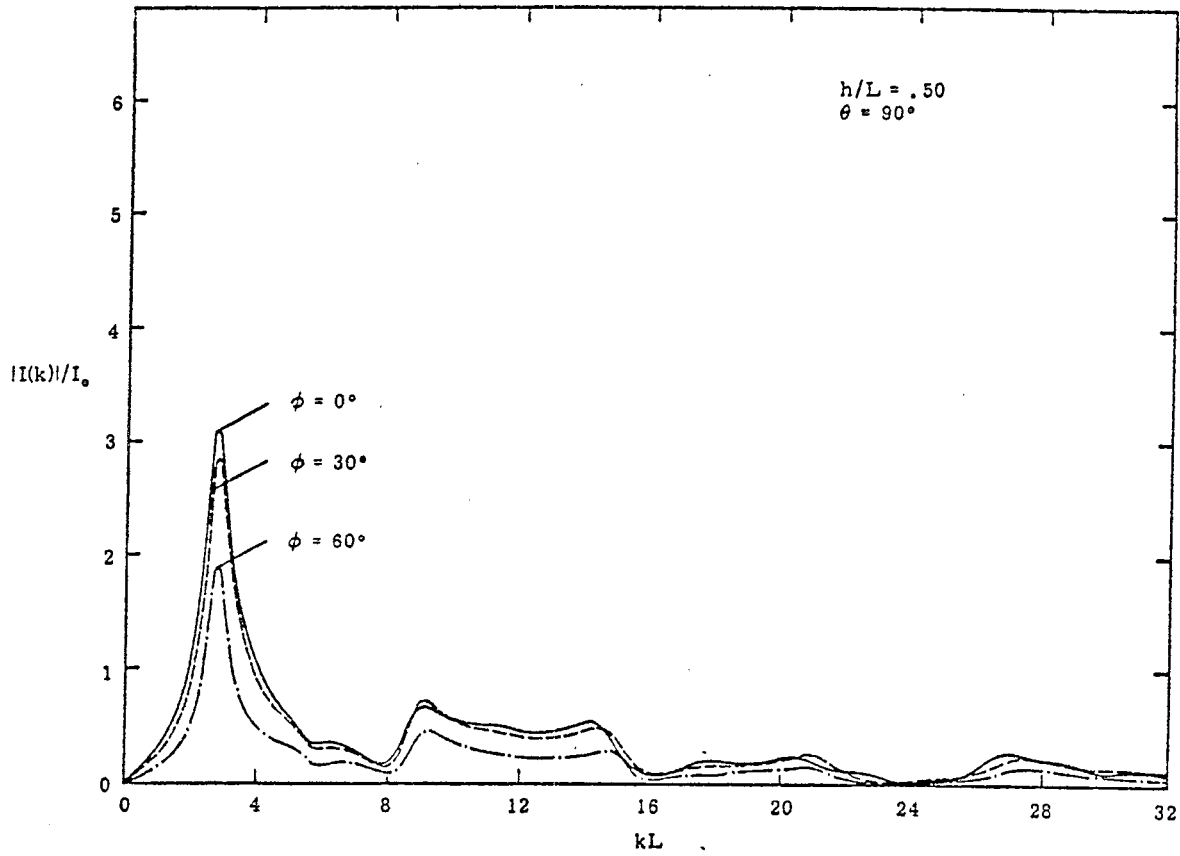


Figure 7a. Magnitude of the impulse spectrum of the current observed at the point  $\xi = .25L$ .

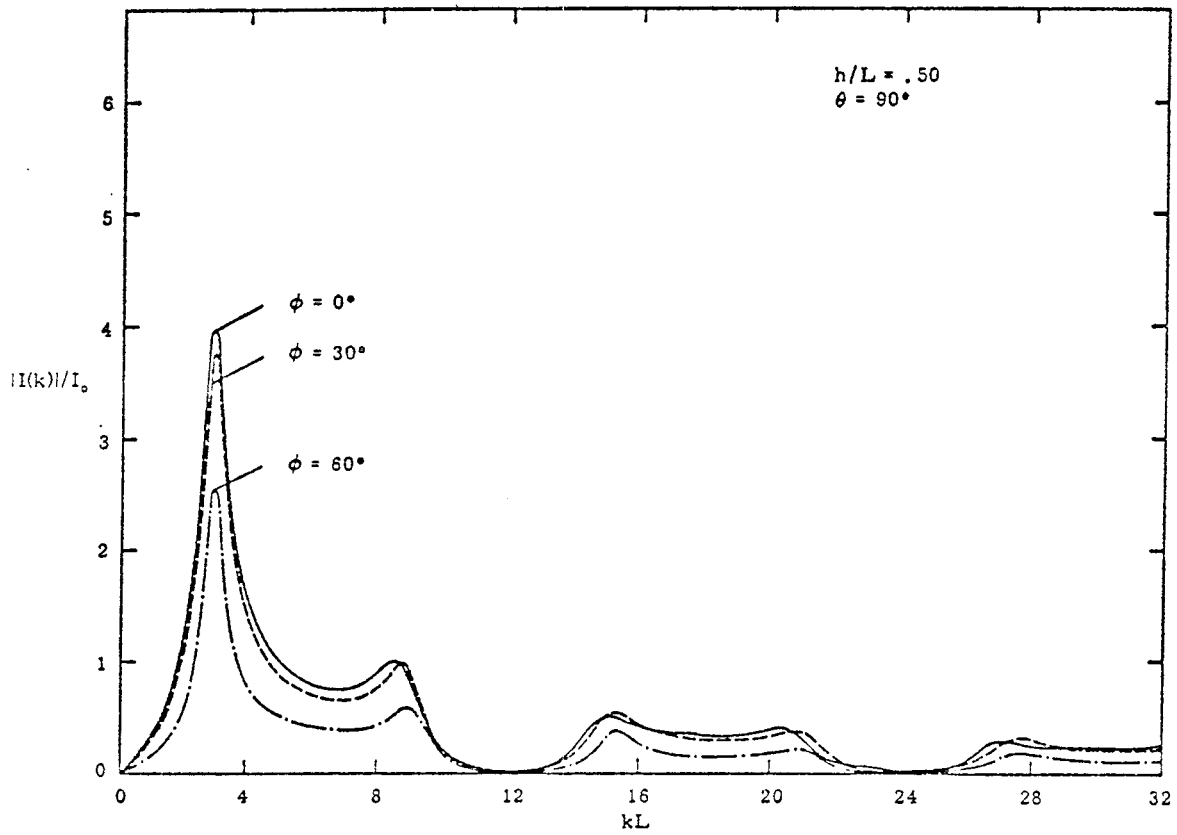


Figure 7b. Magnitude of the impulse spectrum of the current observed at the point  $\xi = .5L$ .

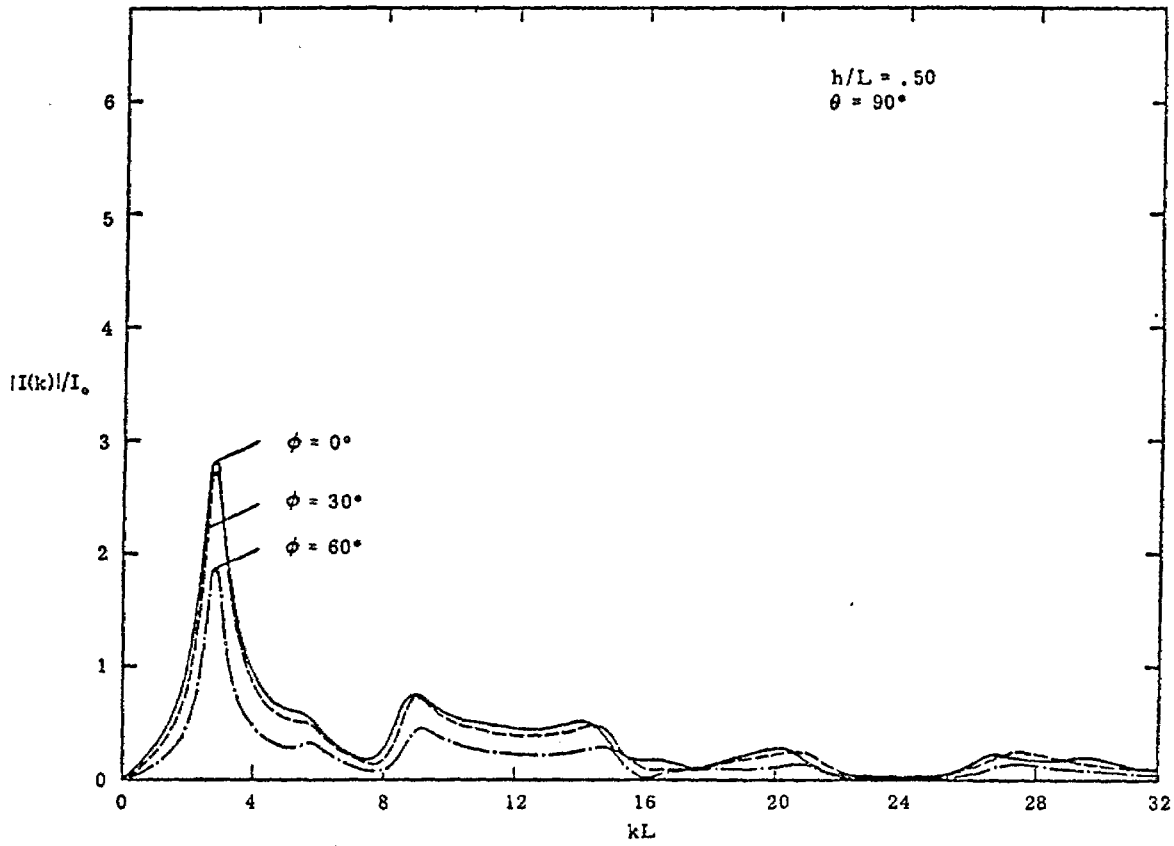


Figure 7c. Magnitude of the impulse spectrum of the current observed at the point  $\xi = .75L$ .

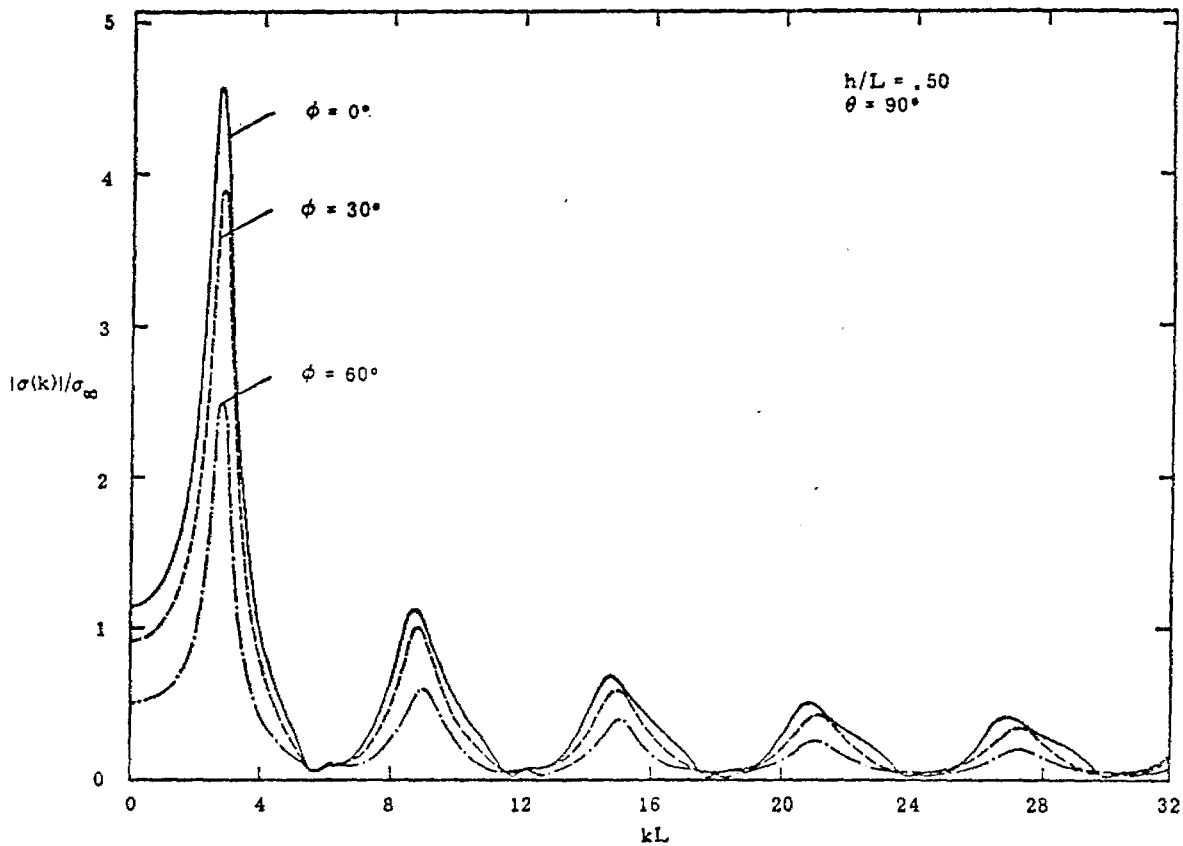


Figure 7d. Magnitude of the impulse spectrum of the linear charge density observed at the point  $\xi = 0$ .

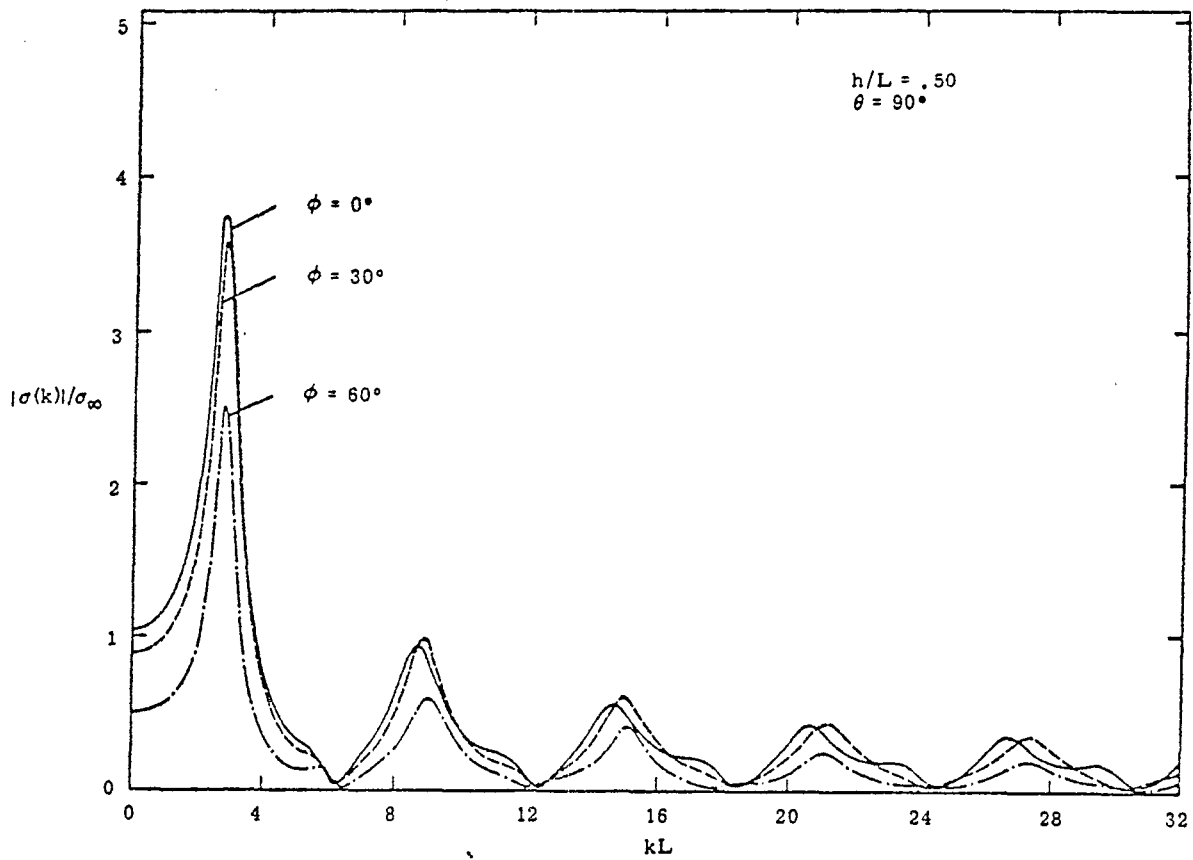


Figure 7e. Magnitude of the impulse spectrum of the linear charge density observed at the point  $\xi = L$ .

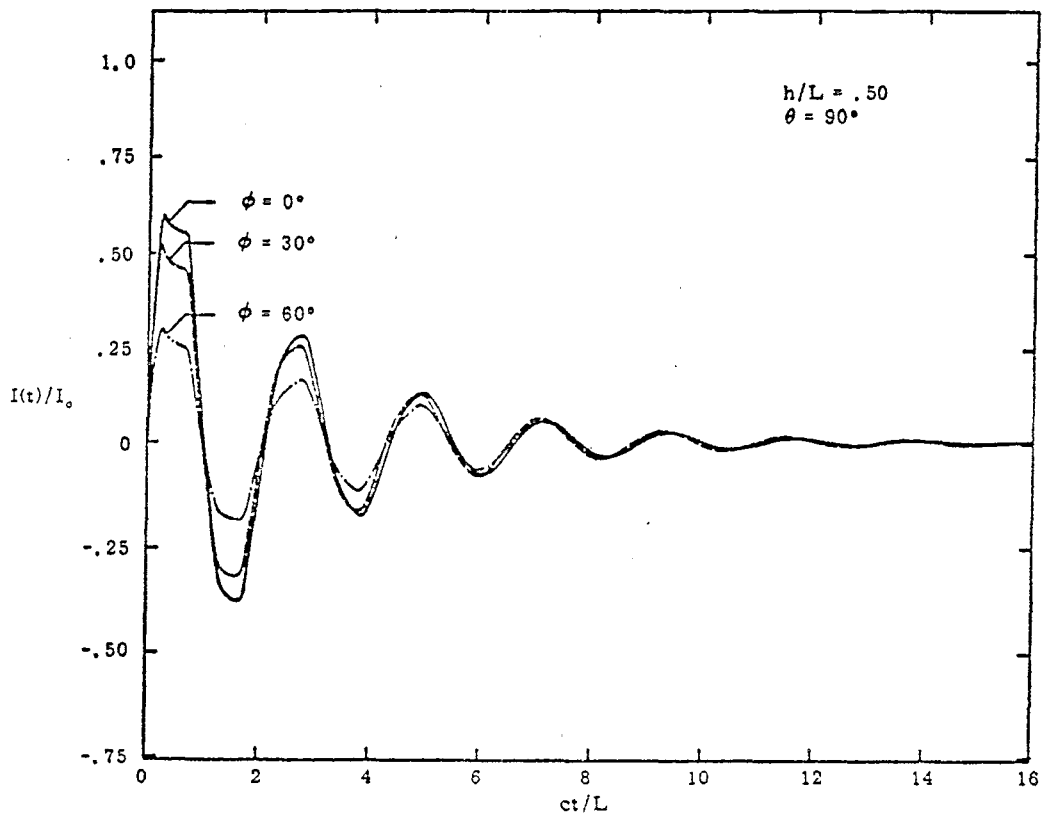


Figure 7f. Time response of the current at  $\xi = .25L$  for an incident step wave.

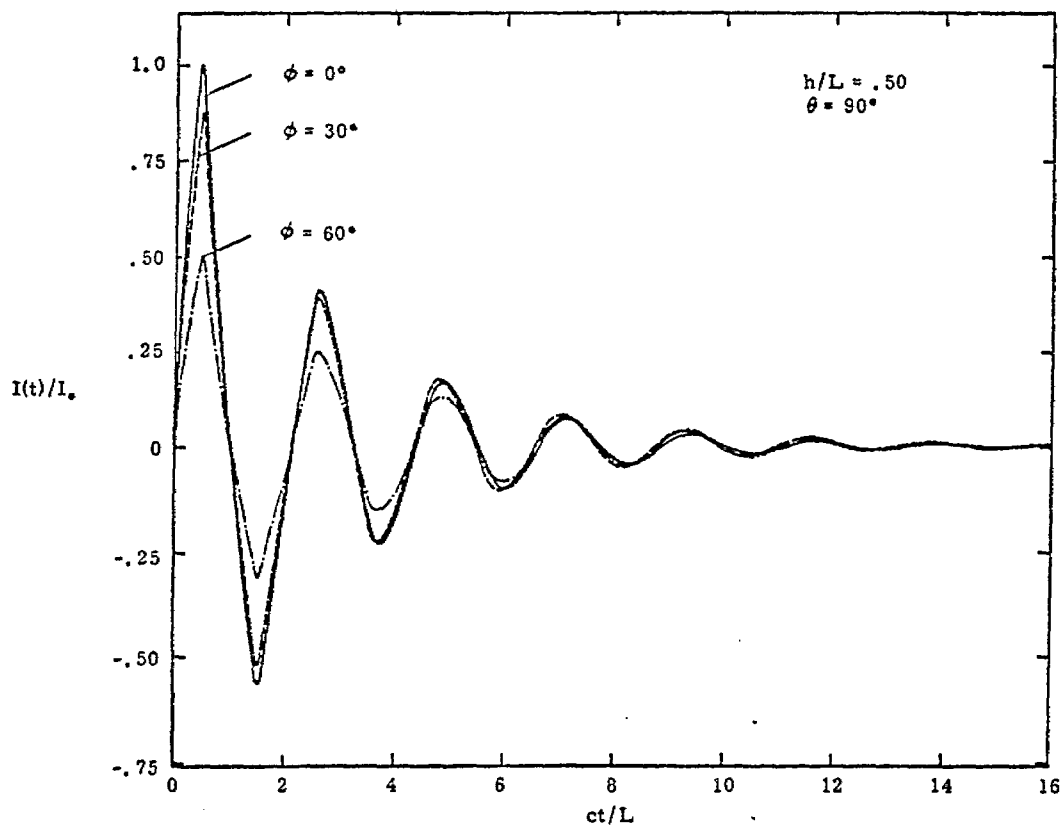


Figure 7g. Time response of the current at  $\xi = .5L$  for an incident step wave.

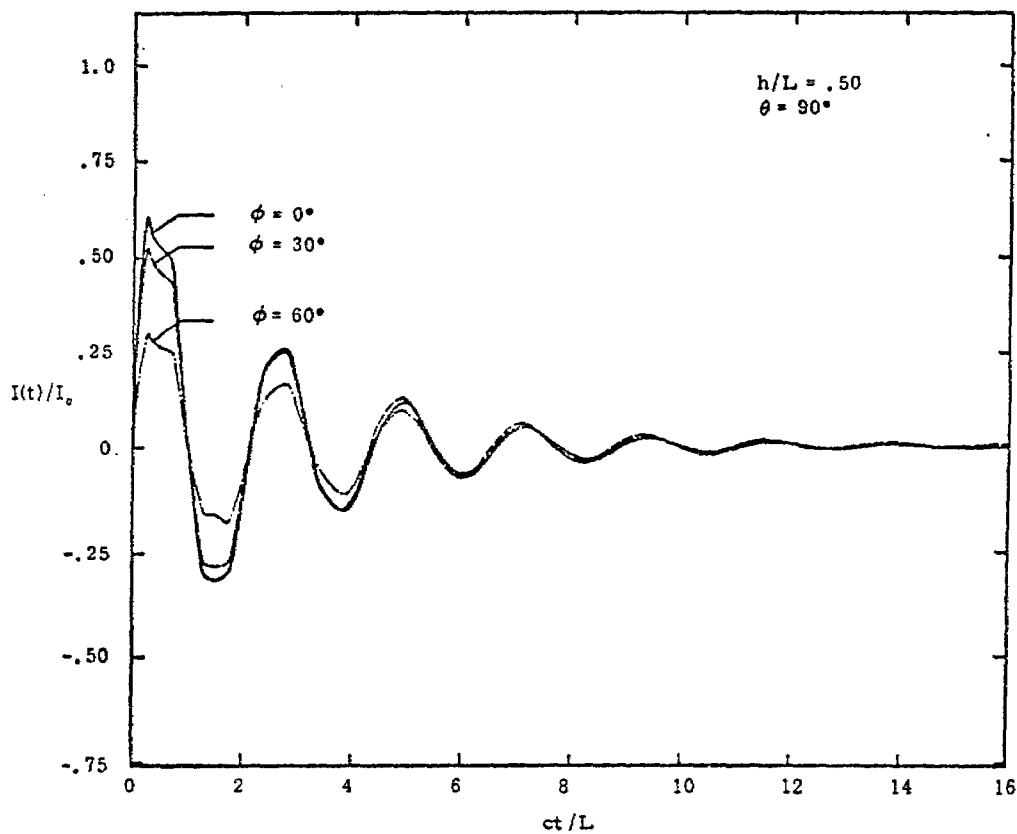


Figure 7h. Time response of the current at  $\xi = .75L$  for an incident step wave.

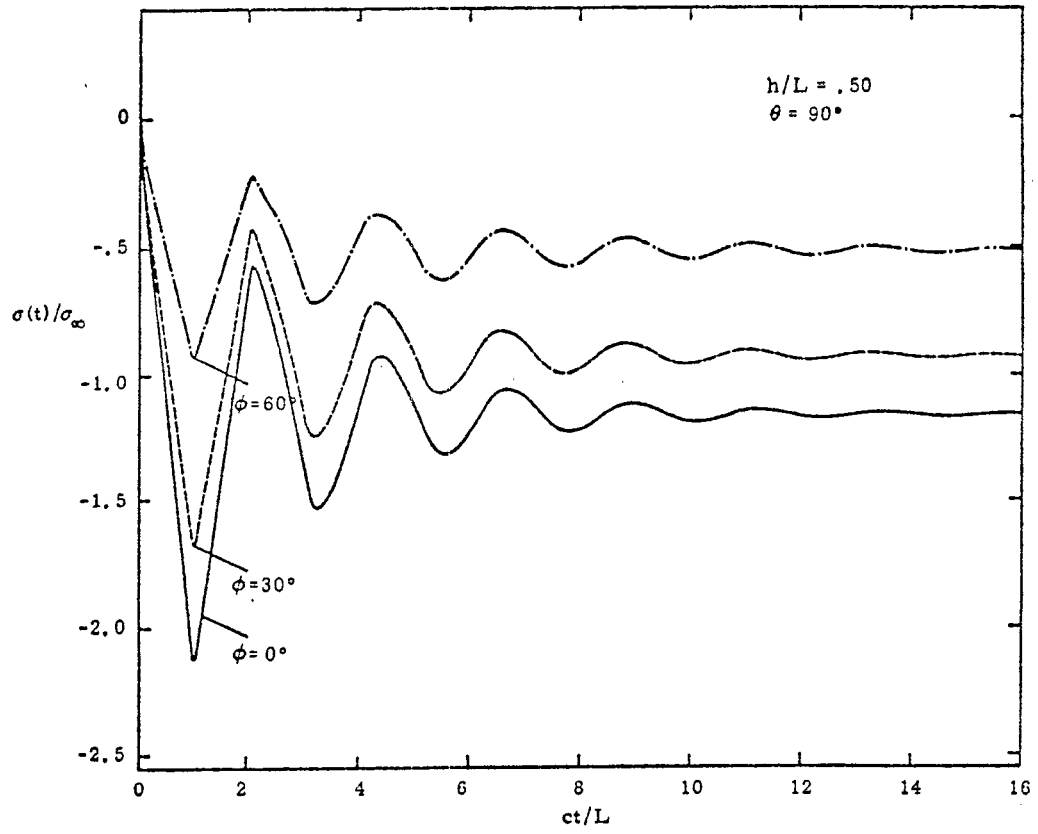


Figure 7i. Time response of the charge density at  $\xi = 0$  for an incident step wave.

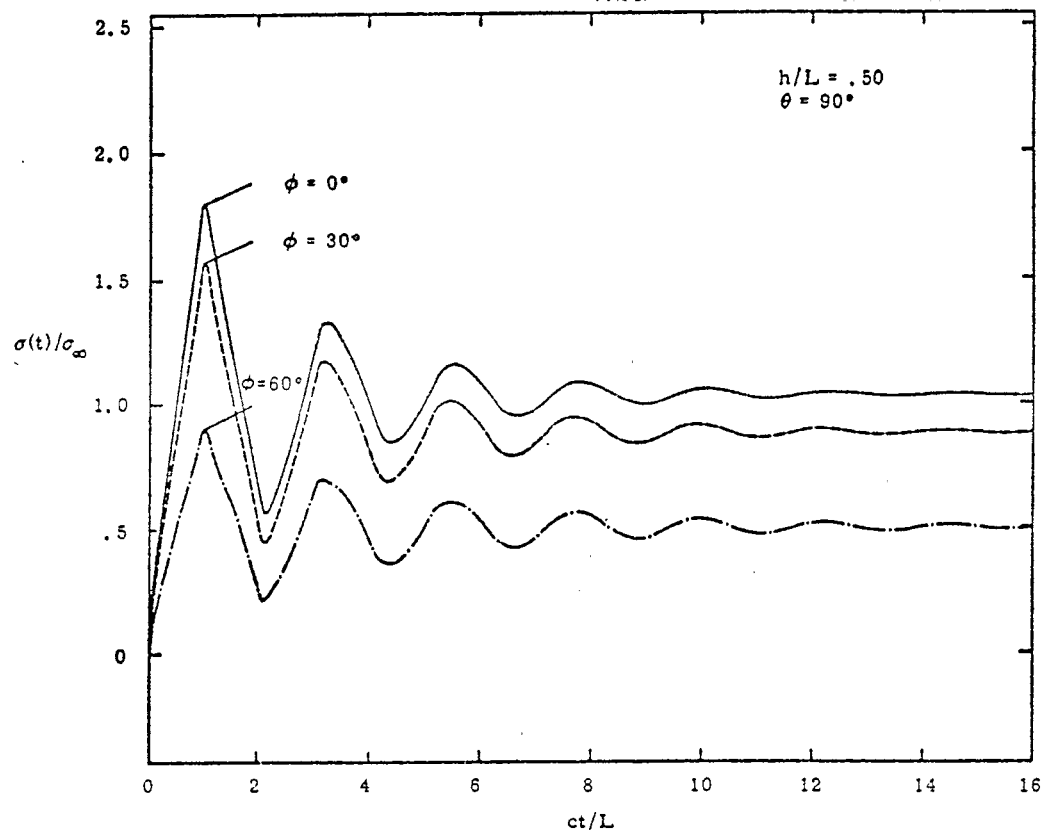


Figure 7j. Time response of the charge density at  $\xi = L$  for an incident step wave.

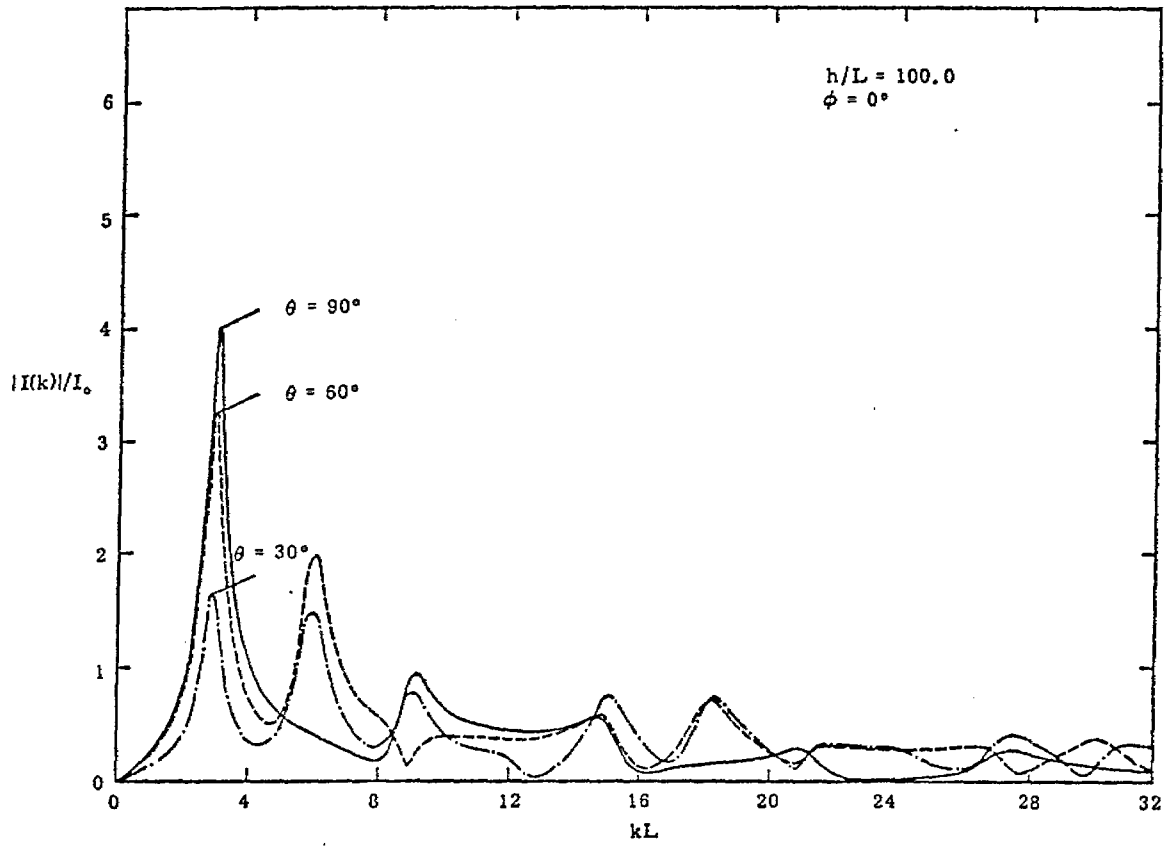


Figure 8a. Magnitude of the impulse spectrum of the current observed at the point  $\xi = .25L$ .

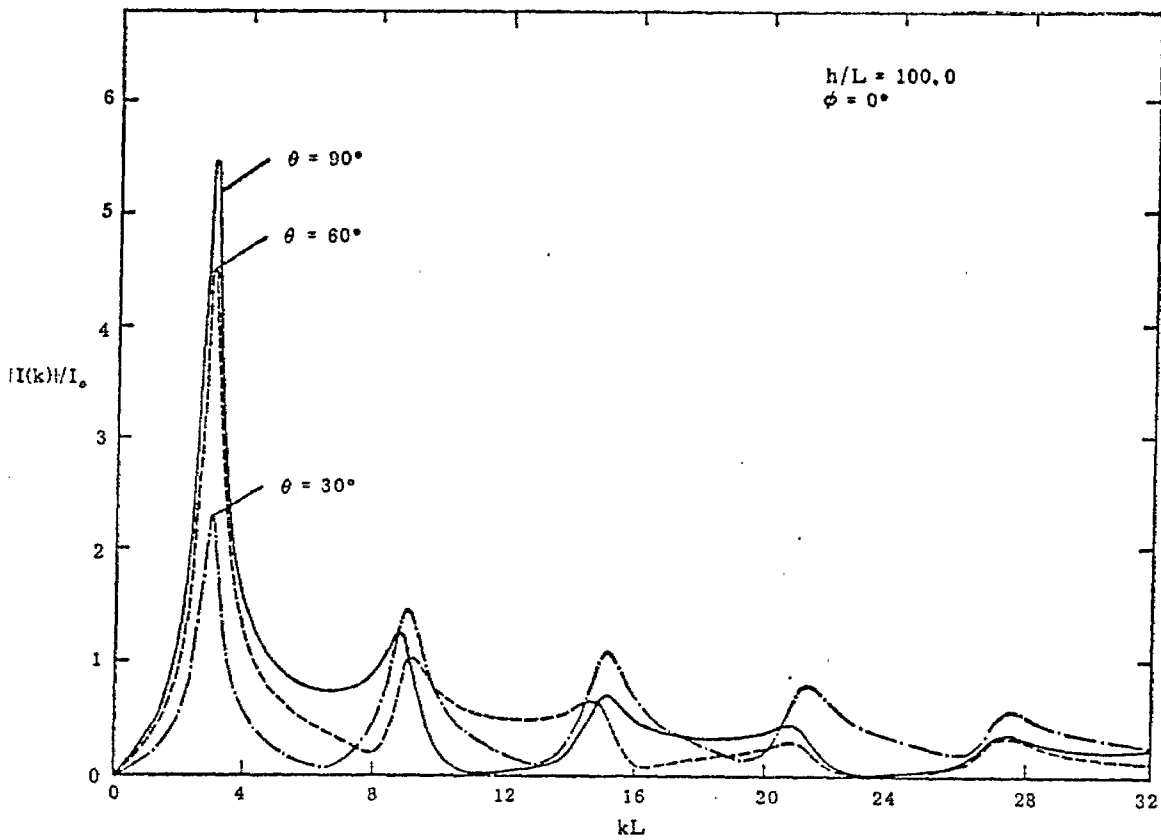


Figure 8b. Magnitude of the impulse spectrum of the current observed at the point  $\xi = .5L$ .

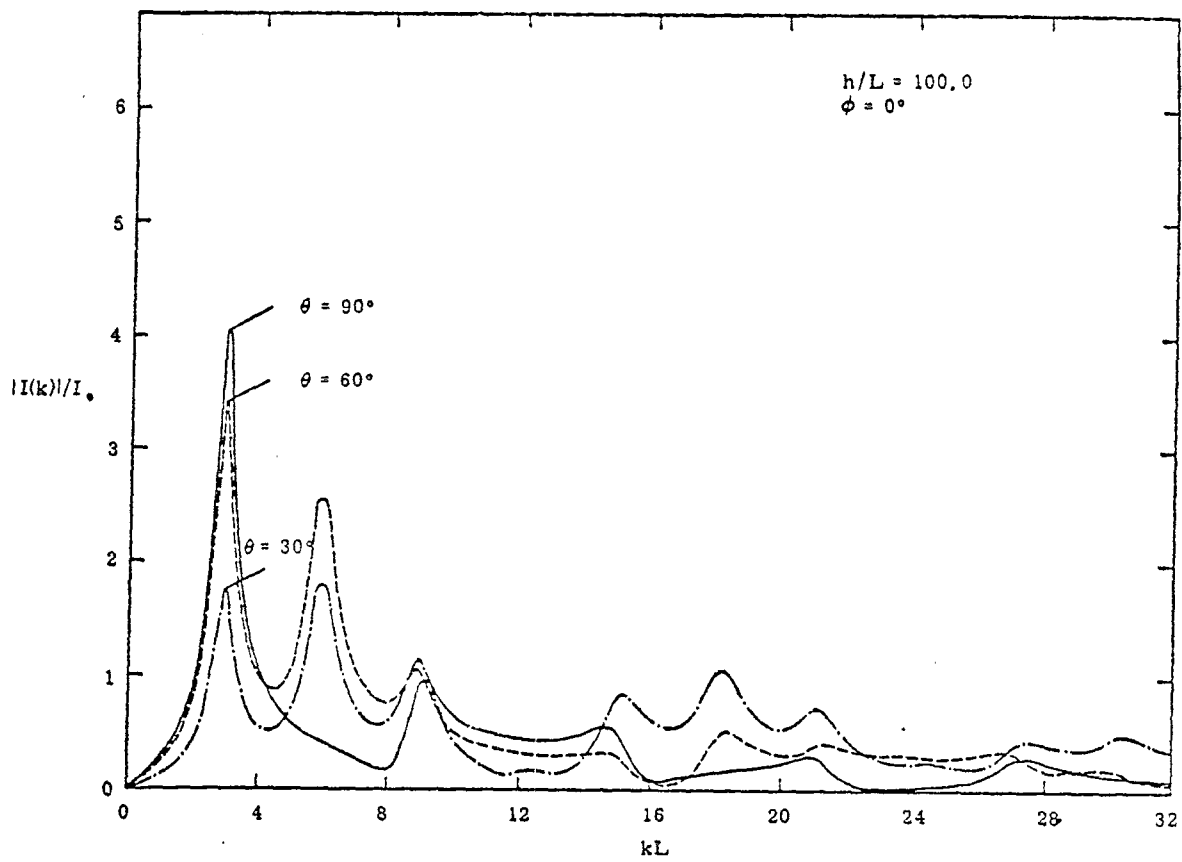


Figure 8c. Magnitude of the impulse spectrum of the current observed at the point  $\xi = .75L$ .

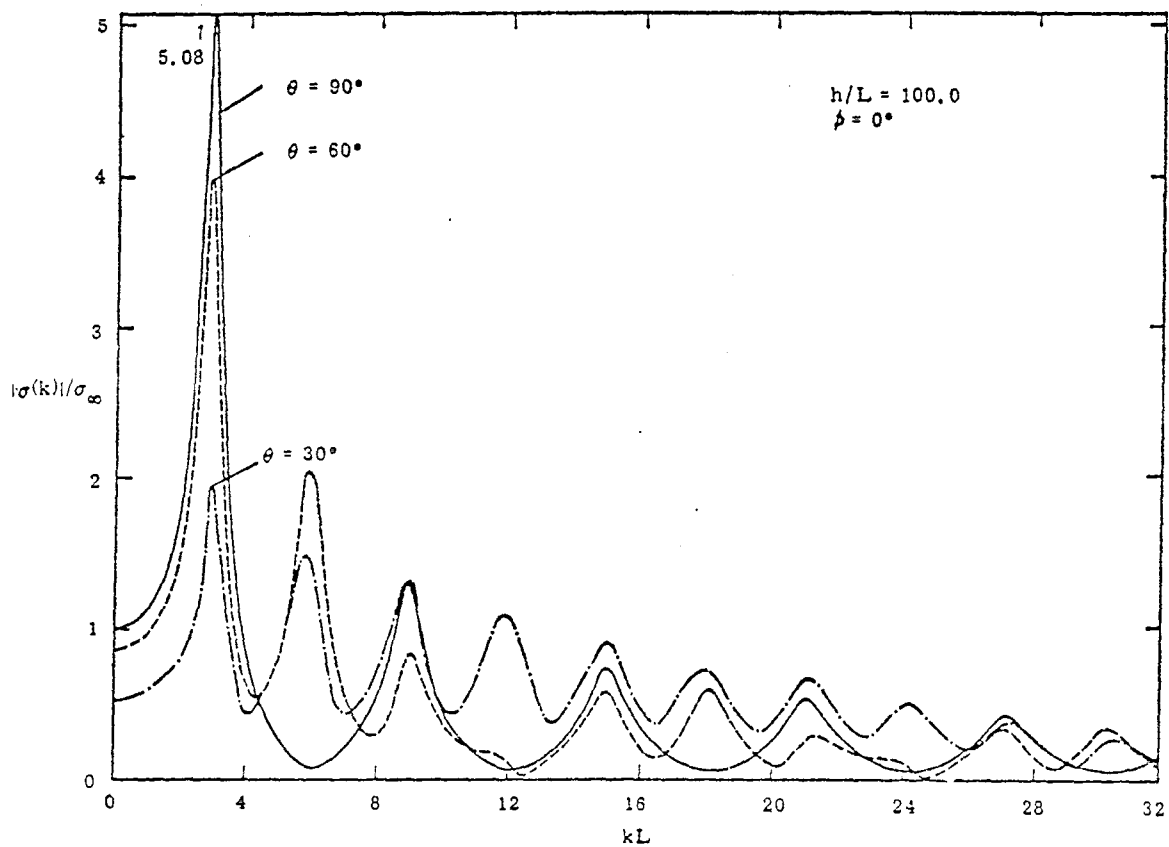


Figure 8d. Magnitude of the impulse spectrum of the linear charge density observed at the point  $\xi = 0$ .

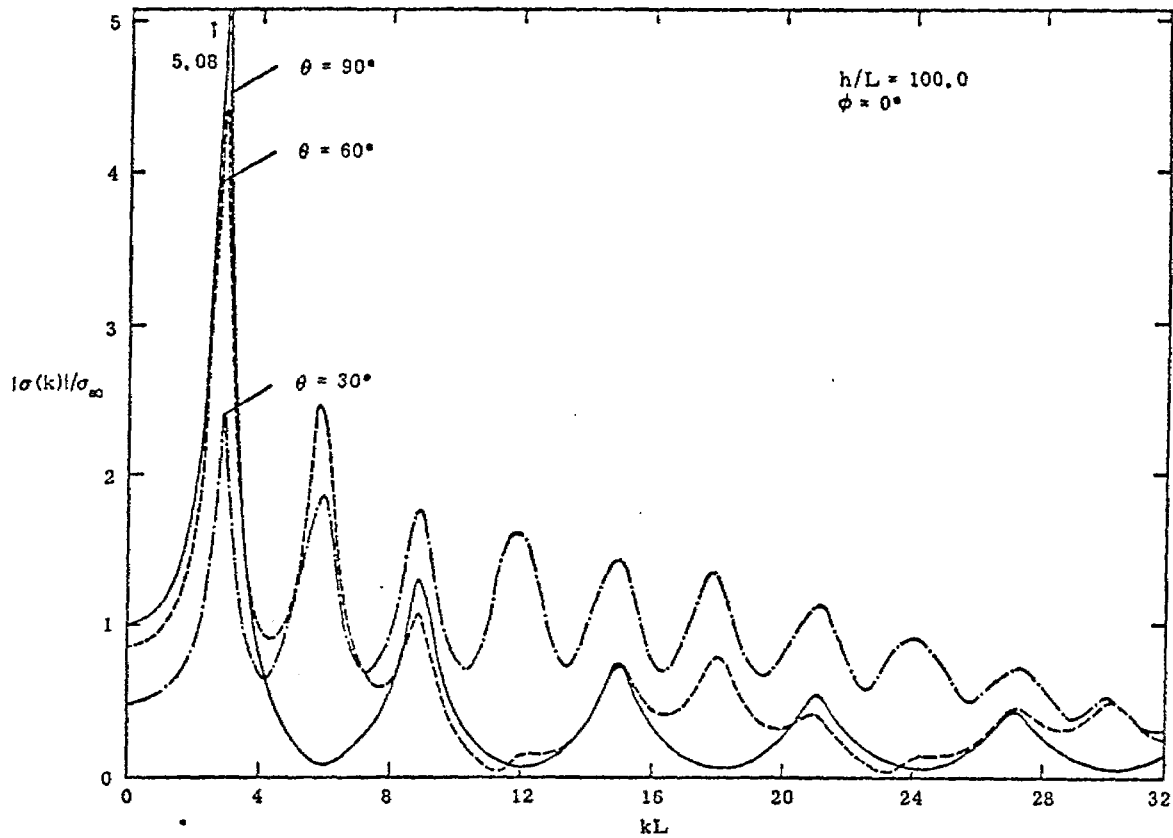


Figure 8e. Magnitude of the impulse spectrum of the linear charge density observed at the point  $\xi = L$ .

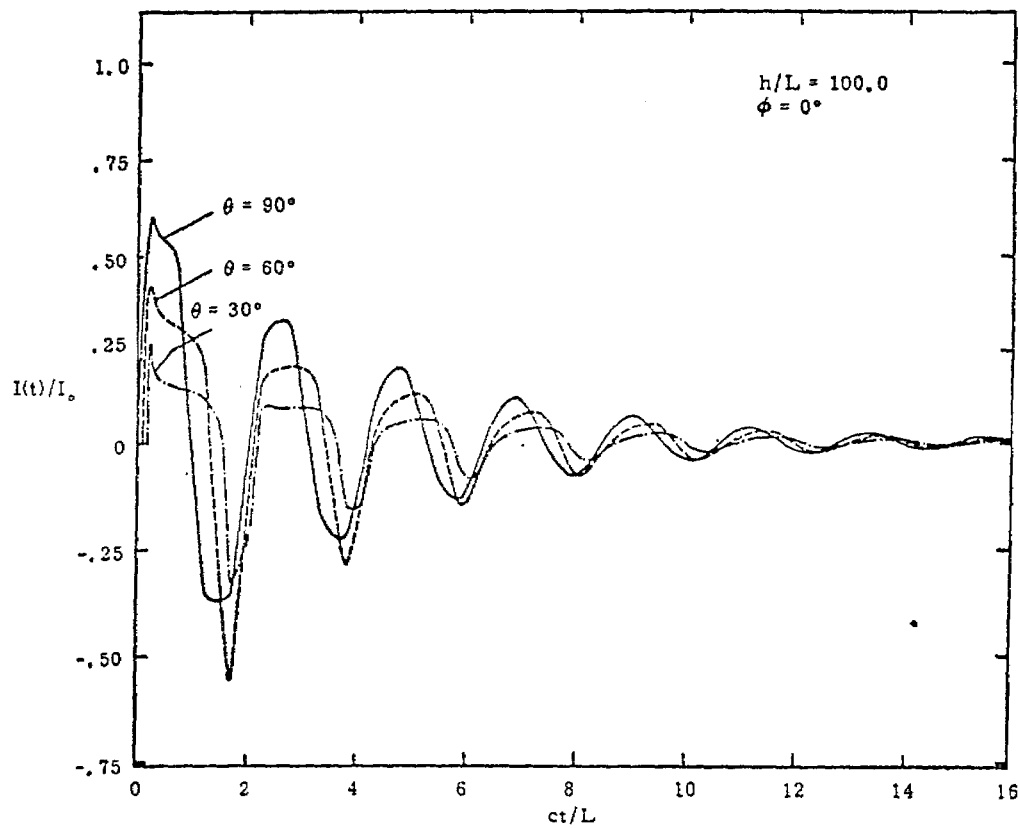


Figure 8f. Time response of the current at  $\xi = .25L$  for an incident step wave.

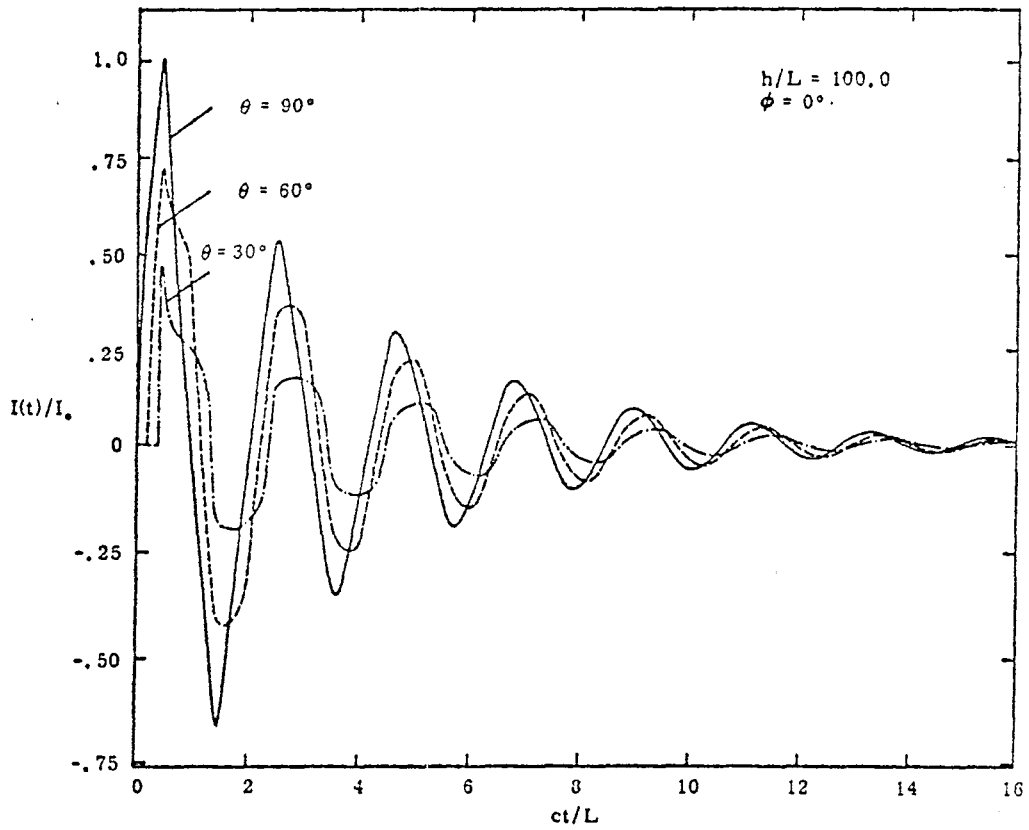


Figure 8g. Time response of the current at  $\xi = .5L$  for an incident step wave.

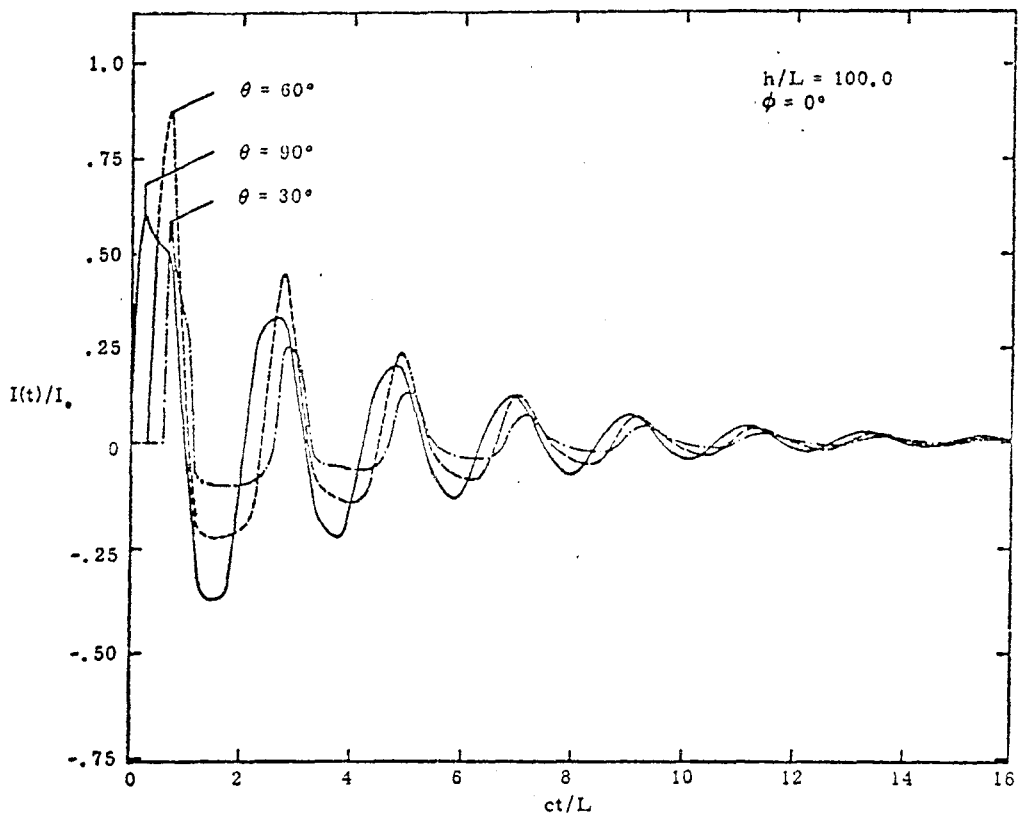


Figure 8h. Time response of the current at  $\xi = .75L$  for an incident step wave.

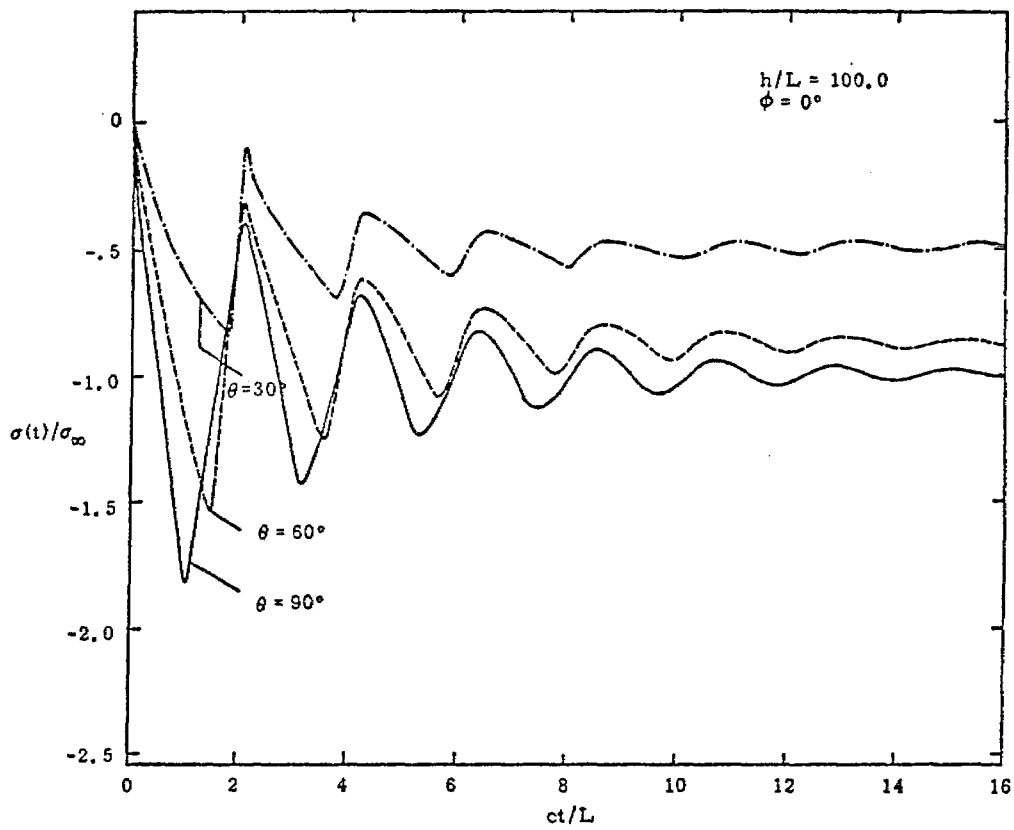


Figure 8i. Time response of the charge density at  $\xi = 0$  for an incident step wave.

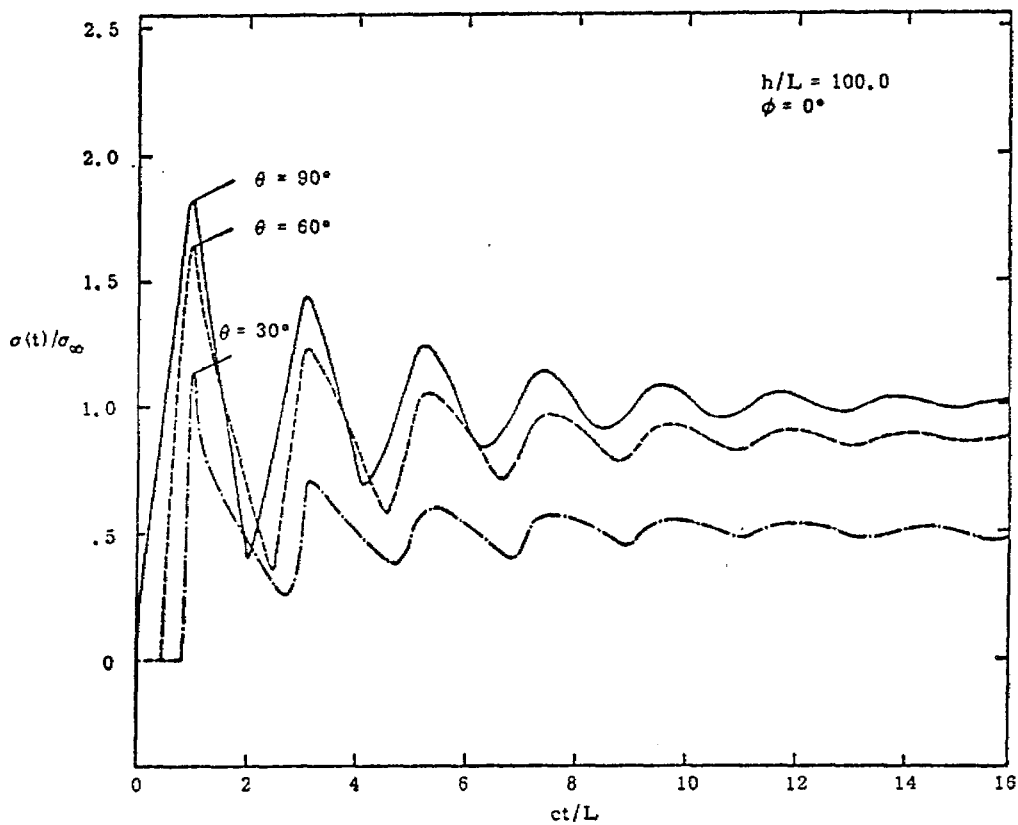


Figure 8j. Time response of the charge density at  $\xi = L$  for an incident step wave.

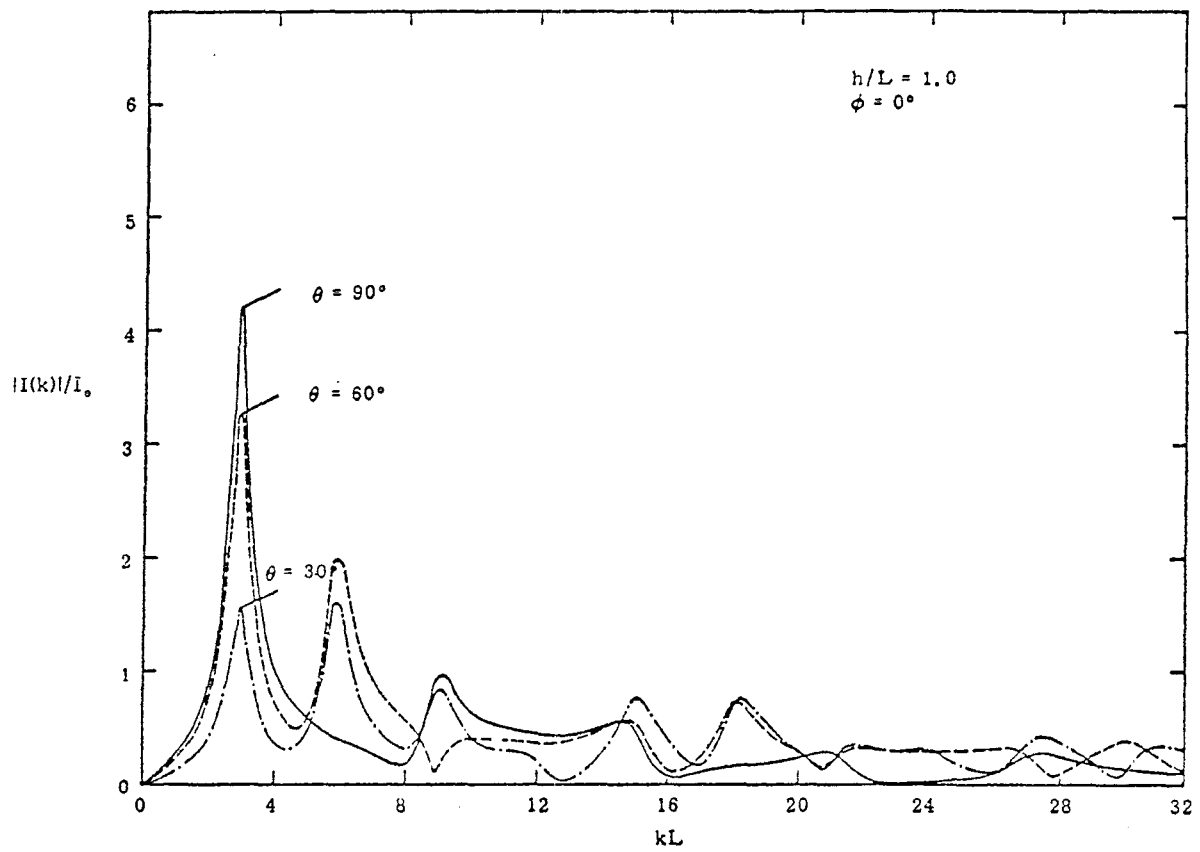


Figure 9a. Magnitude of the impulse spectrum of the current observed at the point  $\xi = .25L$ .

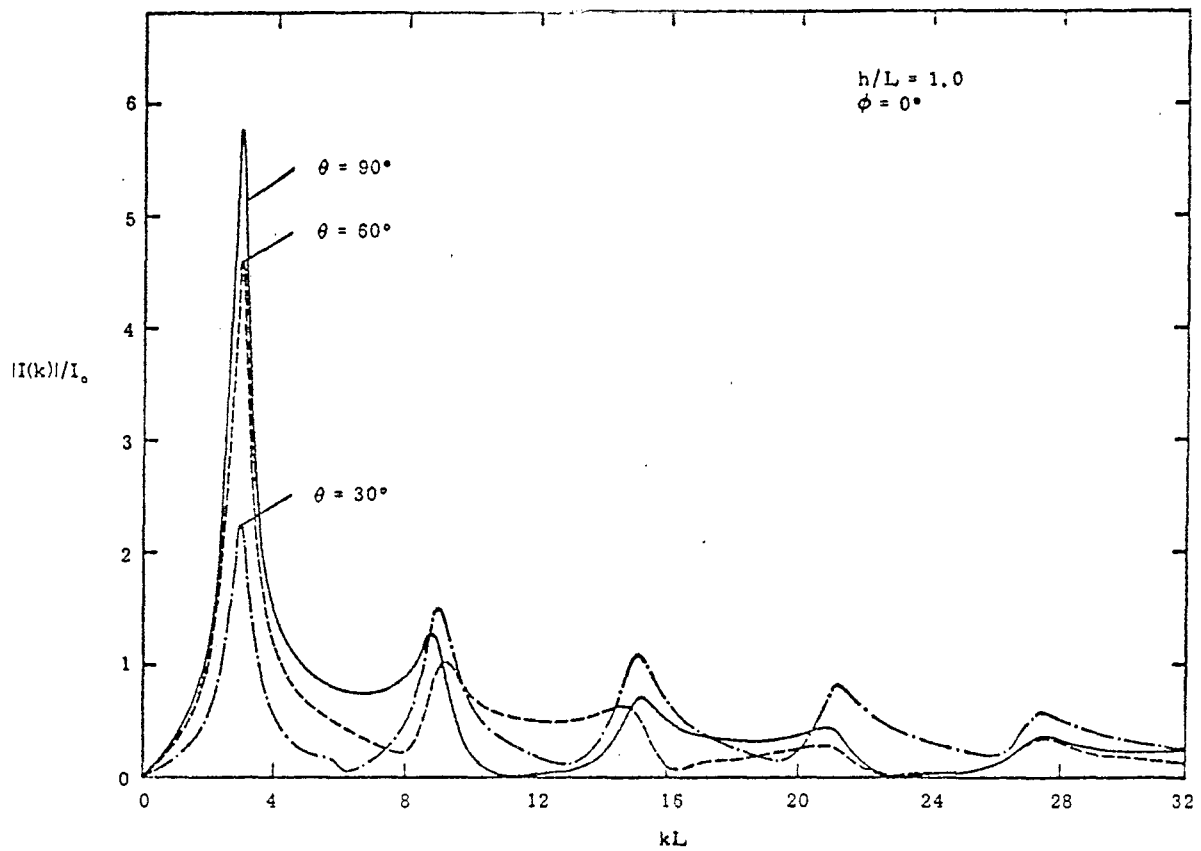


Figure 9b. Magnitude of the impulse spectrum of the current observed at the point  $\xi = .5L$ .

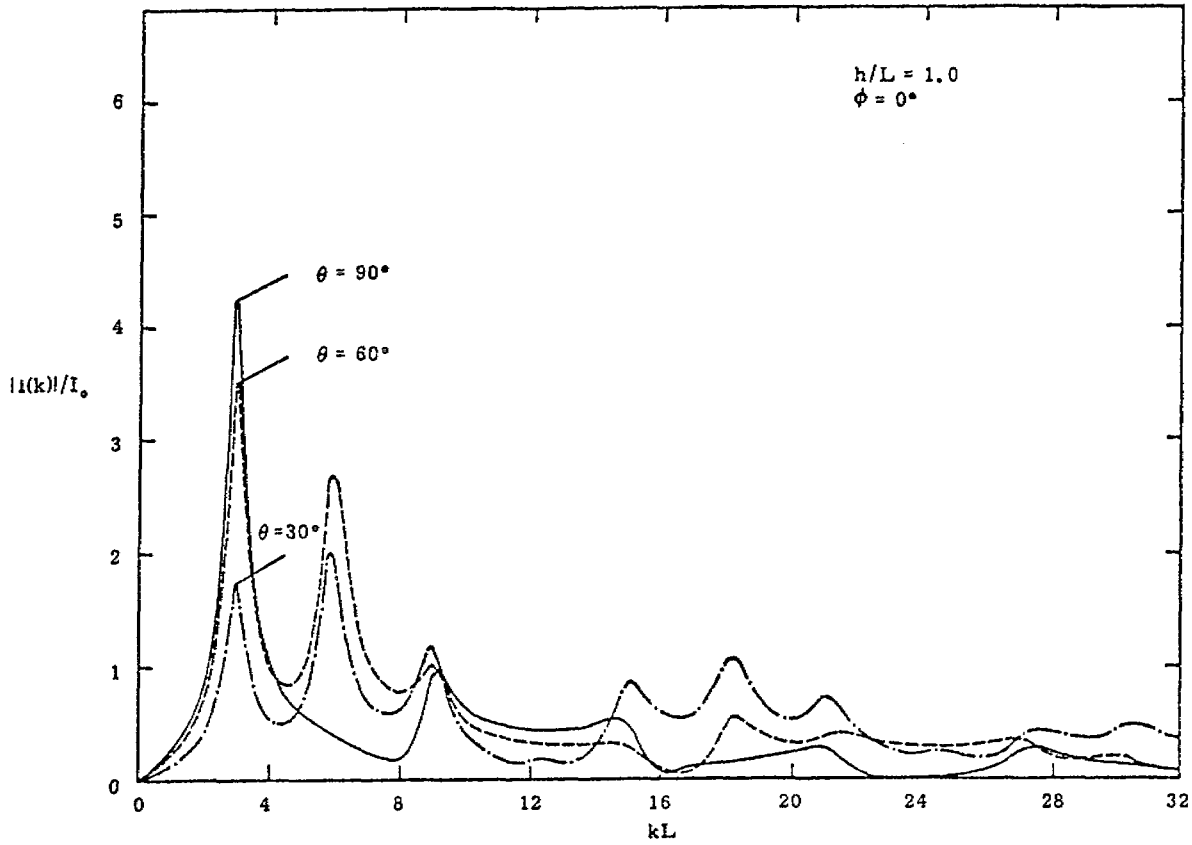


Figure 9c. Magnitude of the impulse spectrum of the current observed at the point  $\xi = .75L$ .

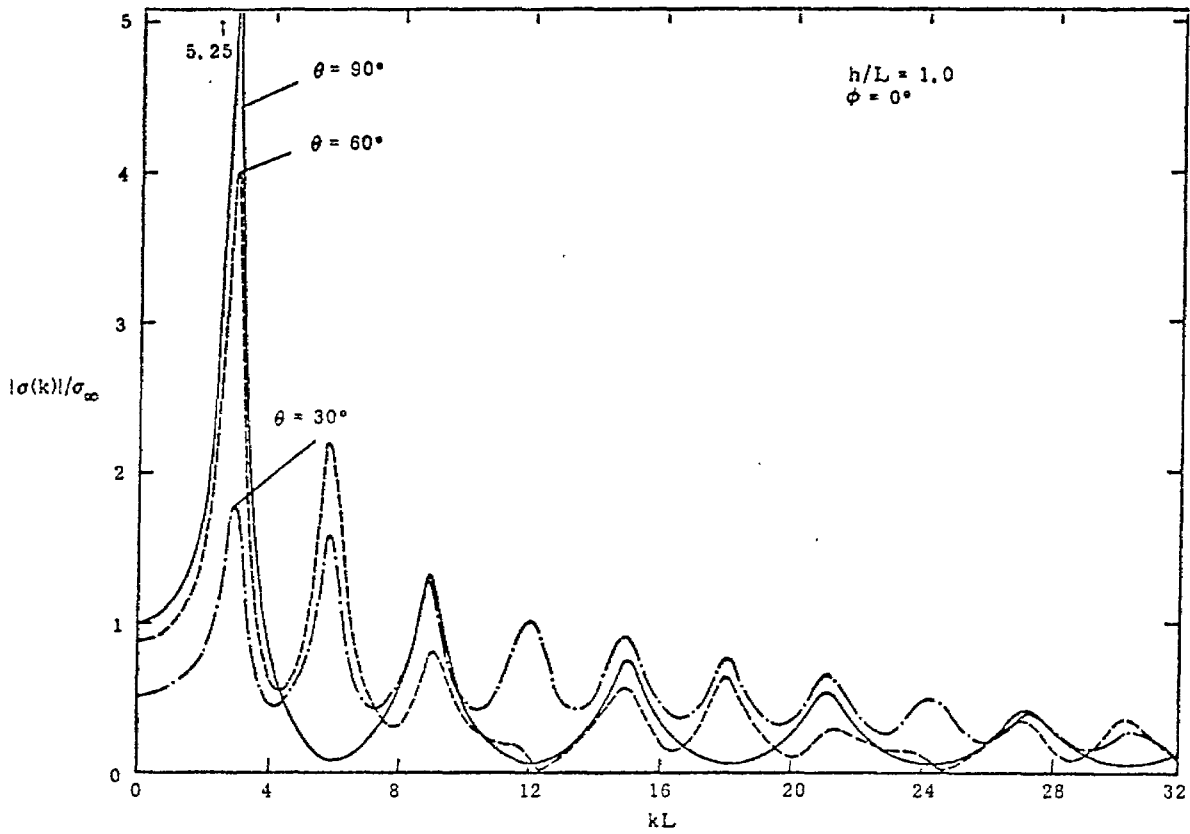


Figure 9d. Magnitude of the impulse spectrum of the linear charge density observed at the point  $\xi = 0$ .

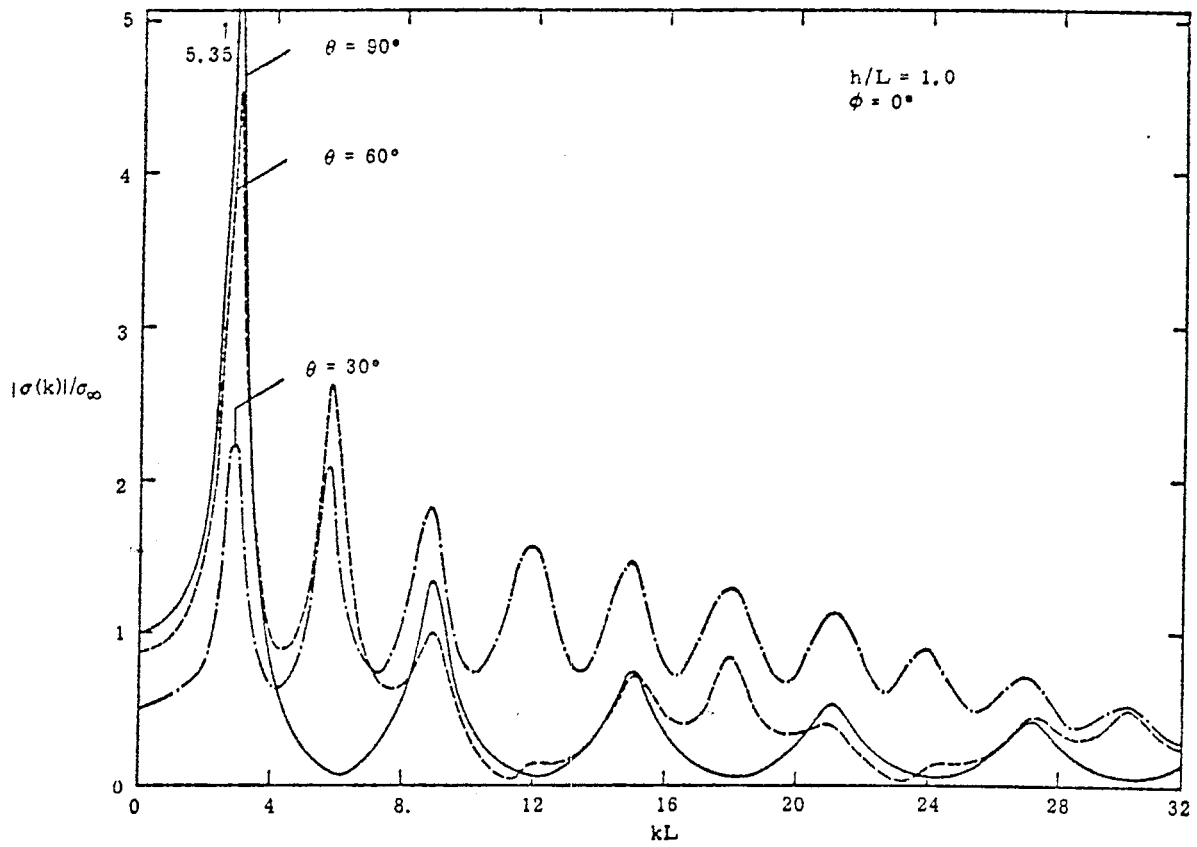


Figure 9e. Magnitude of the impulse spectrum of the linear charge density observed at the point  $\xi = L$ .

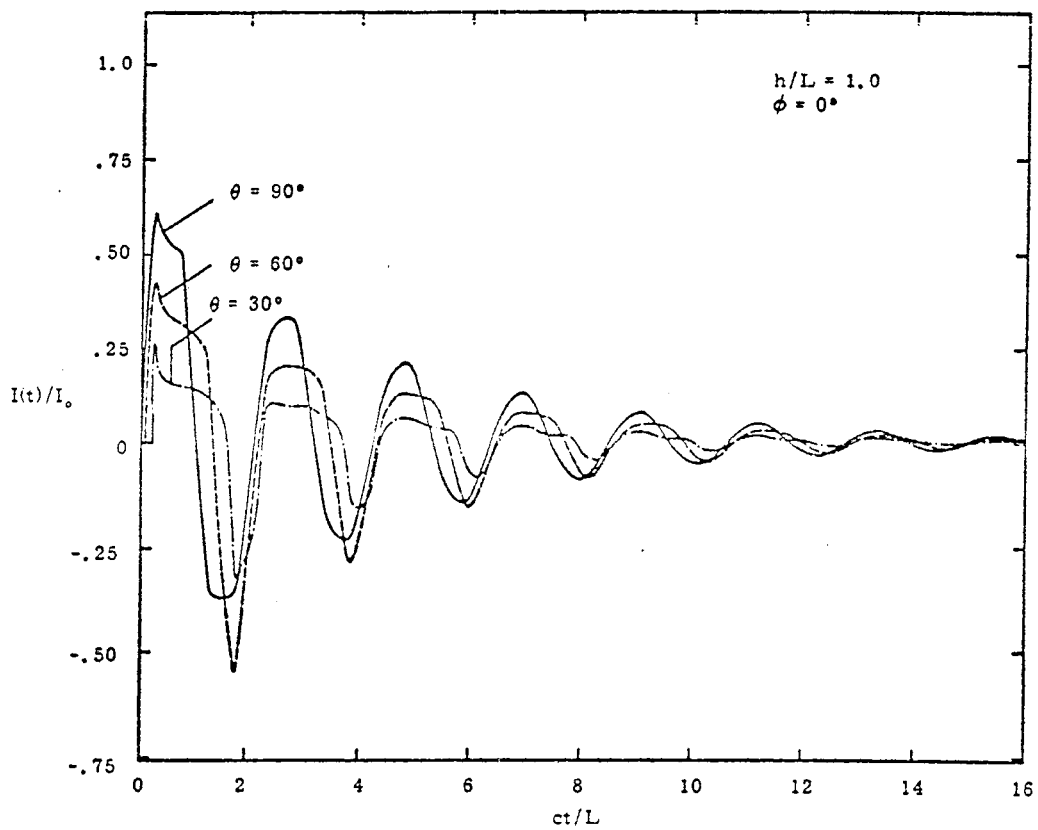


Figure 9f. Time response of the current at  $\xi = .25L$  for an incident step wave.

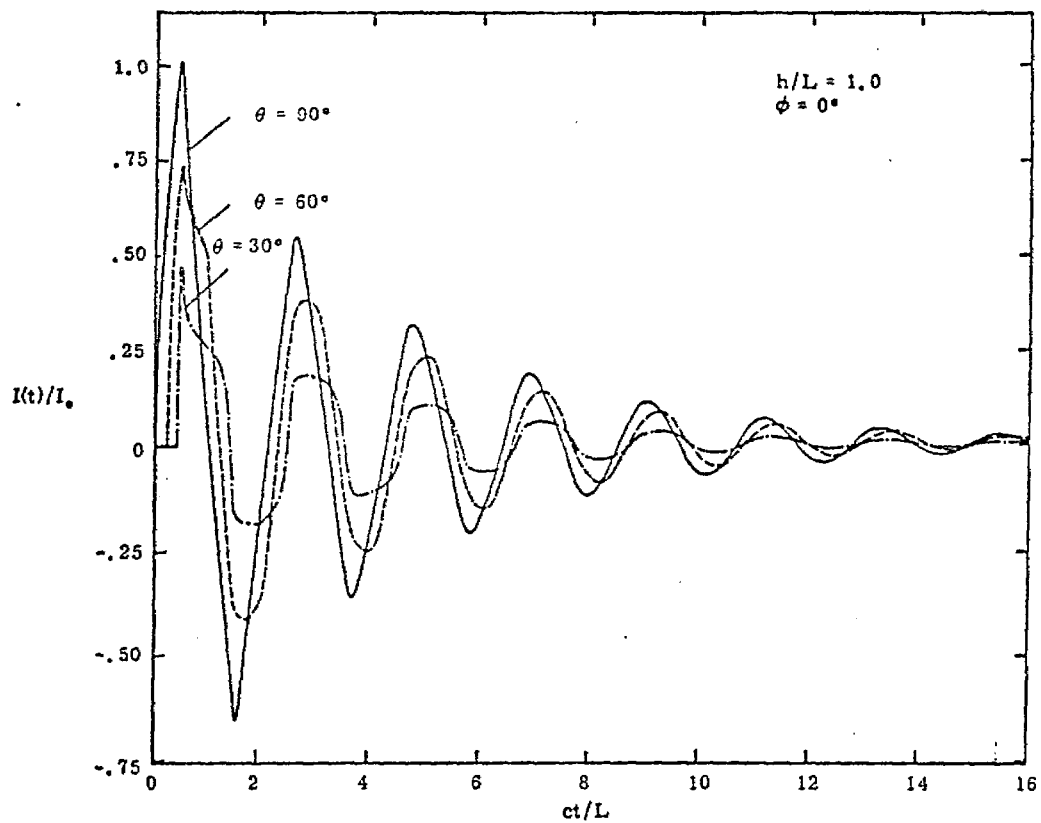


Figure 9g. Time response of the current at  $\xi = .5L$  for an incident step wave.

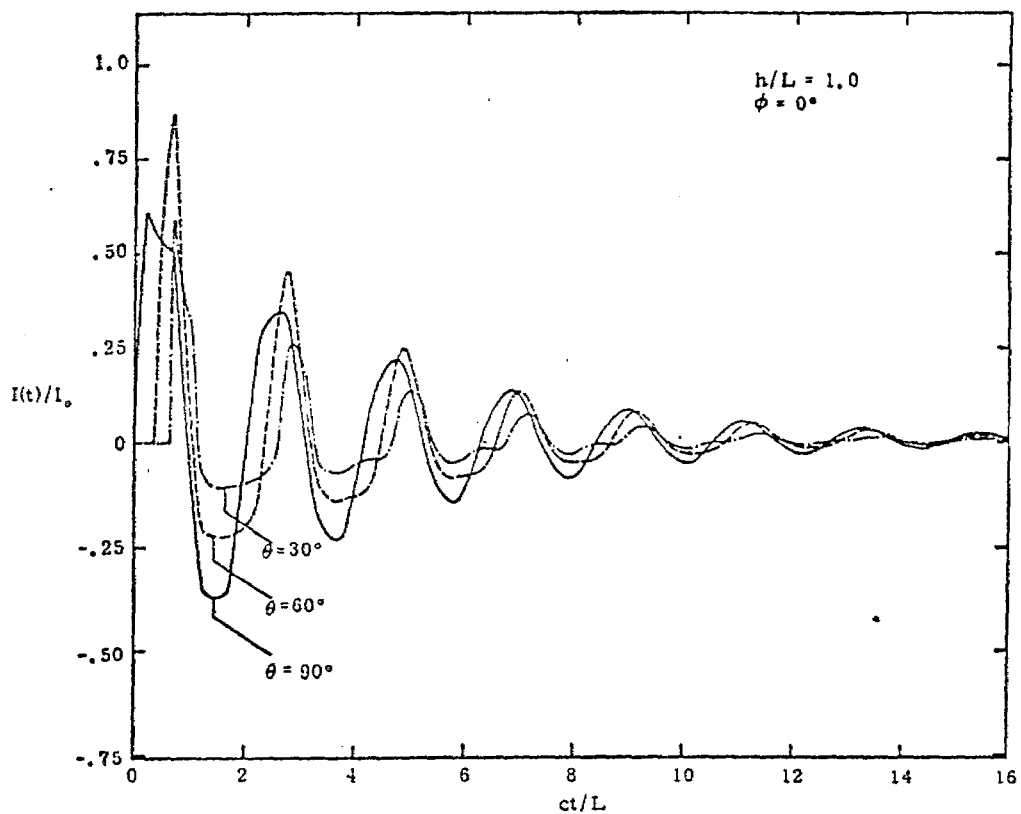


Figure 9h. Time response of the current at  $\xi = .75L$  for an incident step wave.

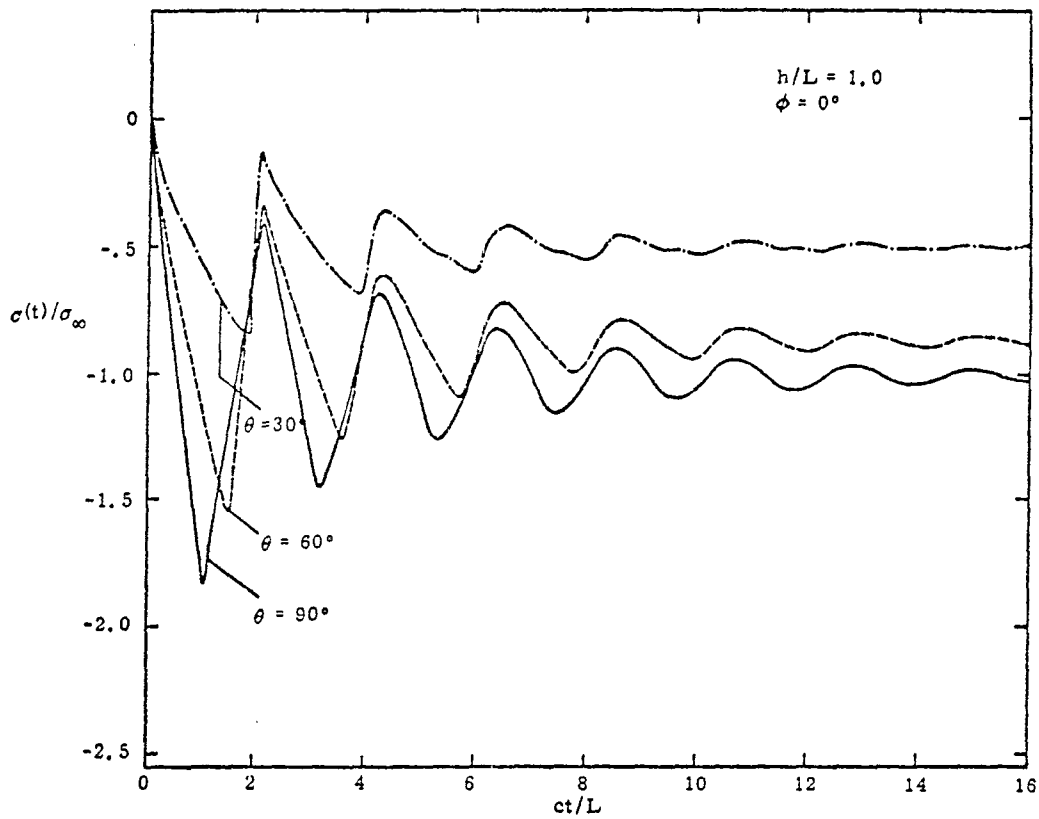


Figure 9i. Time response of the charge density at  $\xi = 0$  for an incident step wave.

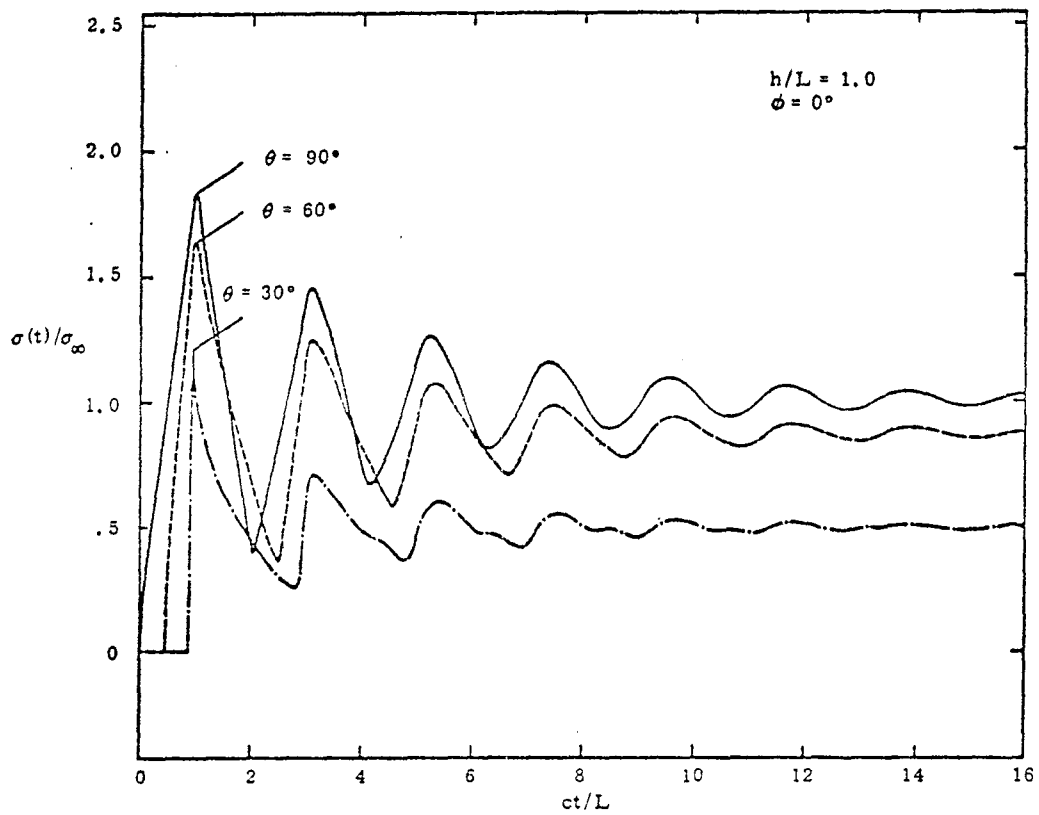


Figure 9j. Time response of the charge density at  $\xi = L$  for an incident step wave.

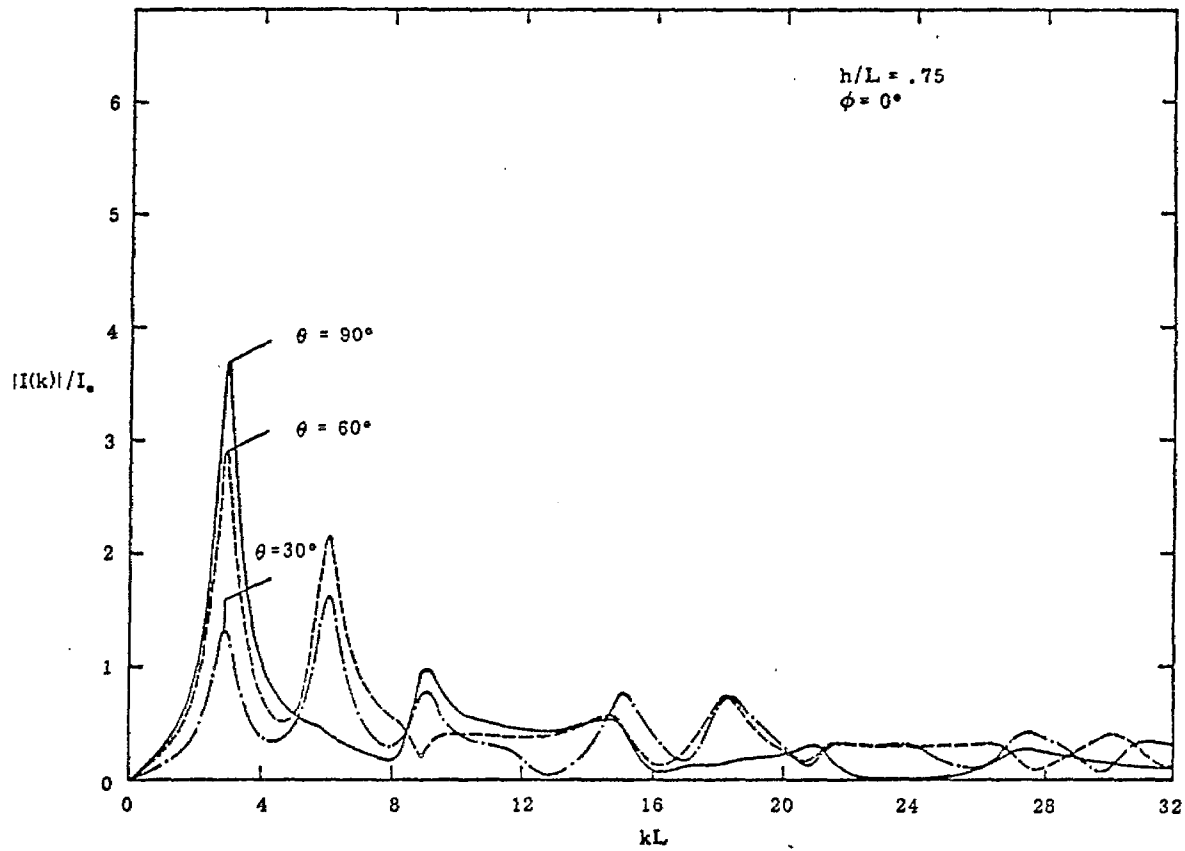


Figure 10a. Magnitude of the impulse spectrum of the current observed at the point  $\xi = .25L$ .

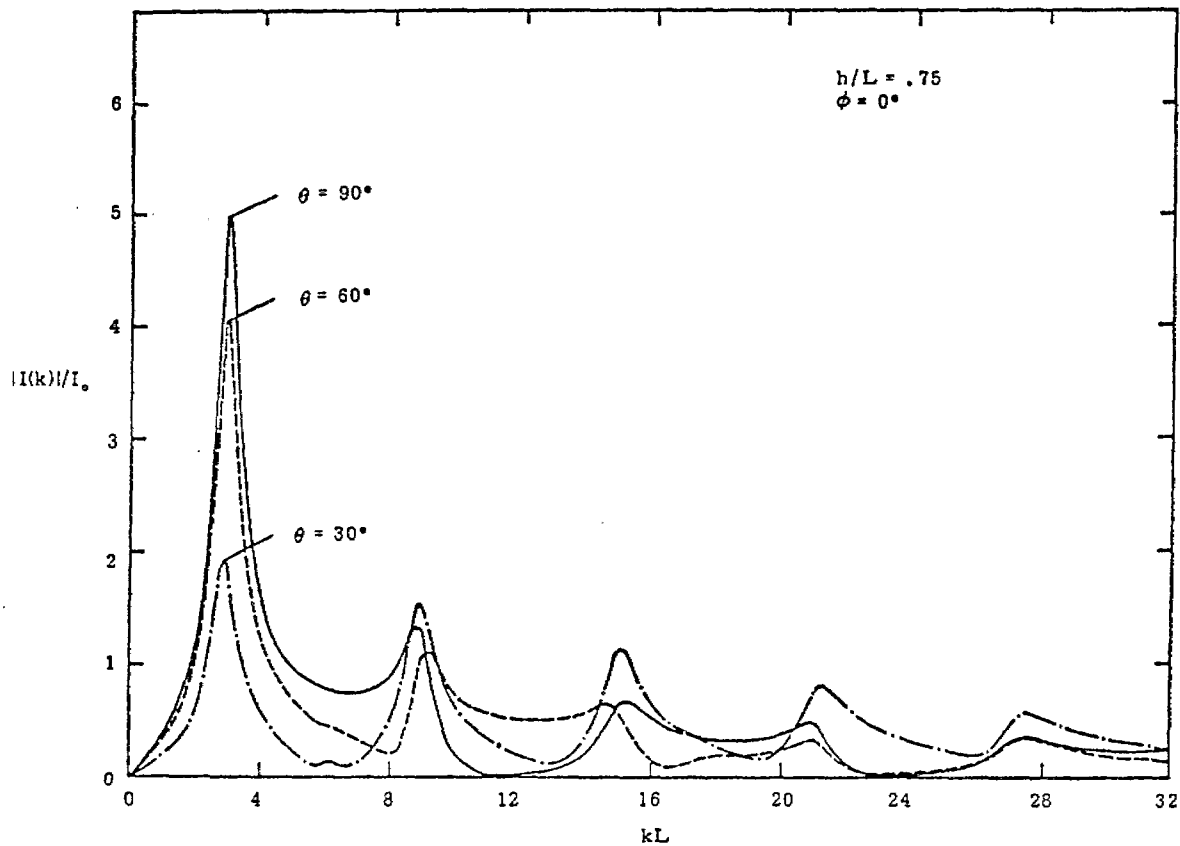


Figure 10b. Magnitude of the impulse spectrum of the current observed at the point  $\xi = .5L$ .

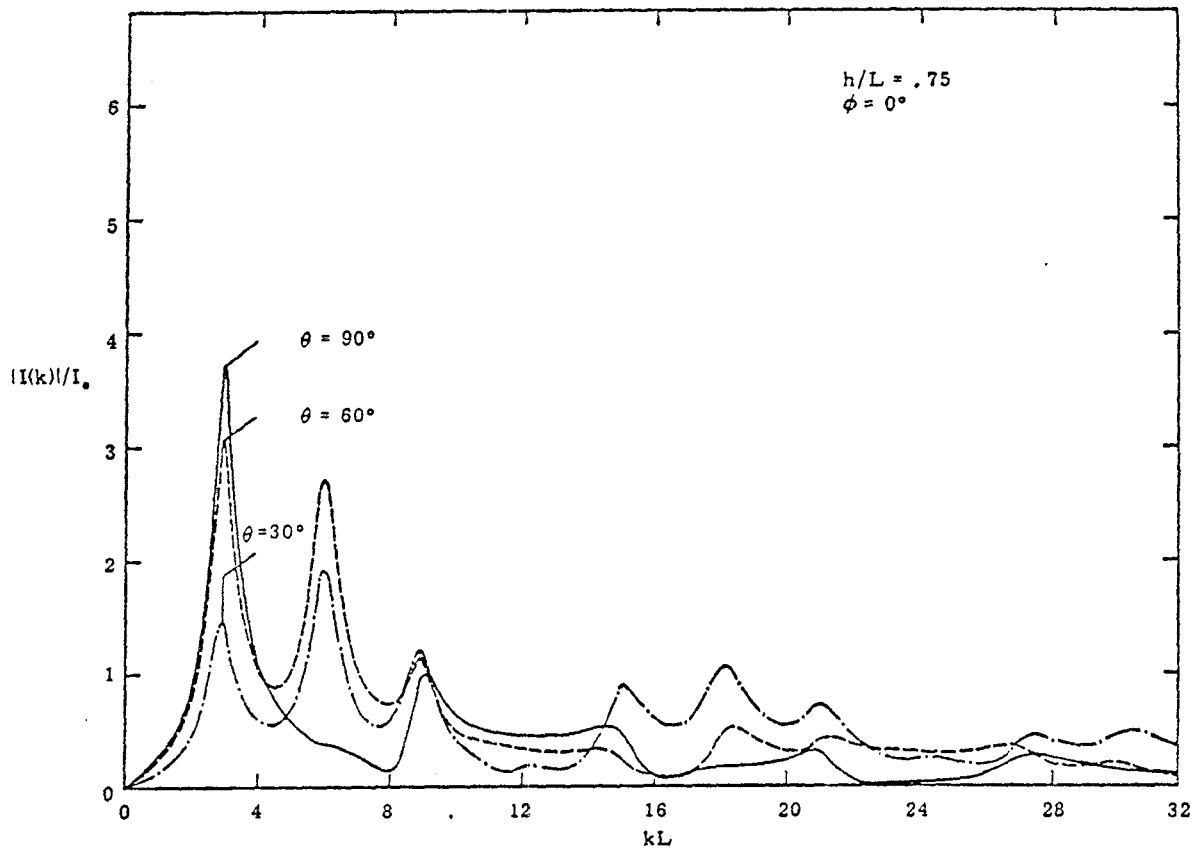


Figure 10c. Magnitude of the impulse spectrum of the current observed at the point  $\xi = .75L$ .

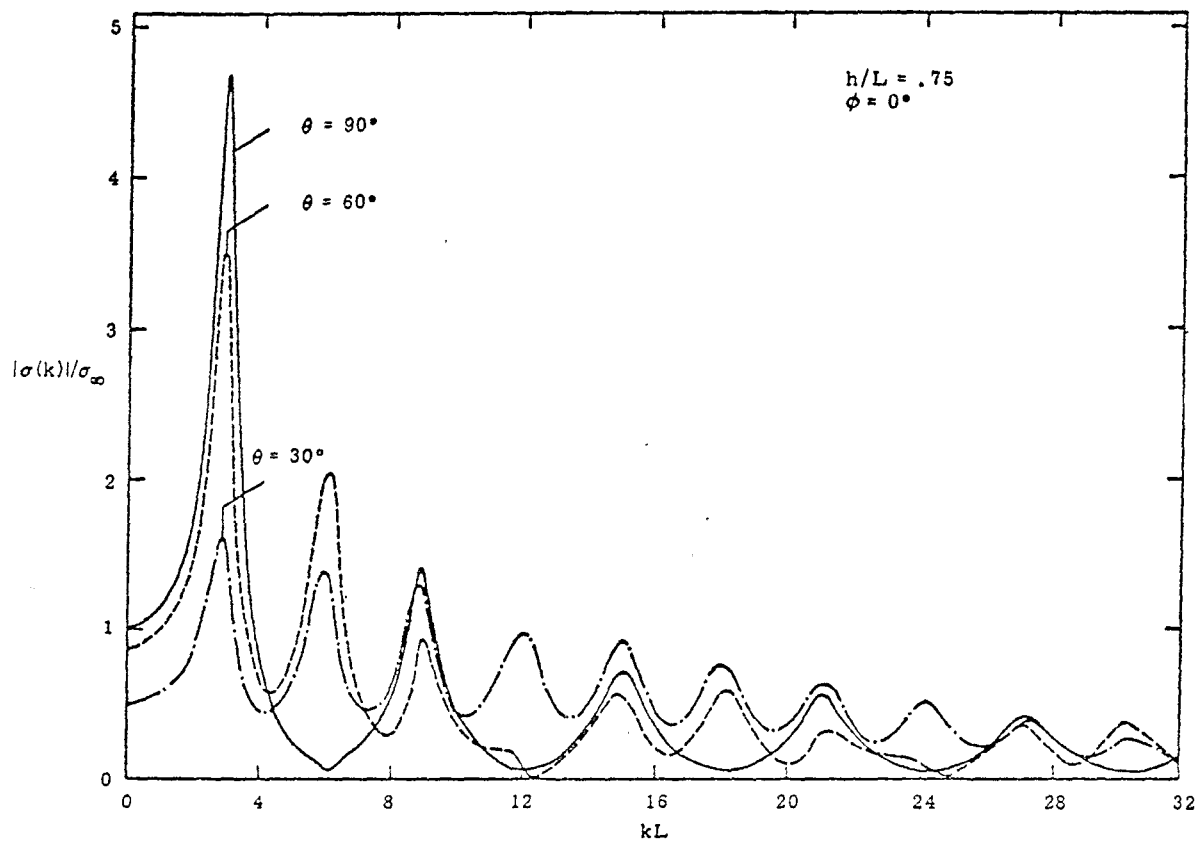


Figure 10d. Magnitude of the impulse spectrum of the linear charge density observed at the point  $\xi = 0$ .

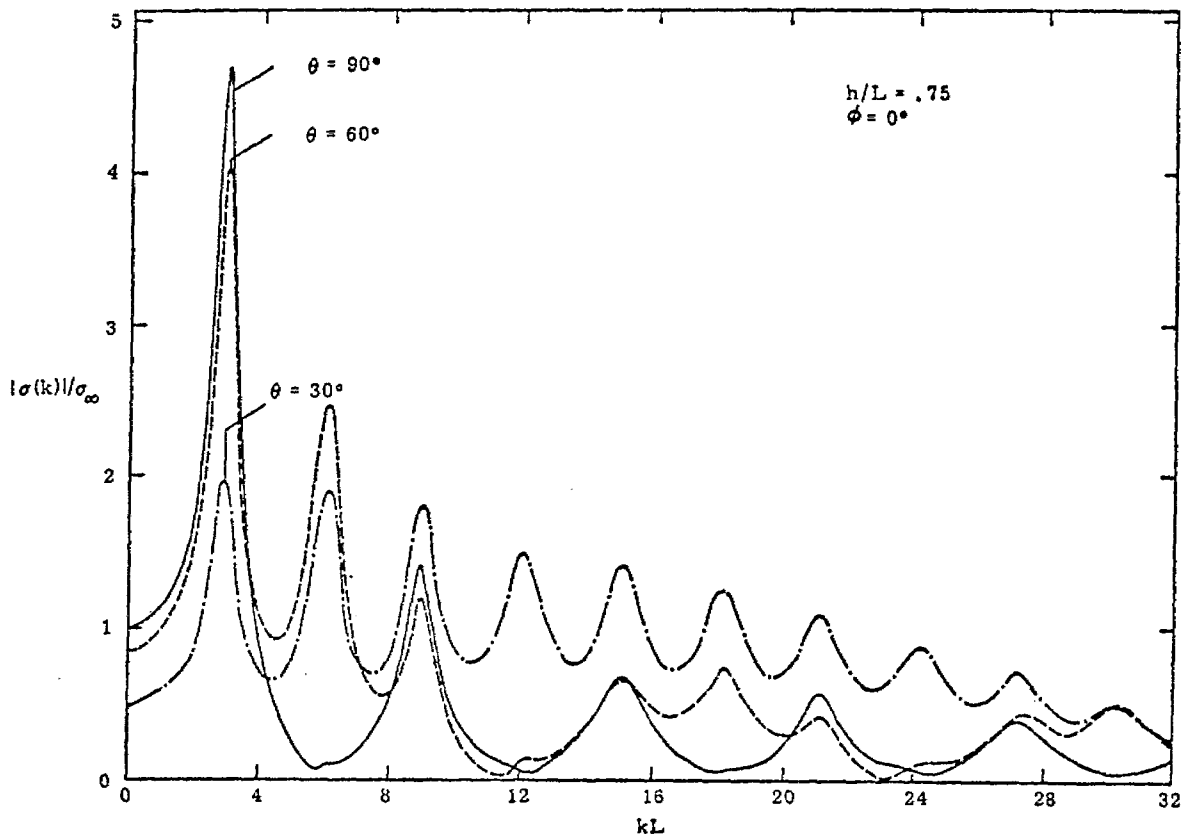


Figure 10c. Magnitude of the impulse spectrum of the linear charge density observed at the point  $\xi = L$ .

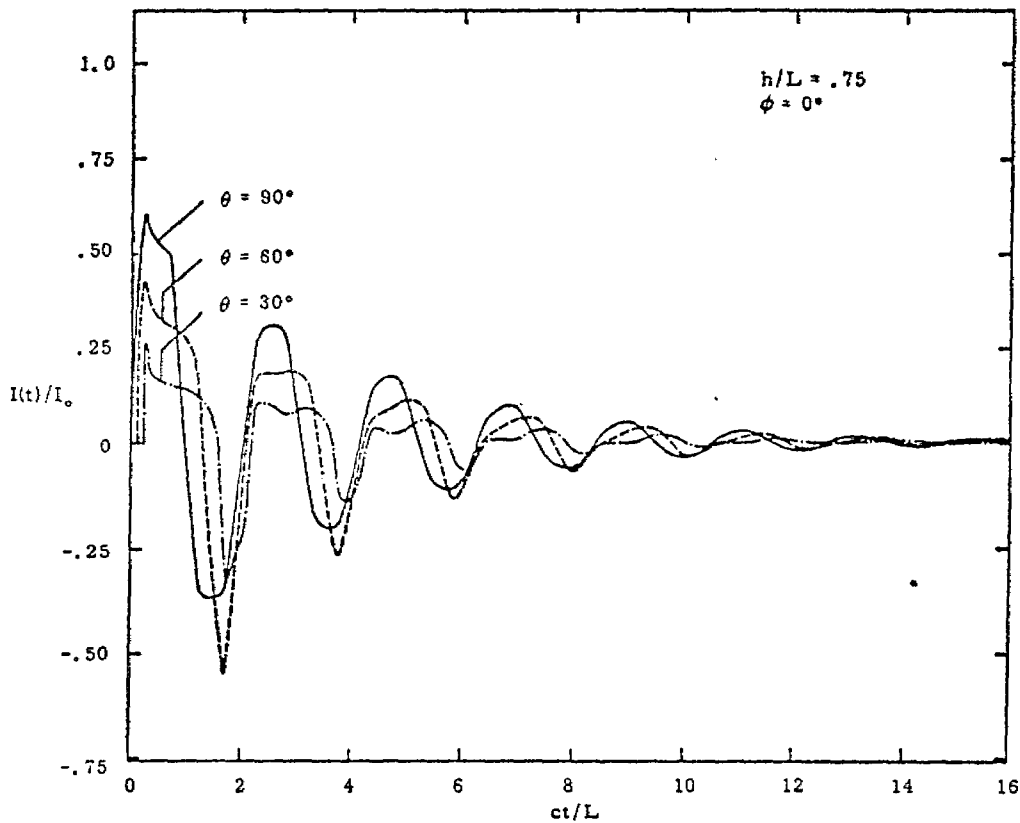


Figure 10f. Time response of the current at  $\xi = .25L$  for an incident step wave.

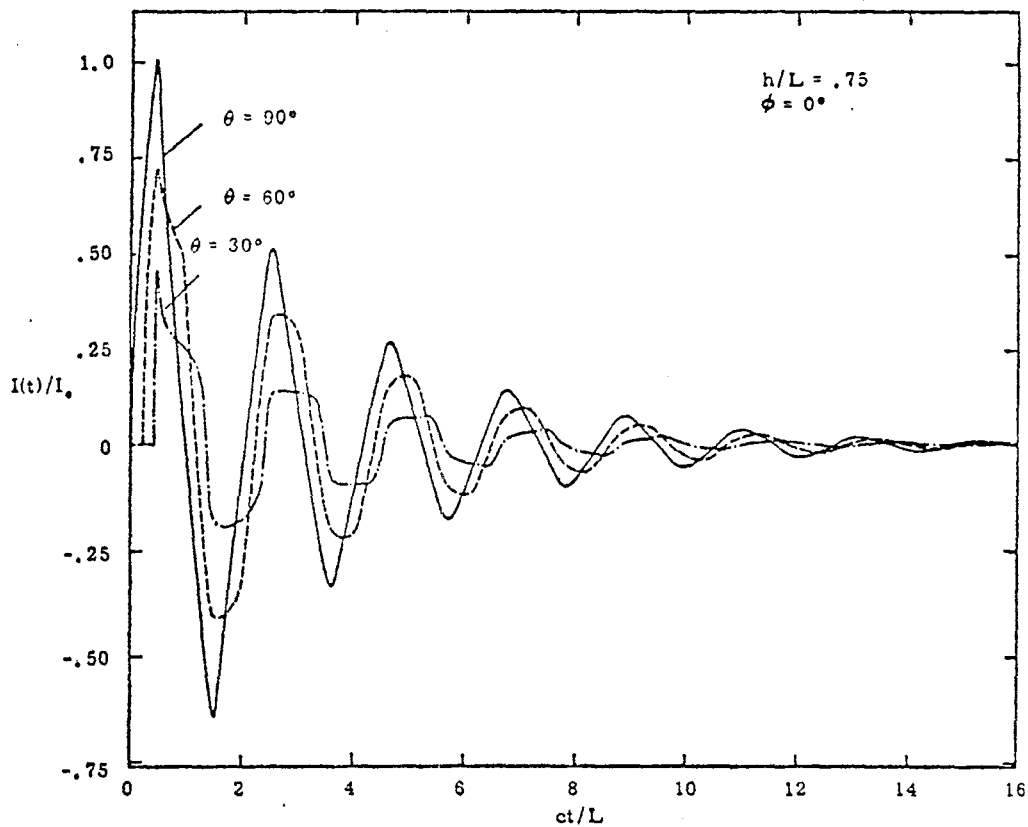


Figure 10g. Time response of the current at  $\xi = .5L$  for an incident step wave.

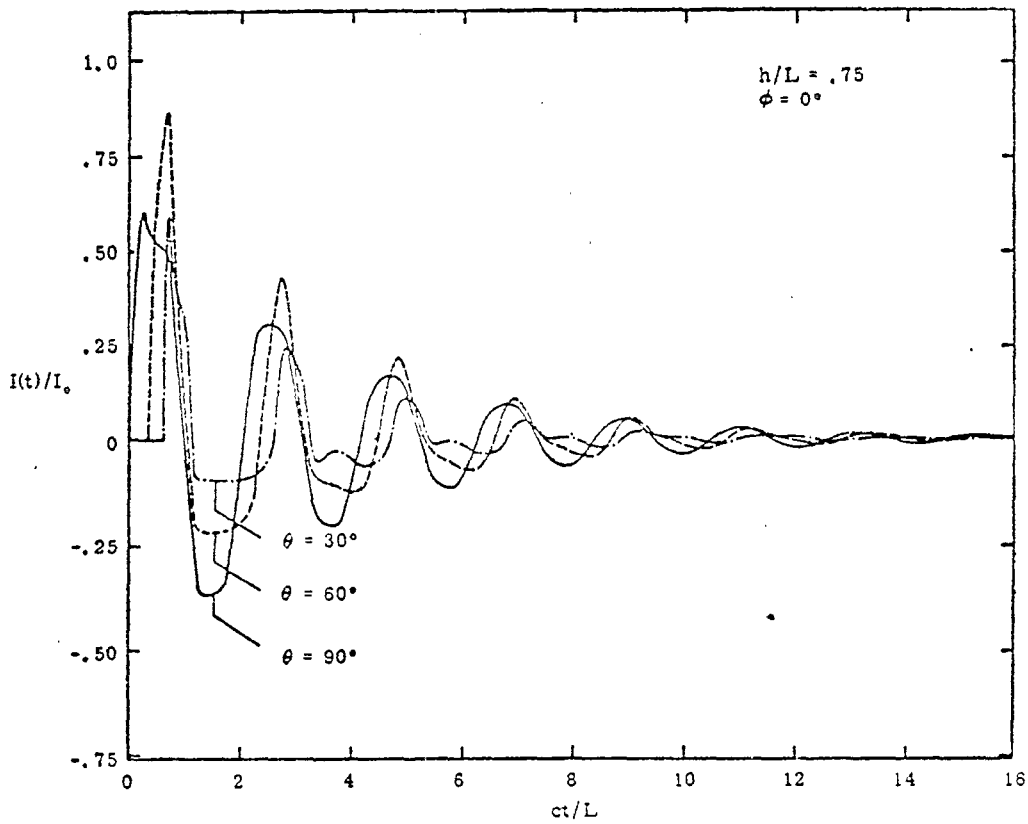


Figure 10h. Time response of the current at  $\xi = .75L$  for an incident step wave.

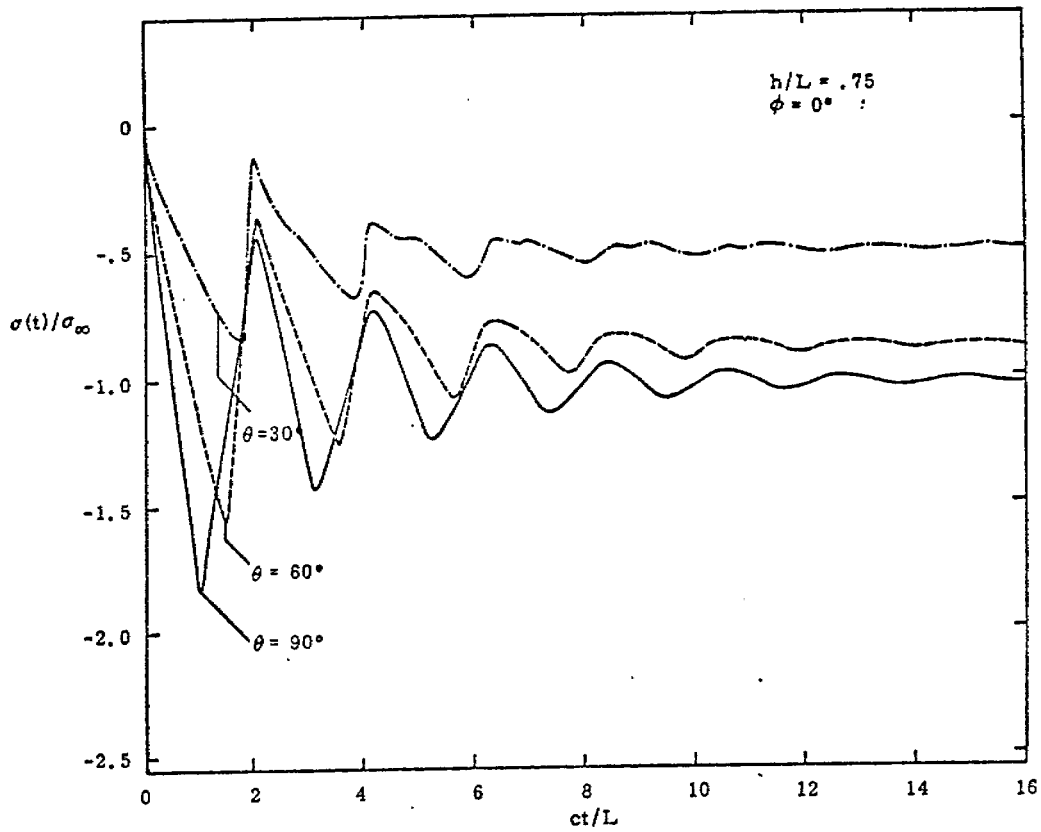


Figure 10i. Time response of the charge density at  $\xi = 0$  for an incident step wave.

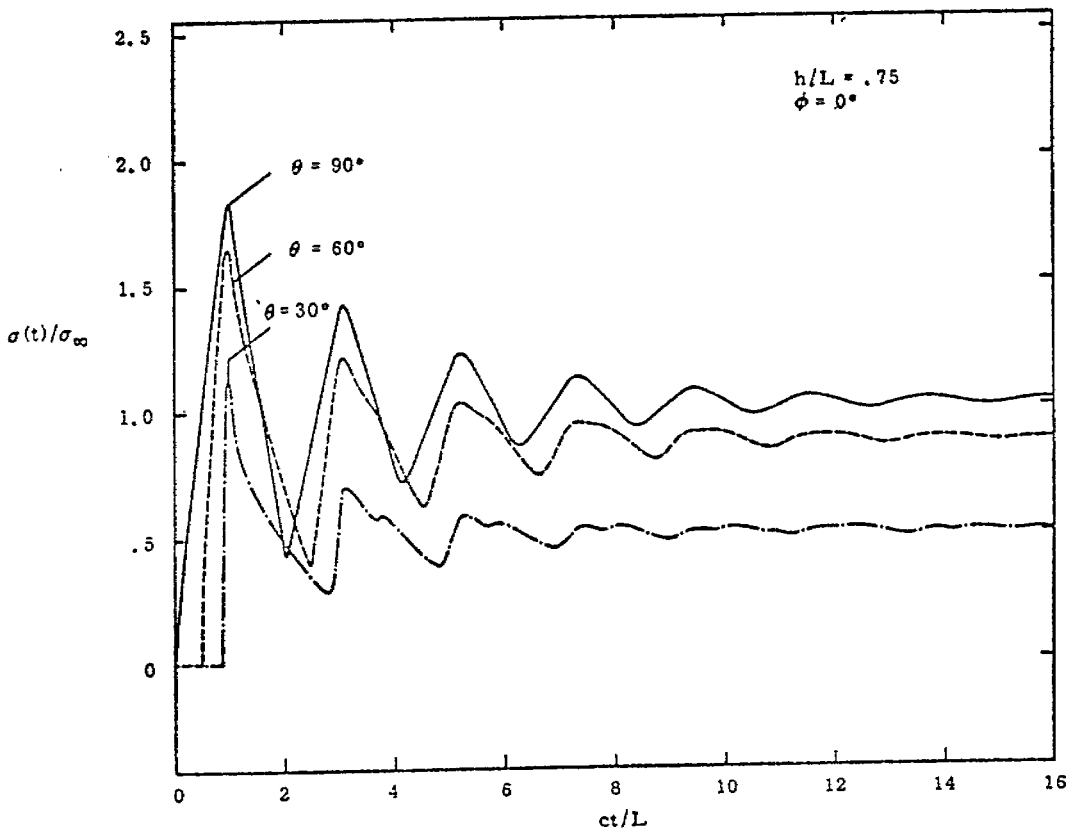


Figure 10j. Time response of the charge density at  $\xi = L$  for an incident step wave.

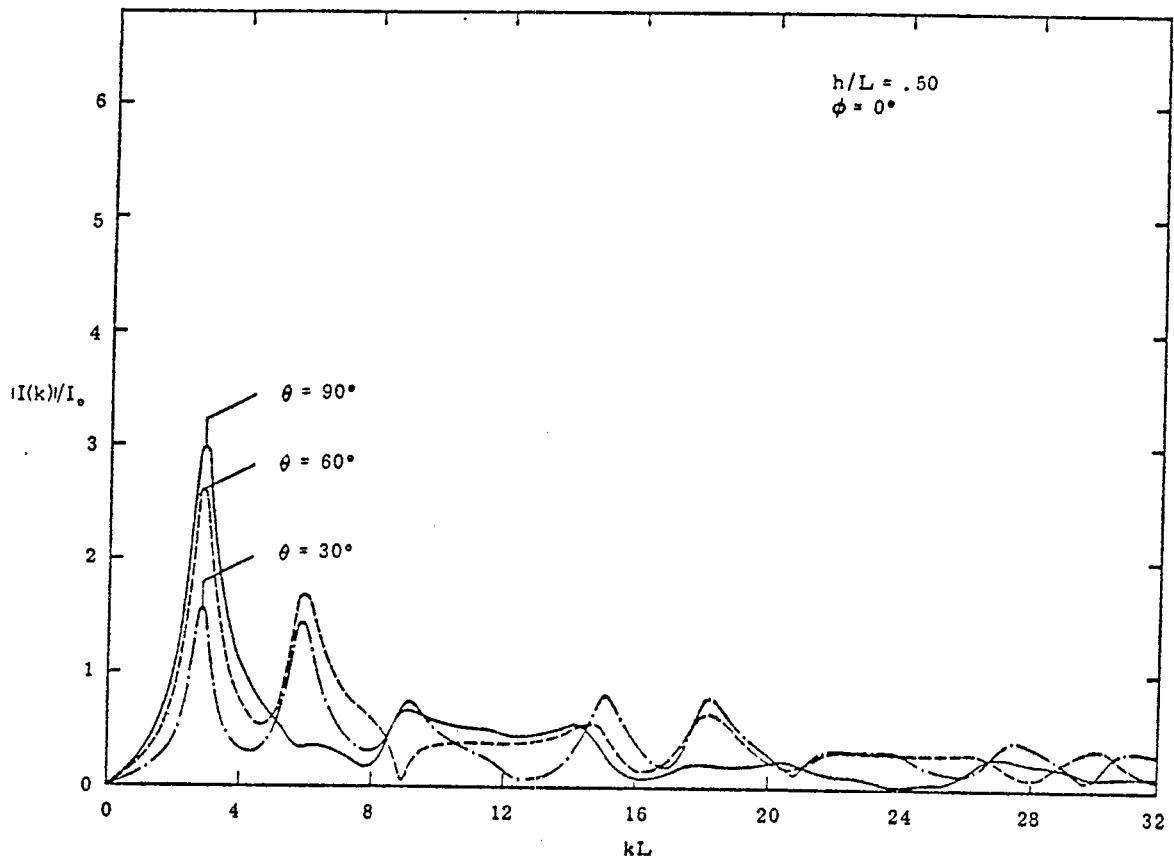


Figure 11a. Magnitude of the impulse spectrum of the current observed at the point  $\xi = .25L$ .

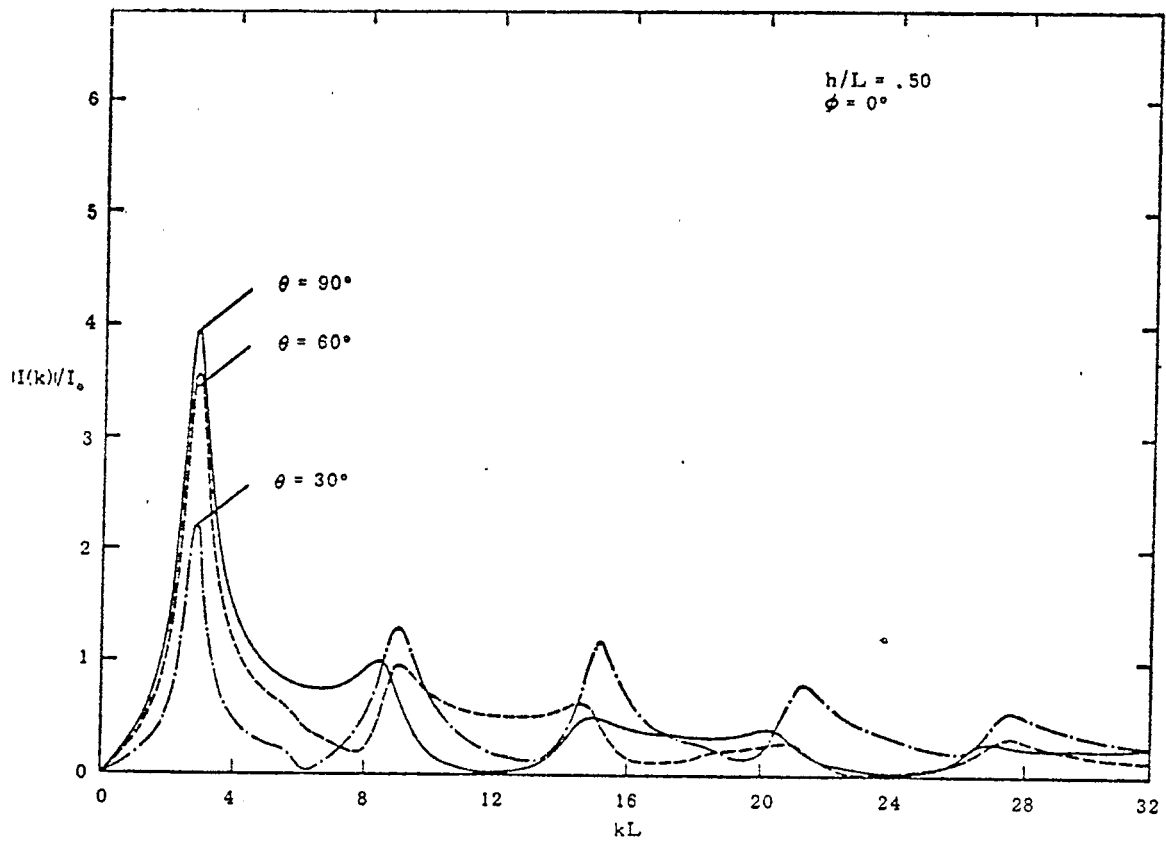


Figure 11b. Magnitude of the impulse spectrum of the current observed at the point  $\xi = .5L$ .

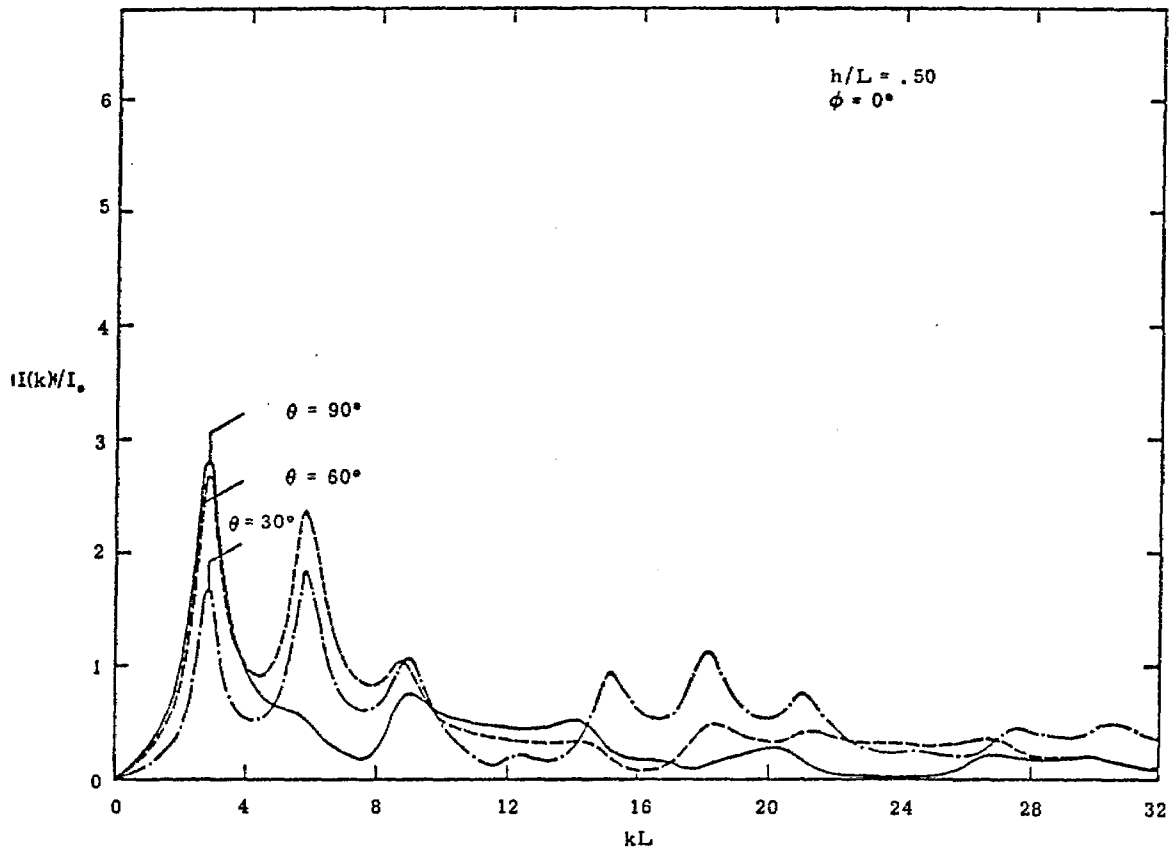


Figure 11c. Magnitude of the impulse spectrum of the current observed at the point  $\xi = .75L$ .

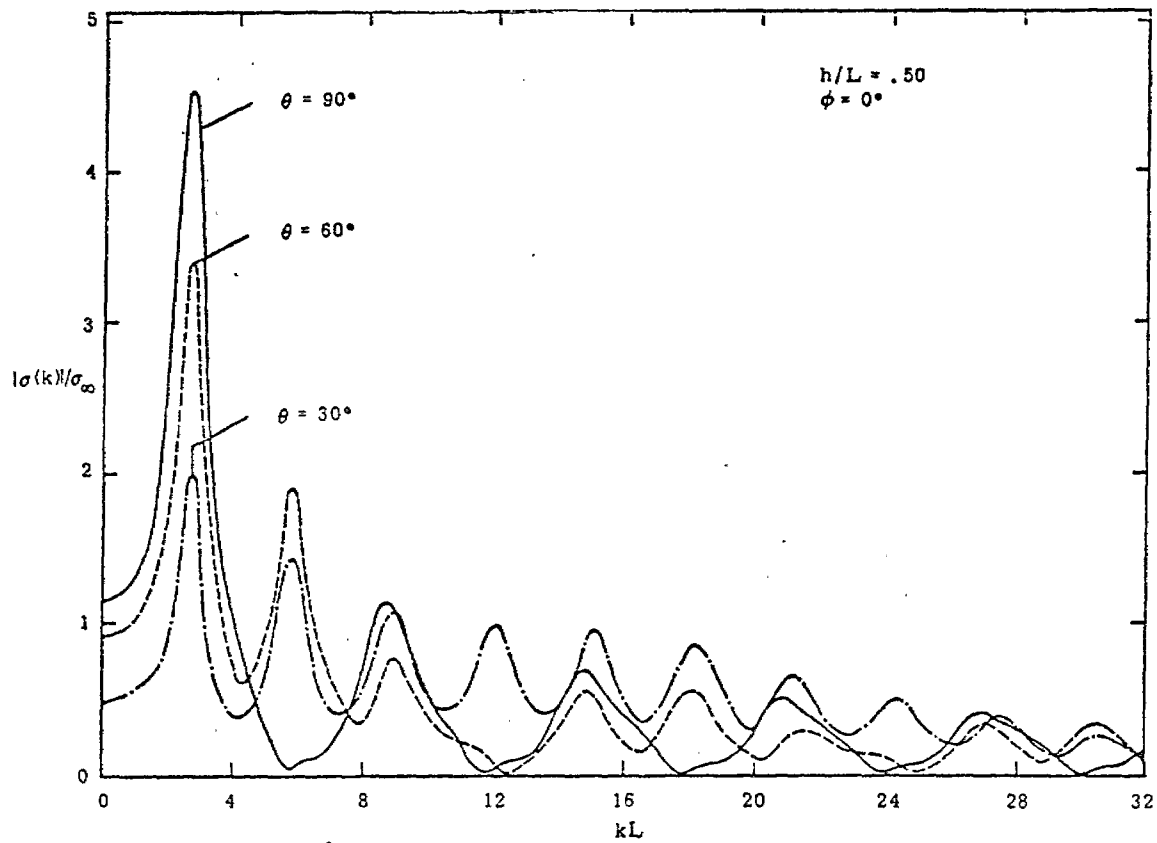


Figure 11d. Magnitude of the impulse spectrum of the linear charge density observed at the point  $\xi = 0$ .

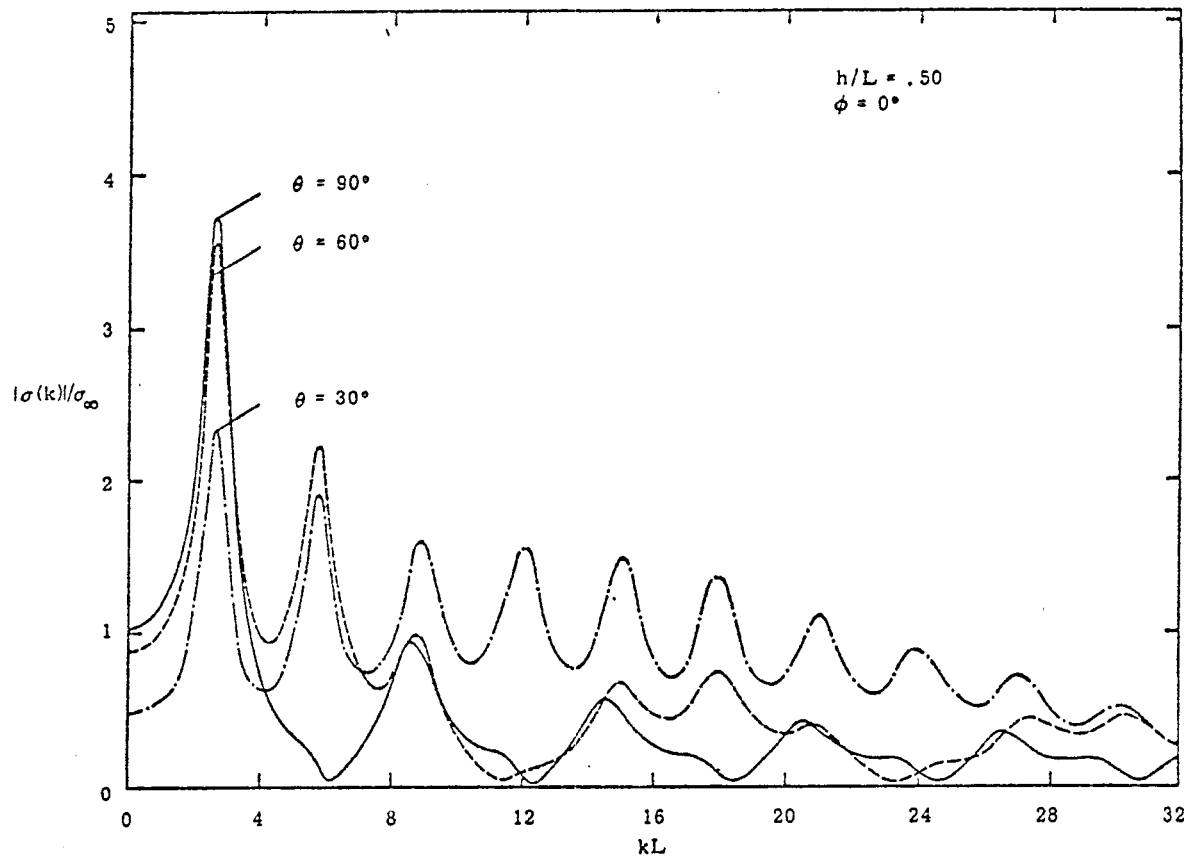


Figure 11e. Magnitude of the impulse spectrum of the linear charge density observed at the point  $\xi = L$ .

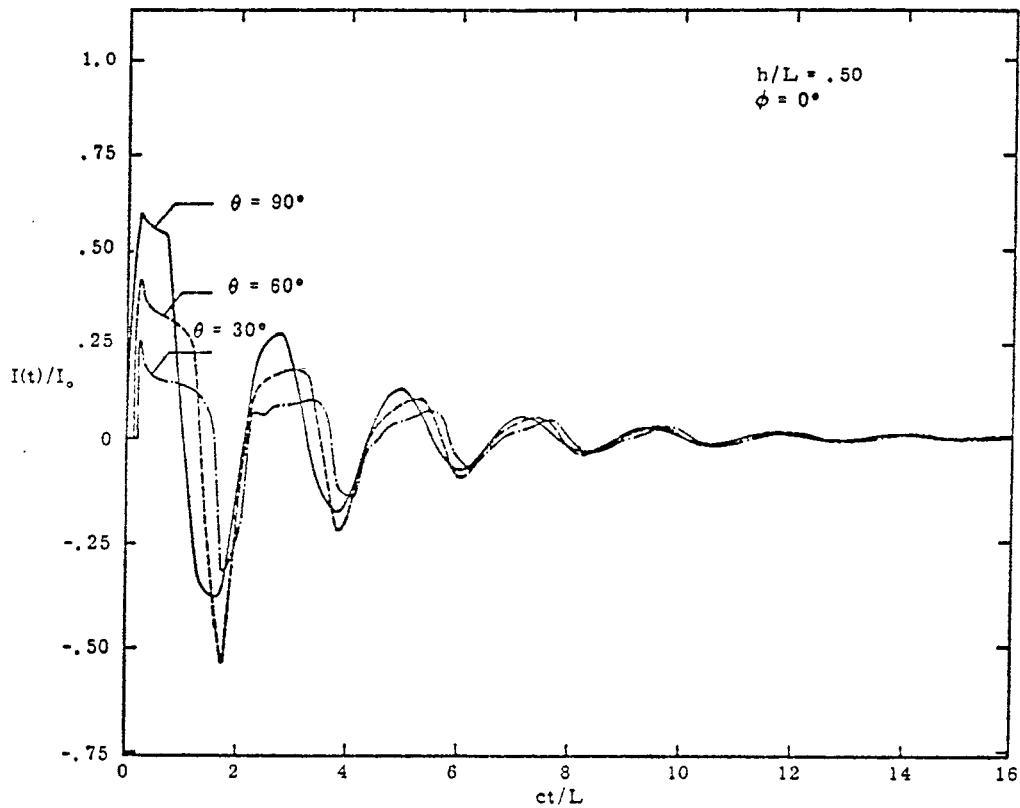


Figure 11f. Time response of the current at  $\xi = .25L$  for an incident step wave.

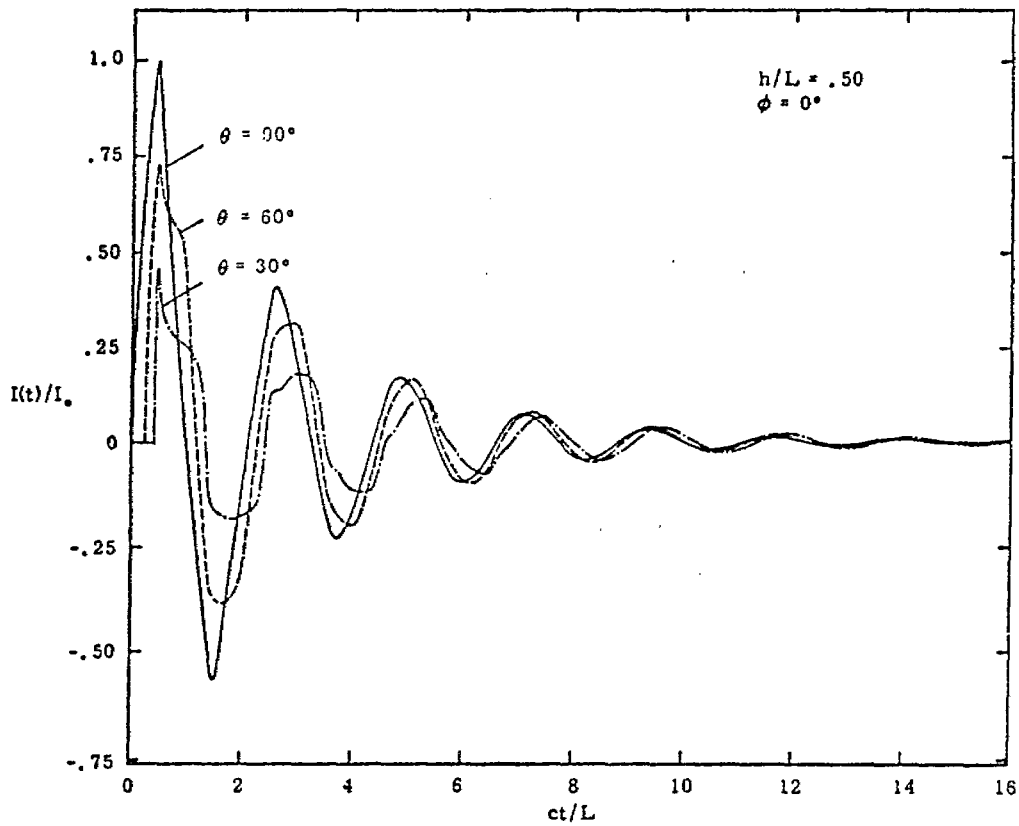


Figure 11g. Time response of the current at  $\xi = .5L$  for an incident step wave.

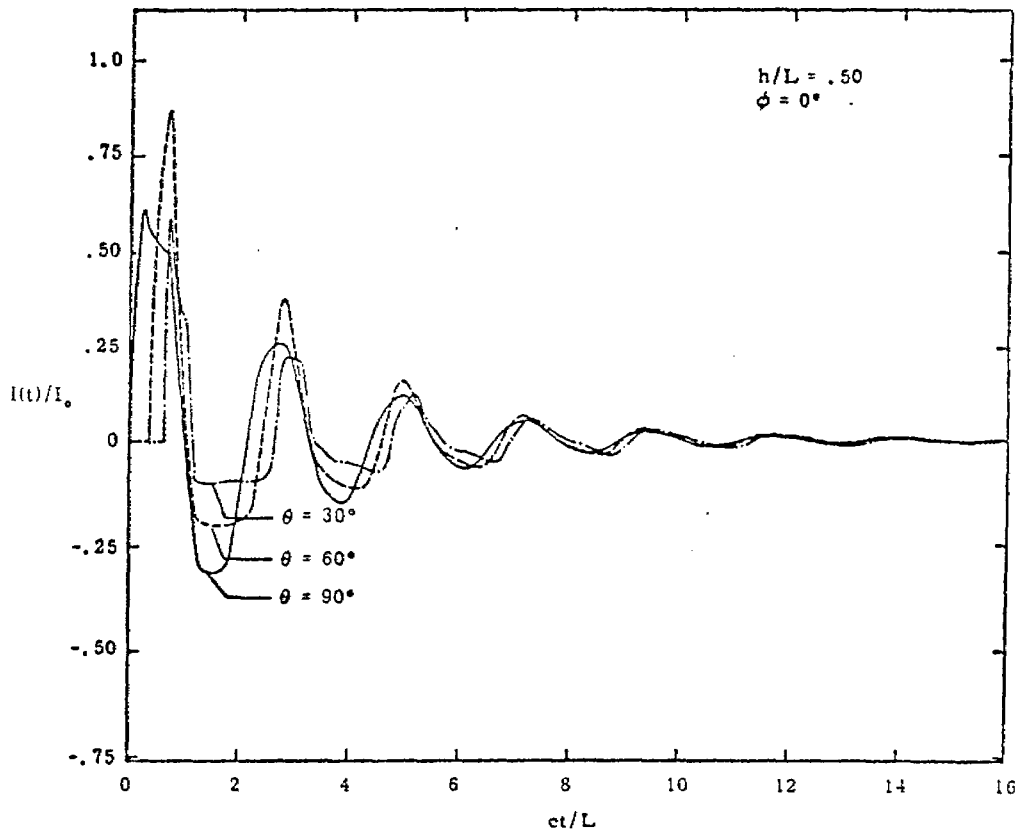


Figure 11h. Time response of the current at  $\xi = .75L$  for an incident step wave.

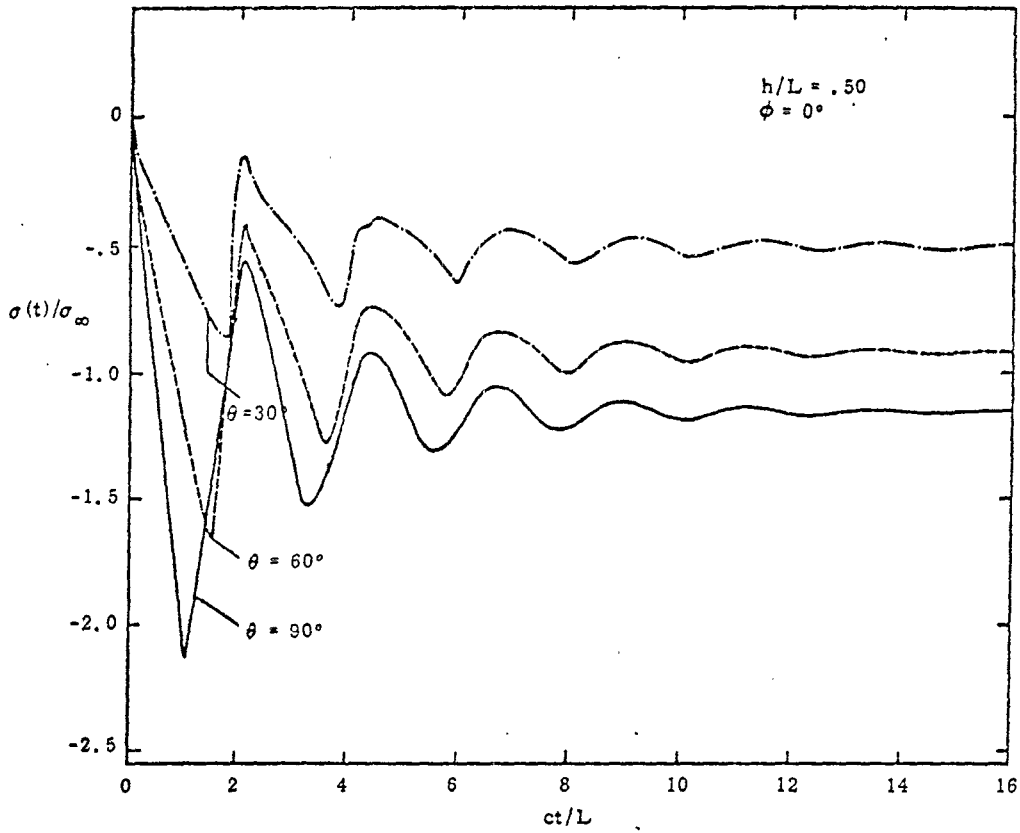


Figure 11i. Time response of the charge density at  $\xi = 0$  for an incident step wave.

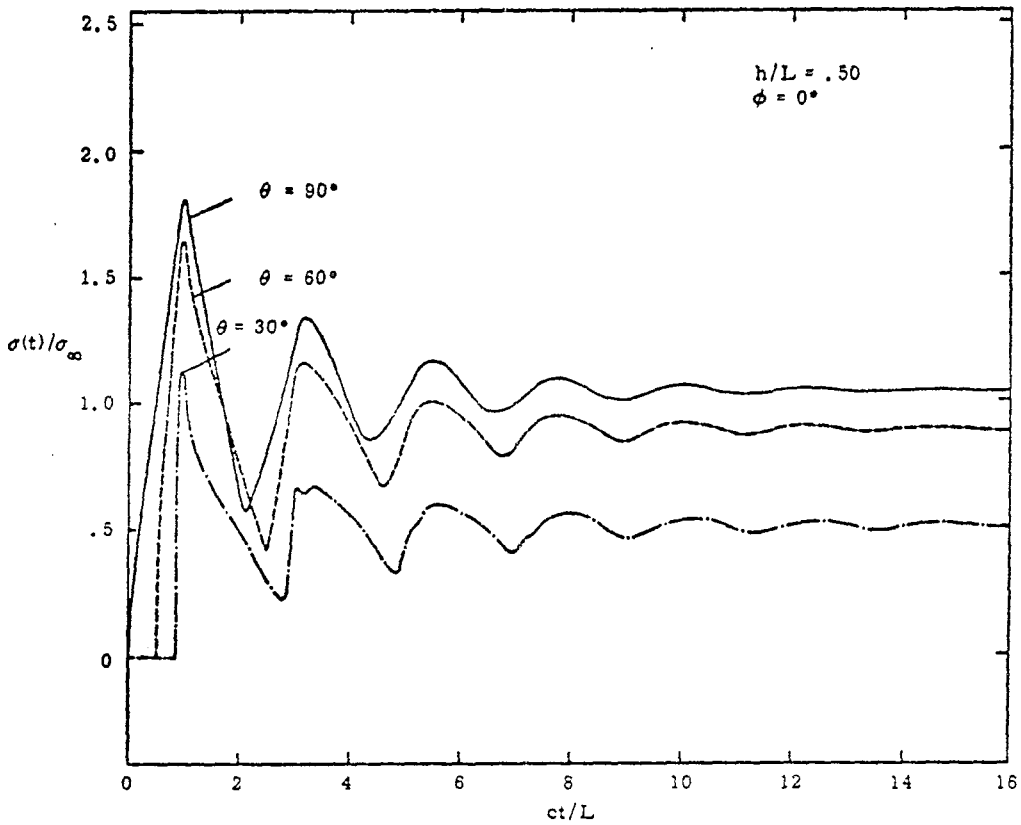


Figure 11j. Time response of the charge density at  $\xi = L$  for an incident step wave.

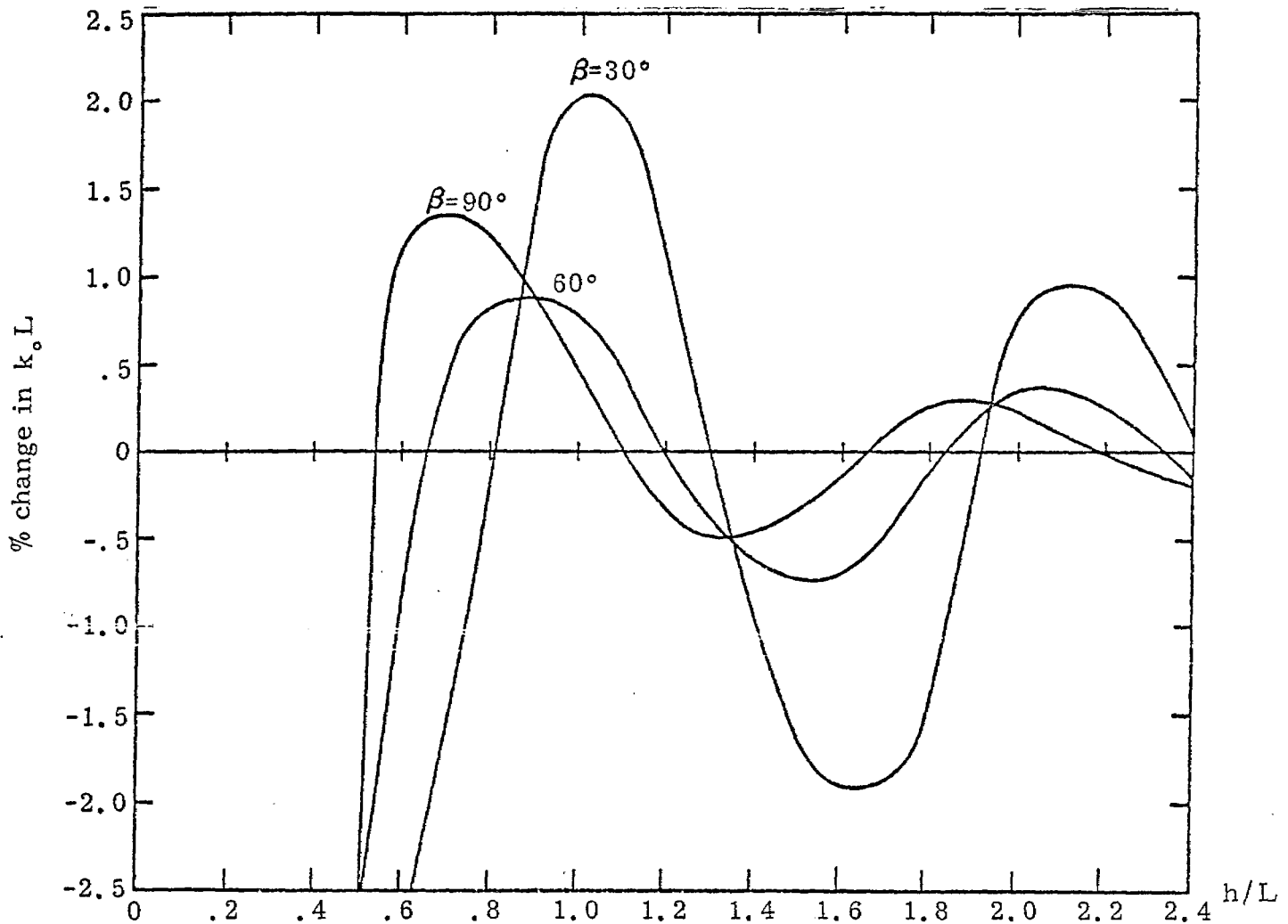


Figure 12. Plots of the percent change of the first resonant frequency of the wire scatterer relative to the free space resonant frequency, shown as a function of  $h/L$  for various values of the inclination angle  $\beta$ .

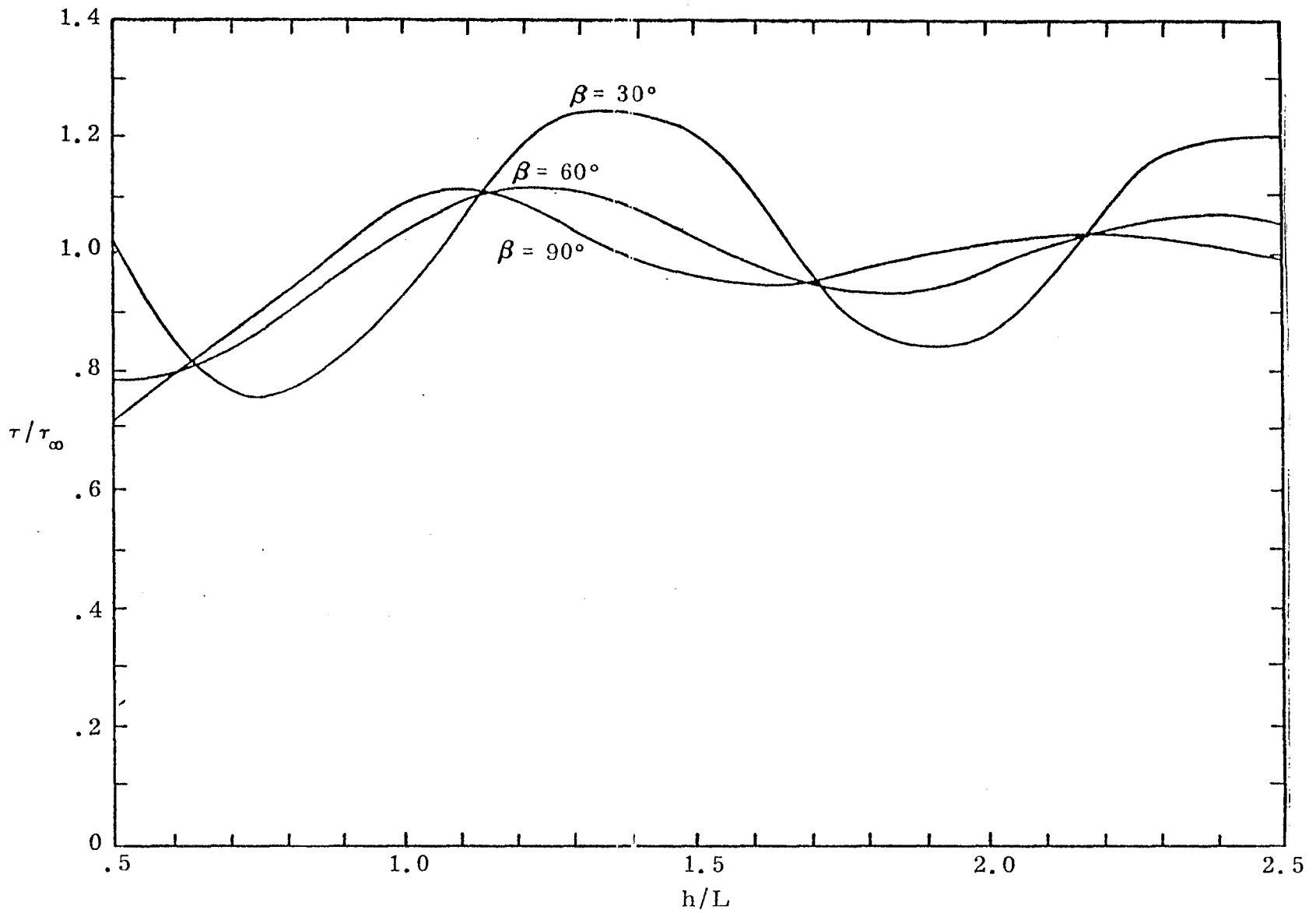


Figure 13. The normalized damping constant  $\tau/\tau_\infty$  for the fundamental mode. Shown as a function of  $h/L$  with  $\beta$  as a parameter. The normalizing factor,  $\tau_\infty$ , is the damping constant for the fundamental mode of the scatterer in free space.

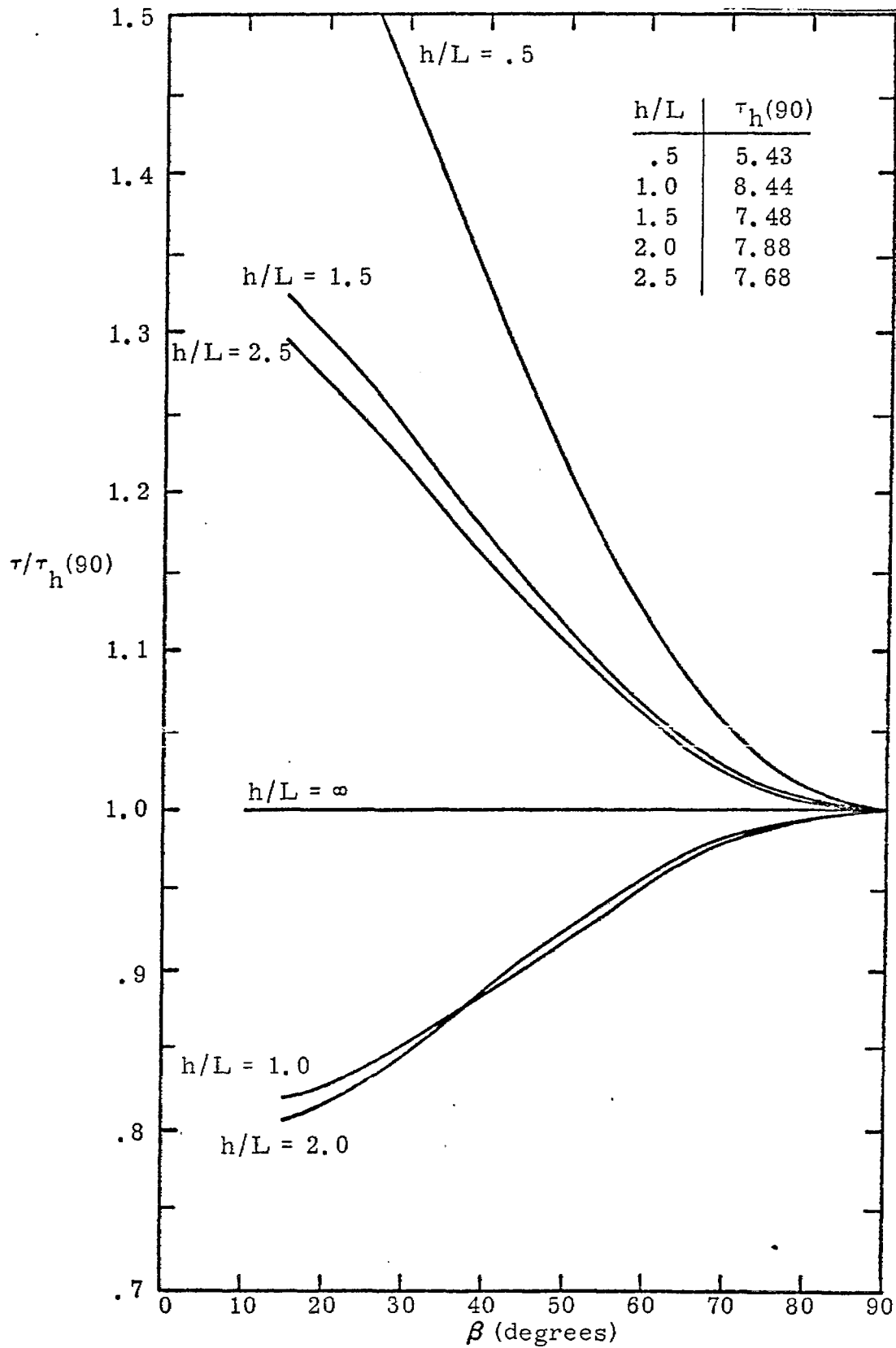


Figure 14. The normalized damping constant  $\tau/\tau_h(90)$  shown as a function of  $\beta$  for  $h/L$  as a parameter. The normalization factor  $\tau_h(90)$ , is the damping constant calculated for  $\beta = 90^\circ$  and the  $h/L$  value under consideration.

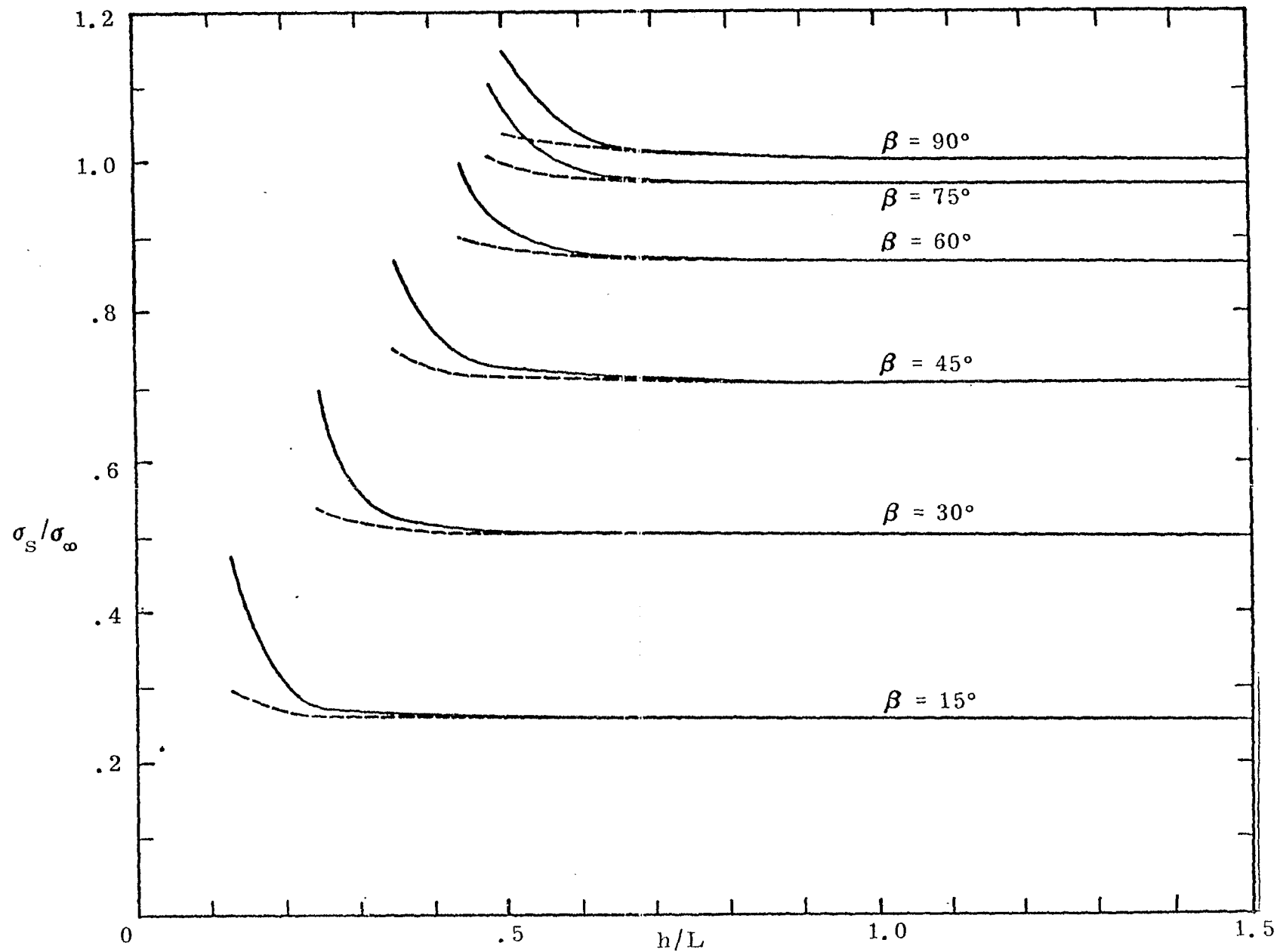


Figure 15. Plots of the late time or static linear charge density induced on the ends of the scattering element shown as a function of  $h/L$  with  $\beta$  as a parameter. The normalizing factor,  $\sigma_\infty$ , is the charge density on the ends of the scatterer in free space and parallel to the incident electric field. The solid line is the charge of  $\xi = 0$  and the dotted is at  $\xi = L$ .

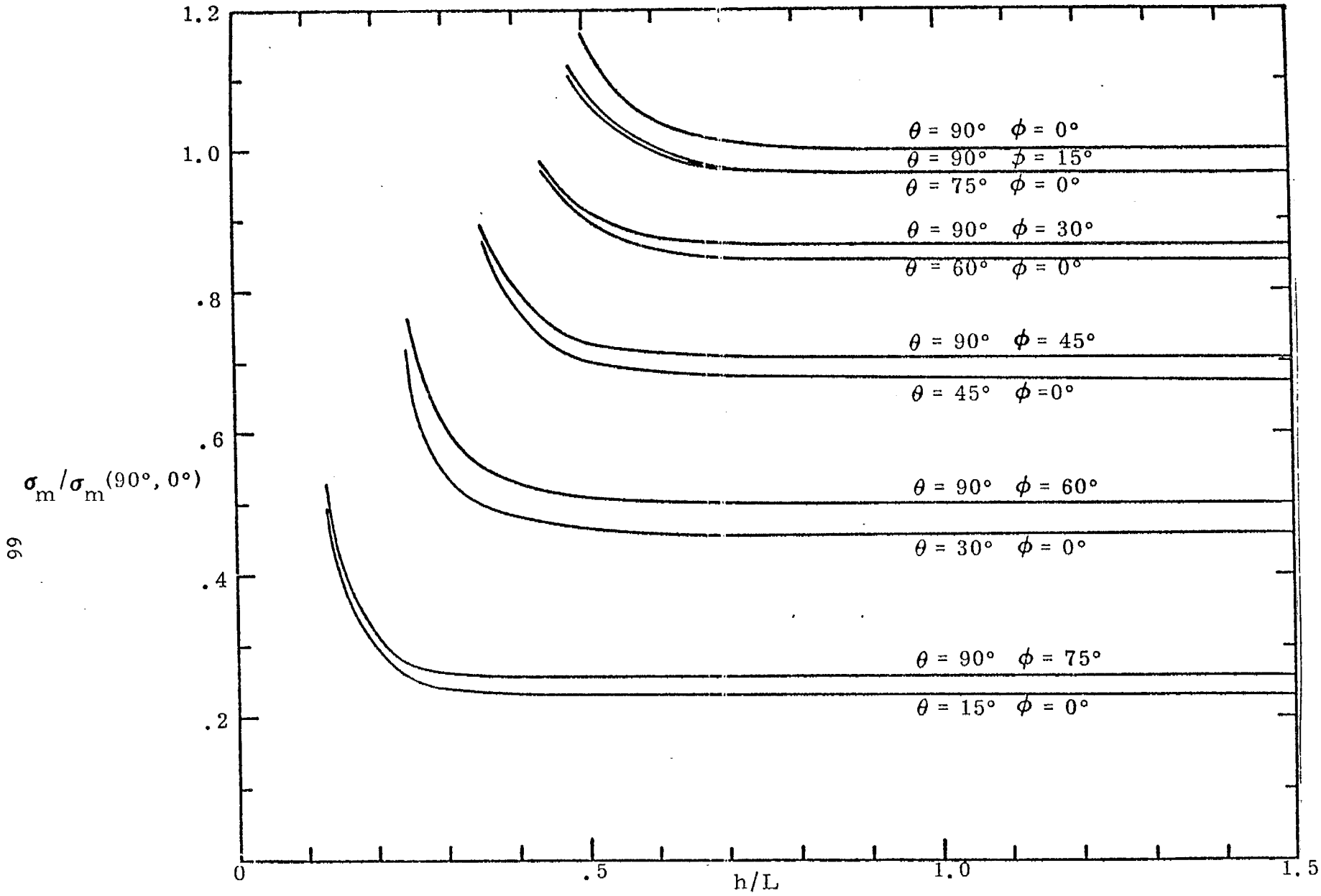


Figure 16. Plots of the field enhancement factor at  $\xi = 0$  (maximum normalized charge density in the time domain) shown as a function of  $h/L$  and for various combinations of the angles  $\theta$  and  $\phi$ . The variation of this quantity at  $\xi = L$  was negligible and not plotted.

## Appendix I

As mentioned in the text, it is necessary to modify the thin-wire approximation in the integro-differential equation for the scattering problem in order to get an accurate time domain response. In this appendix, this problem is discussed in conjunction with the driven antenna problem.<sup>(10)</sup> In the scattering problem, it is not necessary to worry about the gap model as also treated here. Hopefully, this additional information will not cloud the issue at hand, but will serve to shed more light on the use of the numerical methods in antenna and scattering problems.

In attempting to obtain the time response of a thin-wire transmitting antenna by numerical means, there are two ways to proceed. The first is to formulate an integral equation in the frequency domain for the antenna current and upon solving the equation numerically, construct the time response by means of Fourier inversion. The other, perhaps less conventional, approach is to solve the problem directly in the time domain.

The first approach necessitates being able to solve the integral equation for high as well as low frequencies, so as to permit the correct construction of the time response. The customary thin-wire approximation is known to break down at higher frequencies. This can cause appreciable error in the high frequency response of the antenna. Moreover, the model of the driving gap of the antenna influences to a certain extent the frequency response. These effects are briefly discussed in this appendix.

Consider the case of a straight, cylindrical antenna as shown in Figure A1. The antenna has a total length  $L$ , radius  $a$  and is center driven with a gap at  $x = L/2$ . The parameter  $\Omega = 2 \ln(L/a) = 10.0$ , so that the antenna is relatively thin. Neglecting the radiation from the equivalent magnetic current flowing over the gap region and assuming a perfectly conducting wire, the following integro-differential equation of the Pocklington type can be formulated for the antenna current<sup>(7)</sup>

$$-j\omega\epsilon E^{inc}(z) = \int_0^L \int_0^{2\pi} J(z') \left( \frac{d^2}{dz^2} + k^2 \right) \frac{e^{-jk[(z-z')^2 + 4a^2 \sin^2(\phi/2)]^{1/2}}}{4\pi[(z-z')^2 + 4a^2 \sin^2(\phi/2)]^{1/2}} ad\phi dz' . \quad (A1)$$

By assuming that the current can be considered flowing at the center of the wire and that the observation point  $z$  still remains on the cylindrical surface (thin-wire approximation), Pocklington's equation becomes

$$-j\omega\epsilon E^{inc}(z) = \int_0^L I(z') \left( \frac{d^2}{dz^2} + k^2 \right) \frac{e^{-jk[(z-z')^2 + a^2]^{\frac{1}{2}}}}{4\pi[(z-z')^2 + a^2]^{\frac{1}{2}}} dz' . \quad (A2)$$

The numerical solution of this equation by the method of moments has been discussed and illustrated by Harrington<sup>(3)</sup>. In solving these equations for this particular study, the basis functions used are pulse functions defined over a small interval or cell on the antenna. The weighting functions are impulses, thereby yielding a point matching solution.

In the solution by the method of moments, it is necessary to increase the number of cells on the antenna as the frequency increases so that the current will be adequately represented. If it is assumed that the source voltage is applied over one cell only as has been done by Harrington, the effective source region gets smaller and smaller as the number of cells increases. This gives rise to a gap capacitance which grows with frequency and causes the numerical results to differ from those actually expected in a physical situation.

One way to eliminate this problem is to permit the source gap to contain more than just one cell. By doing this and distributing the incident field out over these source cells, the gap size can be considered fixed. One difficulty with this, however, is that as the gap starts to contain more and more cells, the input current of the antenna becomes difficult to define.

The curves of the magnitude of the input antenna currents as a function of  $kL$  in Figure A2 show the effects of the thin-wire approximation and of placing the driving source in just one cell. The solid curve, which is the result of solving equation (A1) with a fixed driving gap of  $L/10$ , shows the expected behavior of the input current at higher frequencies. The dotted curve is the result of solving equation (A1) with the source voltage in only one cell which becomes smaller compared to the antenna length as the frequency increases. The effect of the increasing gap capacitance is observed in a rise in input current with frequency. The dashed curve represents the input current obtained

by using the thin-wire approximation (equation (A2)) and the driving voltage again in just one cell. The divergent nature of the solution is even more serious than in the previous case.

Special attention should be paid to the differences between the dotted and dashed curves, since they have bearing on the accuracy of the thin-wire approximation. Notice that for  $kL > 15$  or so, the results begin to differ, indicating that the thin-wire approximation is breaking down.

In conclusion, it can be said that the use of the thin-wire approximation as well as the variable gap model of the driving source can cause large errors in the high frequency solution of the integral equation for thin antennas. As a result, the time response calculated from such a frequency spectrum will be in error.

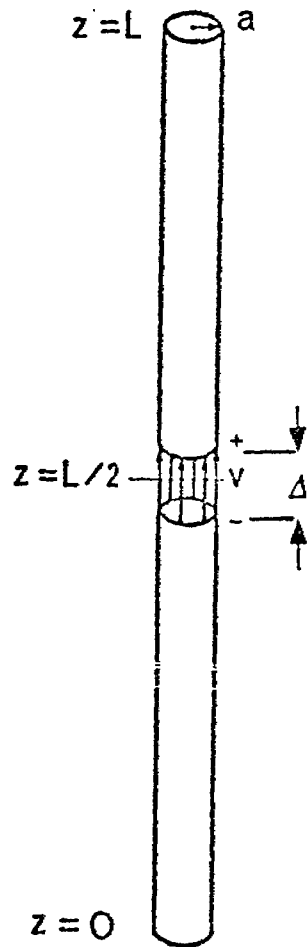


Figure A1. Geometry of the thin-wire, center driven antenna  
 $\Omega = 2 \ln(L/a) = 10$ , and the driving gap  $\Delta = .1L$ .

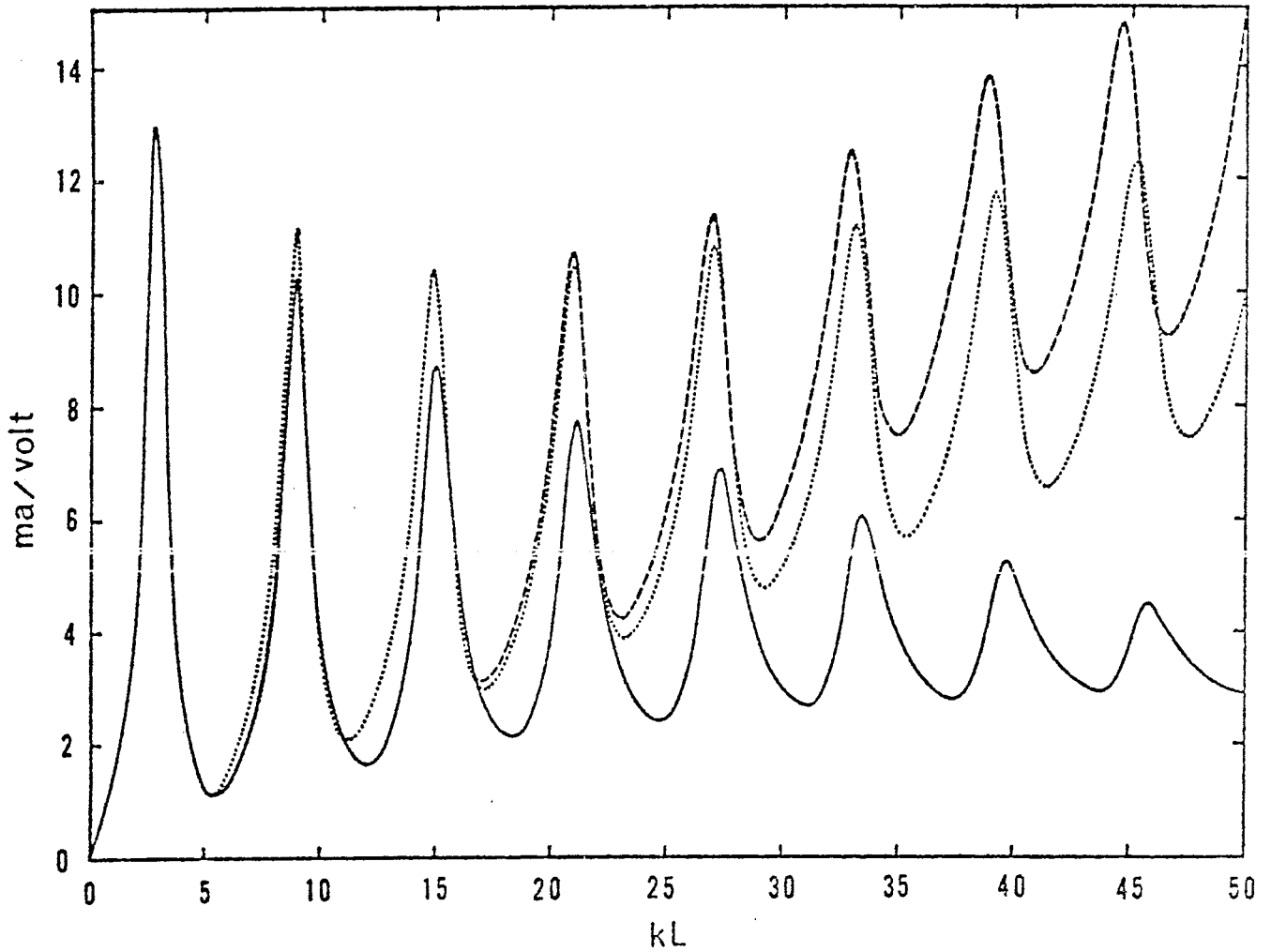


Figure A2. Plots of the magnitudes of the antenna input currents as a function of  $kL$ . (Solid line--exact kernel with fixed gap. Dotted line--exact kernel with variable gap. Dashed line--thin wire kernel with variable gap.)

03 (72)

### References

1. Brigham, E. O., and Morrow, R. E., "The Fast Fourier Transform," IEEE Spectrum, December 1967, pp. 63-70.
2. Cooley, J. W., and Tukey, J. W., "An Algorithm for the Machine Calculation of Complex Fourier Series," Math. Comput., vol. 19, April 1965, pp. 297-301.
3. Harrington, R. F., Field Computation by Moment Methods, Mac Millan, 1968.
4. King, R. W. P., The Theory of Linear Antennas, Harvard University Press, Cambridge, 1956, pp. 119-123.
5. Latham, R. W., and Lee, K. S. H., "Electromagnetic Interaction Between a Cylindrical Post and a Two-Parallel Plate Simulator," EMP Sensor and Simulation Notes, Note 111, July 1970.
6. Marin, L., "A Cylindrical Post Above a Perfectly Conducting Plate, II (Dyanmic Case)," EMP Sensor and Simulation Notes, Note 136, August 1971.
7. Mei, K. K., "On the Integral Equations of Thin-Wire Antennas," IEE Trans. A. P., May 1965, p. 374.
8. Mei, K. K., "Numerical Methods in Electromagnetic Wave Problems," A short course presented at the Harry Diamond Laboratory, Washington, D.C., May 27-June 19, 1968.
9. Tesche, F. M., "On the Numerical Analysis of Thin-Wire Antennas Mounted on a Conducting Sphere," Ph.D. Thesis, The University of California at Berkeley, March 1971.
10. Tesche, F. M., "The Effect of the Thin-Wire Approximation and the Source Gap Model on the High Frequency Integral Equation Solution of Radiating Antennas," to be published in IEEE A.P., March 1972.
11. Tesche, F. M., "On the Behavior of Thin-Wire Scatterers and Antennas Arbitrarily Located Within a Parallel Plate Region, I (The Formulation)," EMP Sensor and Simulation Notes, Note 135, August 1971.